

1989

Ductile Deformation Of The Whitestone Anorthosite By The Parry Sound Shear Zone: Implications For Thrust Tectonics

Hayrettin Koral

Follow this and additional works at: <https://ir.lib.uwo.ca/digitizedtheses>

Recommended Citation

Koral, Hayrettin, "Ductile Deformation Of The Whitestone Anorthosite By The Parry Sound Shear Zone: Implications For Thrust Tectonics" (1989). *Digitized Theses*. 1787.
<https://ir.lib.uwo.ca/digitizedtheses/1787>

This Dissertation is brought to you for free and open access by the Digitized Special Collections at Scholarship@Western. It has been accepted for inclusion in Digitized Theses by an authorized administrator of Scholarship@Western. For more information, please contact tadam@uwo.ca, wlsadmin@uwo.ca.



National Library
of Canada

Bibliothèque nationale
du Canada

Canadian Theses Service

Service des thèses canadiennes

Ottawa, Canada
K1A 0N4

NOTICE

The quality of this microform is heavily dependent upon the quality of the original thesis submitted for microfilming. Every effort has been made to ensure the highest quality of reproduction possible.

If pages are missing, contact the university which granted the degree.

Some pages may have indistinct print especially if the original pages were typed with a poor typewriter ribbon or if the university sent us an inferior photocopy.

Reproduction in full or in part of this microform is governed by the Canadian Copyright Act, R.S.C. 1970, c. C-30, and subsequent amendments.

AVIS

La qualité de cette microforme dépend grandement de la qualité de la thèse soumise au microfilmage. Nous avons tout fait pour assurer une qualité supérieure de reproduction.

S'il manque des pages, veuillez communiquer avec l'université qui a conféré le grade.

La qualité d'impression de certaines pages peut laisser à désirer, surtout si les pages originales ont été dactylographiées à l'aide d'un ruban usé ou si l'université nous a fait parvenir une photocopie de qualité inférieure.

La reproduction, même partielle, de cette microforme est soumise à la Loi canadienne sur le droit d'auteur, SRC 1970, c. C-30, et ses amendements subséquents.

**DUCTILE DEFORMATION OF THE WHITESTONE ANORTHOSITE
BY THE PARRY SOUND SHEAR ZONE:
IMPLICATIONS FOR THRUST TECTONICS**

by
Hayrettin Koral

Department of Geology

**Submitted in partial fulfillment
of the requirements for the degree of
Doctor of Philosophy**

**Faculty of Graduate Studies
The University of Western Ontario
London, Ontario
January 1989**

© Hayrettin Koral 1989



National Library
of Canada

Bibliothèque nationale
du Canada

Canadian Theses Service Service des thèses canadiennes

Ottawa, Canada
K1A 0N4

The author has granted an irrevocable non-exclusive licence allowing the National Library of Canada to reproduce, loan, distribute or sell copies of his/her thesis by any means and in any form or format, making this thesis available to interested persons.

The author retains ownership of the copyright in his/her thesis. Neither the thesis nor substantial extracts from it may be printed or otherwise reproduced without his/her permission.

L'auteur a accordé une licence irrévocable et non exclusive permettant à la Bibliothèque nationale du Canada de reproduire, prêter, distribuer ou vendre des copies de sa thèse de quelque manière et sous quelque forme que ce soit pour mettre des exemplaires de cette thèse à la disposition des personnes intéressées.

L'auteur conserve la propriété du droit d'auteur qui protège sa thèse. Ni la thèse ni des extraits substantiels de celle-ci ne doivent être imprimés ou autrement reproduits sans son autorisation.

ISBN 0-315-49327-5

Canada

ABSTRACT

The Parry Sound Shear Zone occurs in the Grenville Province of the Canadian Pre-cambrian Shield between the predominantly amphibolite facies gneisses of the Britt Domain and the granulite facies mafic rocks and migmatites of the Parry Sound Domain of the Central Gneiss Belt. The shear zone transects the Whitestone Anorthosite, located along the western margin of the Parry Sound Domain, and produces a range of new textures and paragenesis.

Two types of mylonites occur along the intersection between the Whitestone Anorthosite and the Parry Sound Shear Zone. Away from the mylonites, moderately modified anorthosite, exhibiting well-defined schistosity, and weakly modified anorthosite, exhibiting relict igneous textures and ill-defined foliation, occur. Minor planar and anastomosing shear zones are superimposed on modified anorthosites.

The metamorphic mineral assemblages produced in the Whitestone Anorthosite formed under retrogressive conditions. Moderately modified anorthosite, scapolite-bearing planar shear zones and scapolite-bearing mylonites display a mineral assemblage of plagioclase (An₃₄₋₆₀), pargasite, scapolite (Me₆₈₋₇₅), and almandine garnet which suggests middle-upper amphibolite facies conditions of metamorphism. The anorthosites display small chemical modifications compared to the undeformed

Whitestone Anorthosite; CO_2 is the most prominently enhanced component. Weakly modified anorthosite, quartz-bearing anastomosing shear zones and quartz-bearing mylonites consist of plagioclase (An 20-47), hornblende/pargasite, scapolite (Me 57-65) and epidote or almandine garnet which suggest middle-lower amphibolite facies. The anorthosites display significant chemical modifications compared to the undeformed anorthosite; SiO_2 and K_2O are the most dramatically increased components.

Under amphibolite and higher metamorphic conditions, plagioclase in the increasingly modified anorthosites underwent syntectonic recrystallization which produced non-random crystallographic orientation patterns. Quartz, present in ribbons in quartz-rich mylonites and anastomosing shear zones, deformed by dislocation creep resulting in the development of two different preferred crystallographic orientations. Isolated quartz and recrystallized plagioclase in the matrix deformed by grain boundary processes which produced random crystal orientations.

The textural and mineralogical characteristics of the Whitestone Anorthosite in the Parry Sound Shear Zone suggest a history of deformation that extended from granulite facies to lower amphibolite facies conditions. The observed sequence of chemical modifications suggests an evolutionary fluid history resulting from the inverted

metamorphic gradient of an overthrust. The different orientation patterns observed in quartz grains within quartz ribbons suggest the occurrence of different regimes during the latest stages of deformation. The reported zircon U-Pb ages of syn-, and late-tectonic pegmatites indicates this progressive deformation occurred from about 1160 Ma to at least 1120.

ACKNOWLEDGEMENTS

I wish to express my gratitude to Dr. John Starkey of the University of Western Ontario for the advise and guidance he provided to me during the preparation of this thesis. I acknowledge his sincere attitude that made my stay at Western worthwhile.

I wish to thank Dr. W.R. Church and Dr. T. Davidson for their valuable comments and suggestions on several aspects of my thesis.

Special thanks are due to Dr. C.T. Wu for helping me with my chemical analyses, and R. Barnett for introducing me to the electron microprobe. Thanks are also due to K. Cunnison, A. McNeill for their comments about the thesis, to Y. Dilek, S. Talman, G. Albino, D. Dillon, E. Prosh, S. Simigian and W. Stone for their friendship, support and assistance during difficult times. John Forth and Walt Harley prepared thin and probe sections, they are thanked for their contribution.

Finally, I am very much indebted to Ozan Sungurlu of Turkish Oil Company, Dr. Yucel Yilmaz of Istanbul Technical University and M. Brian Bayly of Rensselaer Polytechnic Institute for their contribution to my basic knowledge in geology.

This study was supported by the grants from the Geological Survey of Turkey and the Natural Sciences and Engineering Research Council of Canada to Dr. J. Starkey.

TABLE OF CONTENTS

	Page
CERTIFICATE OF EXAMINATION	ii
ABSTRACT	iii
ACKNOWLEDGEMENTS	vi
TABLE OF CONTENTS	viii
LIST OF PHOTOGRAPHIC PLATES	xii
LIST OF TABLES	xiii
LIST OF FIGURES	xv
CHAPTER 1 - INTRODUCTION	1
1.1 Purpose and Scope	1
1.2 Location and Access	2
CHAPTER 2 - PREVIOUS WORK	4
2.1 Tectonic Framework	4
2.2 Parry Sound Shear Zone	10
2.3 Whitestone Anorthosite	11
CHAPTER 3 - DEFORMATION OF THE WHITESTONE ANORTHOSITE IN THE PARRY SOUND SHEAR ZONE.....	24
3.1 General Statement	24
3.2 Profiles of the Whitestone Anorthosite	
at the Intersection with the Parry Sound Shear Zone	24

3.3 Composite cross-section of the Whitestone Anorthosite.....	
at the Intersection with the Parry Sound Shear Zone	43
3.4 Principal Features of the Whitestone Anorthosite.....	
at the Intersection with the Parry Sound Shear Zone	46
3.4.1 Deformed Anorthosite	46
3.4.1.1 Weakly Modified Anorthosite	46
3.4.1.2 Moderately Modified Anorthosite	47
3.4.1.3 Strongly Modified Anorthosite	48
3.4.1.4 Mylonites	48
3.4.2 Local Shear Zones	54
3.4.2.1 Anastomosing Shear Zones	54
3.4.2.2 Planar Shear Zones	60
3.5 Summary	64

CHAPTER 4 - MINERAL ASSEMBLAGES OF THE WHITESTONE ANORTHOSITE ...	
IN THE PARRY SOUND SHEAR ZONE	67
4.1 General Statement	67
4.2 Increasingly Modified Anorthosites	68
4.2.1 Original Anorthosite	68
4.2.2 Weakly Modified Anorthosite	71
4.2.3 Moderately Modified Anorthosite	74
4.2.4 Strongly Modified Anorthosite	77
4.2.5 Mylonites	79
4.3 Local shear zones	94
4.3.1 Anastomosing Shear Zones	94
4.3.2 Planar shear zones	96
4.4 Summary	102

CHAPTER 5 - GEOCHEMISTRY OF THE WHITESTONE ANORTHOSITE	
AT THE INTERSECTION WITH THE PARRY SOUND SHEAR ZONE	112
5.1 General Statement	112
5.2 Analytical Methods	112
5.3 Results	115
5.3.1 Deformed Anorthosite	116
5.3.2 Local Shear Zones	137
5.5 Summary	171
CHAPTER 6 - QUARTZ AND PLAGIOCLASE FELDSPAR FABRICS IN.....	
THE WHITESTONE ANORTHOSITE	173
6.1 General Statement	173
6.2 Method	173
6.3 Results	174
6.3.1 Quartz Fabric	174
6.3.2 Feldspar Fabric	183
6.4 Summary	187
CHAPTER 7 - DISCUSSION: RESULTS AND GEOLOGICAL IMPLICATIONS ...	199
7.1 Intracrystalline Deformation	199
7.2 Kinematic History	203
7.3 Tectonic Evolution	204
7.4 Fluid Evolution	210
CHAPTER 8 - CONCLUSIONS	214

APPENDIX A - SAMPLE LOCATIONS	216
APPENDIX B - CALCULATIONS OF SHEAR STRAINS AND DISPLACEMENTS ..	218
APPENDIX C - ELECTRON MICROPROBE ANALYSES	219
APPENDIX D - GEOCHEMICAL ANALYSES	248
APPENDIX E - ORIENTATION DATA	255
REFERENCES	259
VITA	268

LIST OF PLATES

Plate	Description	Page
3-1	Photographs of the progressively modified anorthosite.	50
3-2	Photograph and photomicrographs mylonites.	53
3-3	Photographs of local shear zones.	66
4-1	Photomicrographs of plagioclase.	105
4-2	Photomicrographs of amphibole garnet and scapolite.	107
4-3	Photomicrographs of epidote, muscovite, microcline and quartz.	109
4-4	Photomicrographs of oxides and sulphides.	111

LIST OF TABLES

Table	Description	Page
2-1	Modal analyses of the marginal anorthosite.	14
2-2	Average chemical and modal compositions of the Whitestone Anorthosite.	19
4-1	Analysis of a primary pyroxene from the unmodified Whitestone Anorthosite.	70
4-2	Chemical analyses and mean grain sizes of plagioclase grains in the Whitestone Anorthosite sampled across the Parry Sound Shear Zone.	83
4-3	Chemical analyses and mean grain sizes of amphibole grains in the Whitestone Anorthosite sampled across the Parry Sound Shear Zone.	85
4-4	Analyses of scapolite in the Whitestone Anorthosite sampled across the Parry Sound Shear Zone.	91
4-5	Analyses of garnet in the Whitestone Anorthosite sampled across the Parry Sound Shear Zone.	93
4-6	Chemical analyses and mean grain sizes of plagioclase grains from a planar shear zone and an anastomosing shear zone.	99
4-7	Analyses of scapolite from a planar shear zone.	101
5-1	Abundances of major elements expressed as oxides in increasingly modified Whitestone Anorthosite in the Parry Sound Shear Zone.	119
5-2	Compositional changes in increasingly modified Whitestone Anorthosite in the Parry Sound Shear Zone.	124

5-3	Oxidation state of iron in increasingly modified Whitestone Anorthosite in the Parry Sound Shear Zone.	133
5-4	Abundances of major elements, expressed as oxides, in samples from an anastomosing shear zone.	140
5-5	Compositional changes associated with an anastomosing shear zone.	155
5-6	Oxidation state of iron in an anastomosing shear zone.	159
5-7	Abundances of major elements, expressed as oxides, in samples from a planar shear zone.	164
5-8	Compositional changes associated with a planar shear zone.	168
5-9	Oxidation state of iron in a planar shear zone.	170

LIST OF FIGURES

Figure	Description	Page
2-1	Simplified geologic map of the Central Gneiss Belt near Parry Sound.	6
	Y-Y of Figure 1-1, showing the tectonic features of the central part of the Central Gneiss Belt.	9
3-1	Modal mineral distributions in the Whitestone Anorthosite.	16
3-1	Location map of the Whitestone Anorthosite and the cross-cutting Parry Sound Shear Zone.	26
3-2	Schematic cross-section of the Whitestone Anorthosite along traverse I.	30
3-3	Outcrop areas along traverse II.	33
3-4	a) Anorthositic metagabbro at outcrop area A traverse II; b) Stereographic projection of 89 foliation poles and lineations from outcrop area A.	35
3-5	Schematic cross-section of the Whitestone Anorthosite along the section of (X-Y-Z) of Figure 3-3.	37
3-6	Anorthositic metagabbro lens in mylonite. section line of Figure 3-7 marked (X-Y).	40
3-7	Schematic cross-section of the Whitestone Anorthosite along the section line (X-Y) of Figure 3-6.	42
3-8	Composite cross-section of the progressively modified Whitestone Anorthosite across the Parry Sound Shear Zone.	45

3-9	a) Diagram showing progressive rotation of the schistosity in a shear zone.	
	b) Diagram showing the angles between the orientation of the schistosity and the shear zone boundary at locations 1 & 2 in Figure 3-9a.	56
3-10	Shear strain-distance curves derived from geometric analyses of schistosity across two anastomosing shear zones.	59
3-11	Variation of shear strain across two planar shear zones.	63
4-1	The (^{vi}Al):(^{iv}Al) ratio and the (100 Na/Ca+Na):(100 Al/Si+Al) ratio in amphiboles from progressively modified anorthosite in the Parry Sound Shear Zone.	87
4-2	The (Al+Fe+Ti):(^{iv}Al) ratio and the (100 Na/Ca+Na):(100 Al/Si+Al) in amphiboles from the progressively modified Whitestone Anorthosite, compared with data from various occurrences of mafic schists in the world.	89
5-1	Component ratio diagram for modified anorthosite from the Parry Sound Shear Zone.	121
5-2	Composition-volume diagram showing the transformation of unmodified anorthosite (PS-85-17) to weakly modified anorthosite	125
5-3	Composition-volume diagram showing the transformation of unmodified anorthosite (PS-85-17) to moderately modified anorthosite (PS-85-2).	127
5-4	a&b Composition-volume diagram showing the transformation of moderately modified anorthosite (PS-85-2) to type I mylonite (PS-85-5).	129
5-5	Composition-volume diagram showing the transformation of moderately modified anorthosite (PS-85-2) to type II mylonite	

	(PS-85-4).	132
5-6	Block-diagram of an anastomosing shear zone in weakly modified anorthosite indicating the locations of analyzed samples across the Parry Sound shear zone.	142
5-7	Component ratio diagram for specimens from an anastomosing shear zone.	144
5-8	Composition-volume diagram showing the transformation of weakly modified anorthosite (PS-85-7) to weakly modified anorthosite near an anastomosing shear zone (PS-85-7a).	147
5-9 a&b	Composition-volume diagram showing the transformation of weakly modified anorthosite near the anastomosing shear zone (PS-85-7a) to anorthosite at less deformed edge of the shear zone (PS-85-7b).	149
5-10	Composition-volume diagram showing the transformation of anorthosite from the less deformed edge of the anastomosing shear zone (PS-85-7b) to the strongly deformed center of the shear zone (PS-85-7c).	152
5-11	Compositional variation of the Whitestone anorthosite across an anastomosing shear zone.	157
5-12	Block-diagram of a planar shear zone in moderately modified anorthosite indicating the locations of analyzed samples.	162
5-13	Composition-volume diagram showing the transformation of moderately modified anorthosite (PS-85-2) to the strongly deformed center of a planar shear zone (PS-85-2b).	166
6-1	Quartz c-axis orientation patterns in type II mylonite.	177

6-2	Quartz c-axis orientation patterns in anastomosing shear zones.	180
6-3	The distribution of the poles to 1011 of quartz in anastomosing shear zone specimen PS-85-16 and type II mylonite specimen PS-85-12.	182
6-4	Orientation diagrams of the optical directions X, Y and Z of plagioclase grains from weakly modified anorthosite specimen PS-85-7.	186
6-5	Orientation diagrams of the optical directions X, Y and Z of plagioclase grains from moderately modified anorthosite specimen PS-85-2.	188
6-6	Orientation diagrams of the optical directions X, Y and Z of plagioclase grains from strongly modified anorthosite specimen PS-86-14.	190
6-7	Orientation diagrams of the optical directions X, Y and Z of plagioclase grains in type I mylonite specimen PS-86-5.	192
6-8	Orientation diagrams of the optical directions X, Y and Z of plagioclase grains in type II mylonite specimen PS-86-4.	194
6-9	Orientation diagrams of the optical directions X, Y and Z of plagioclase grains in the strongly deformed center of a planar shear zone (specimen PS-85-2b).	196
7-1	Kinematic model for the Whitestone Anorthosite.	207

CHAPTER 1

INTRODUCTION

1.1 PURPOSE AND SCOPE

Current models for shear zones in the earth's crust place them in two principal domains: a shallow brittle domain and a deep ductile domain. Stick-slip behavior characterizes the former, and plastic flow dominates the latter (Sibson, 1977). A transition zone occurs between the two domains. The Parry Sound Shear Zone, in which the present study area is located, is a ductile shear zone.

There are a number of published studies of the structures and deformation processes in the deep ductile domain (e.g. Wilson, 1975; Kerrich et al., 1977; Ramsay and Allison, 1979; Ramsay, 1980; Beach, 1980; Borges and White, 1980; Jensen and Starkey, 1985; Platt and Behrmann, 1986; Segall and Simpson, 1986; Sinha et al., 1986; Law, 1986; Vauchez, 1987). Although some of these studies investigate the significance of the structures or processes in relation to the progression of deformation across the shear zone (e.g. Ramsay, 1979; Beach, 1980; Jensen and Starkey, 1985; Sinha et al., 1986; Law, 1986), few consider the implications of different stages of deformation within the shear zone in terms of a complex

history of regional deformation. The purpose of this thesis is to study the deformation and metamorphism of the Whitestone Anorthosite where it is intersected by the Parry Sound Shear Zone, and to attempt to relate these to the regional tectonics.

The analysis presented here is threefold: first, the significance of observed progressive textural, structural, and mineralogical changes associated with the shear zone is investigated; second, the relation of rock chemistry to deformation is examined; third, the fabrics of two major rock forming minerals are studied. On the basis of the results of these studies, a model for the kinematic history of the Parry Sound Shear Zone is proposed.

1.2 LOCATION AND ACCESS

The study area is located near Parry Sound on Georgian Bay, Lake Huron, in the Grenville Province of the Canadian Shield. It includes a major tectonic discontinuity, the Parry Sound Shear Zone which contains a variety of deformed rocks including large bodies of anorthosites. One of these, the Whitestone Anorthosite, is intersected by the Parry Sound Shear Zone, and is the subject of this study.

Access to the area south-west of Parry Sound is provided by local roads branching off highway 69B.

Locations north-east of Parry Sound are reached by roads branching off highway 124. Exposure is generally good.

CHAPTER 2

PREVIOUS WORK

2.1 TECTONIC FRAMEWORK

The detailed geology of the Parry Sound area was virtually unknown prior to 1981. Quirke (1930) and Hewitt (1967) had recognized the presence of different rock units in the region, and Wynne-Edwards (1972) had reported the occurrence of metamorphic domains. However, there was little explanation of the regional distribution of these units. This was probably in part due to the poor prospect of economically important mineralization in the area.

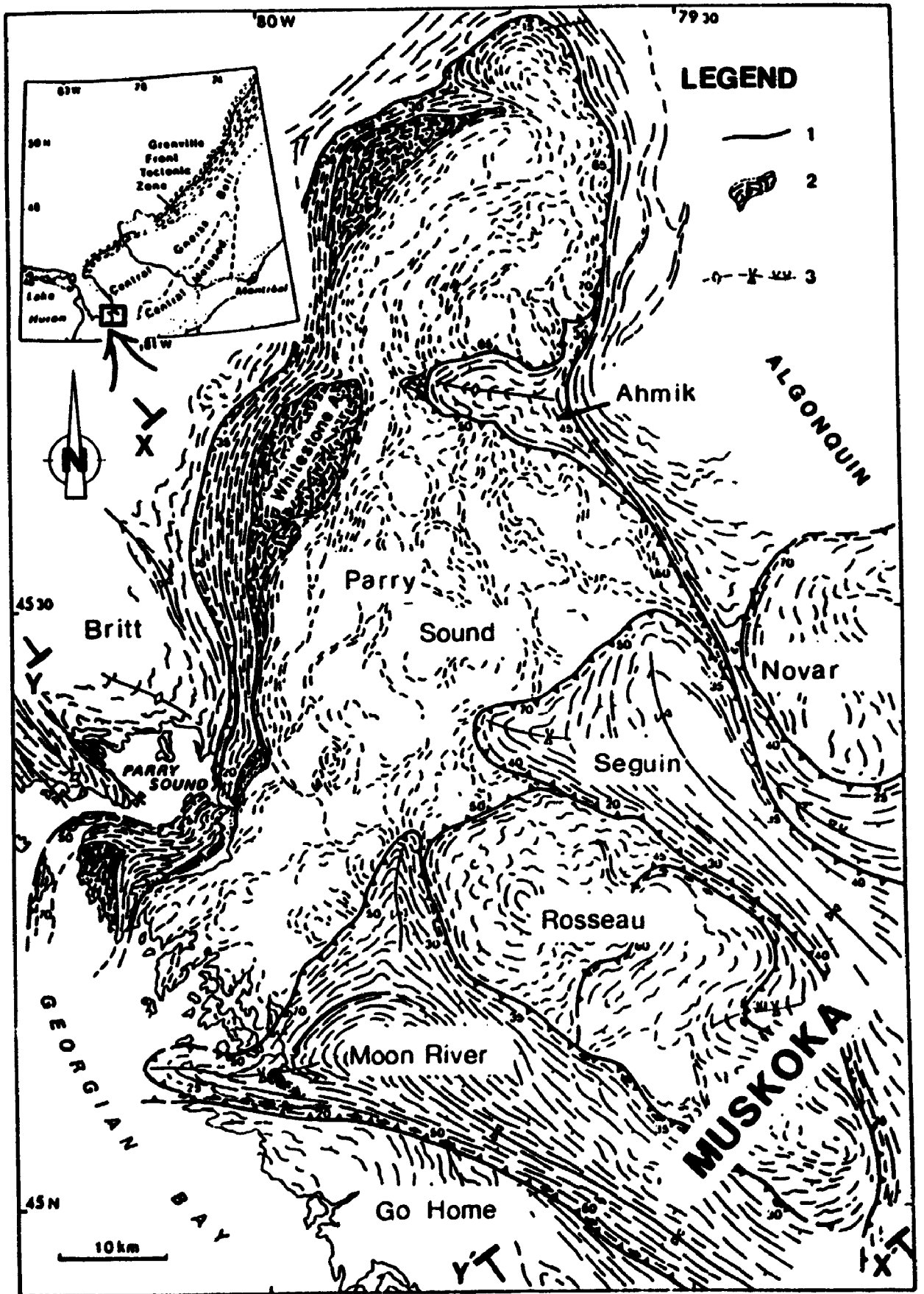
Davidson and Morgan (1981) presented the first evidence for the complex geology of the Parry Sound area. They suggested the occurrence of several structural domains and subdomains on the basis of distinctive tectonic characteristics (Fig. 2-1). The major domains are the Britt, Parry Sound, Muskoka and Algonquin. The Muskoka Domain is, in turn, subdivided into the Seguin, Rosseau, Moon River and Go Home Subdomains.

The Britt Domain is a highly metamorphosed terrain, composed of ortho- and paragneisses and migmatites. The metamorphic grade ranges from middle to upper amphibolite facies (Davidson and Morgan, 1981).

Figure 2-1. Simplified geologic map of the Central Gneiss Belt near Parry Sound (Reproduced from Davidson, 1982b). X-X' and Y-Y' indicate the lines of the cross-sections of Fig 2-2. Inset map shows the geographical location of the Parry Sound area.

LEGEND:

- 1: domain boundary with dips indicated;
- 2: anorthosite, related gabbro and equivalent gneiss;
- 3: antiform, synform, overturned synform.



The Parry Sound Domain is a northeasterly trending terrain, which occurs above the Britt Domain. It is dominated by mafic rocks, spatially discontinuous mafic gneisses and large, lens-shaped gabbroic anorthosite bodies. The metamorphic grade ranges from amphibolite to granulite facies (Davidson and Morgan, 1981).

The Muskoka Domain lies to the east of the Parry Sound Domain. It comprises northwest trending belts of amphibolite facies gneisses and rocks of higher metamorphic grade which exhibit less regular structural trends. The Algonquin Domain lies still further east.

Zones of highly deformed rocks occur along the margins of these domains. Gneisses, migmatites and mylonites occur at the boundary of the Britt Domain with the Grenville Front to the west (Stockwell et al., 1970; Wynne-Edwards, 1972; La Tour, 1979). Tectonized gneisses and mylonites occur at the boundary between the Parry Sound and Britt Domains and mylonites are located at the southern boundary of the Parry Sound Domain with neighboring subdomains. Each of these domains is interpreted as an allochthonous crustal segment in a wide orogenic belt analogous to the Himalayas (Davidson et al., 1982a). Generalized cross-sections through this area are shown in Fig. 2-2.

Figure 2-2. Schematic geologic cross-sections along X-X' and Y-Y' of Figure 2-1, showing the tectonic features of the central part of the Central Gneiss Belt. The stipple indicates the location of the Whitestone Anorthosite.

BD : Britt Domain

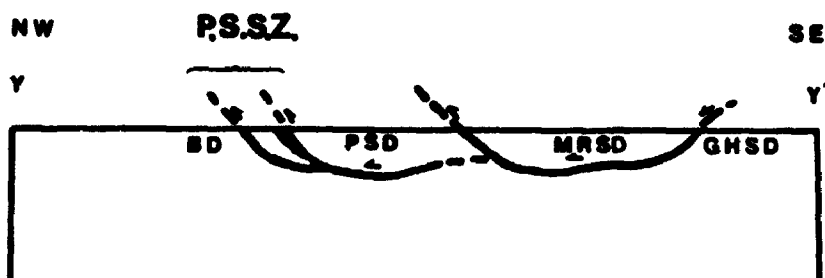
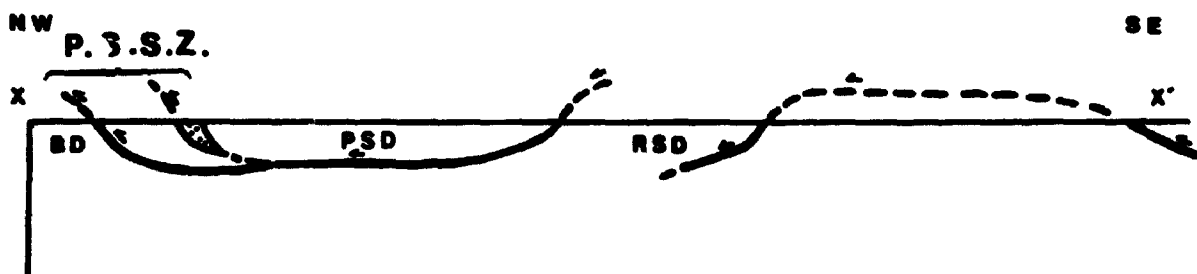
PSSZ : Parry Sound shear zone

PSD : Parry Sound Domain

RSD : Rosseau Subdomain

MRS : Moon River Subdomain

GHSD : Go Home Subdomain



Scale: 0 10km

2.2 PARRY SOUND SHEAR ZONE

A highly deformed zone occurs at the northern boundary of the Parry Sound Domain and is marked by the presence of mylonites, highly tectonized rocks and amphibolites. It occurs between the predominantly amphibolite facies quartzo-feldspatic gneisses of the Britt Domain and the granulite facies mafic rocks and migmatites of the overlying Parry Sound Domain. This highly deformed zone has been called the Parry Sound Shear Zone, and interpreted as a large deep-seated tectonic discontinuity (Davidson and Morgan, 1981; Davidson, 1984) (see Fig. 2-2).

North of Parry Sound, the Parry Sound Shear Zone is characterized by pelitic gneisses containing disoriented blocks of metamorphosed anorthosite, metadiorite and amphibolite that outcrop for nearly 30 km along strike (Davidson et al., 1982b). Near Parry Sound, the shear zone is characterized by lithologically distinct tectonites that tend to be continuous laterally for long distances. South of Parry Sound, the shear zone is characterized by migmatites, amphibolites, mylonites, and bands of anorthositic gneisses which continue over long distances (Davidson et al., 1982b). The mafic gneisses which overly the Parry Sound Shear Zone contain large lens-shaped masses of relatively well-preserved gabbroic anorthosites.

The most prominent of these is the Whitestone Anorthosite which occurs at the western margin of the Parry Sound Domain (Davidson et al., 1982b; Davidson, 1984).

2.3 WHITESTONE ANORTHOSITE

The Whitestone Anorthosite is a lens-shaped body, nearly 16 km long and 0.5 to 6 km wide, which occurs in a sequence of metasediments and metavolcanic rocks located along the western margin of the Parry Sound Domain. It is generally a well-preserved igneous mass, but shows evidence of severe deformation at its western margin where it is intersected by the eastern margin of the Parry Sound Shear Zone (see Fig. 2-1) (Davidson and Morgan, 1981).

The Whitestone Anorthosite was first studied by Lacy (1960) near the Dunchurch area. He recognized its dome shape and reported the occurrence of mineralogical and textural changes near its margin. He noted that layered anorthosite, which is typical of the margin, is enriched in scapolite, pyrite and ferro-magnesian minerals. He indicated that scapolite replaced plagioclase, particularly where it was granulated and displayed mortar texture. Lacy presented two modal analyses as representative of the marginal anorthosite (Table 2-1).

21:

Table 2-1 Modal analyses of the marginal anorthosite
(Taken from Lacy, 1960).

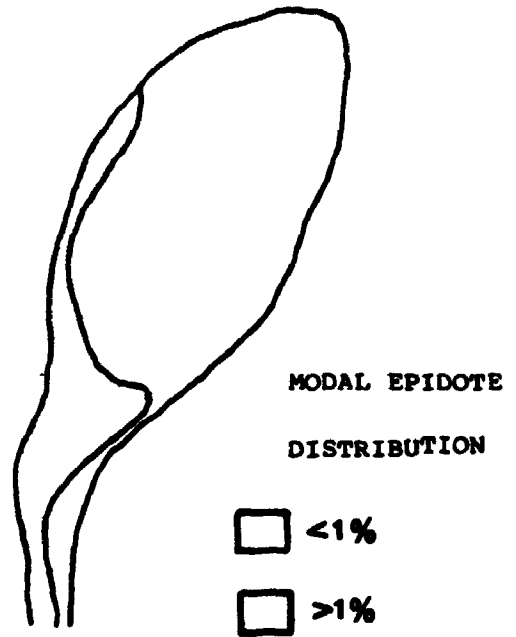
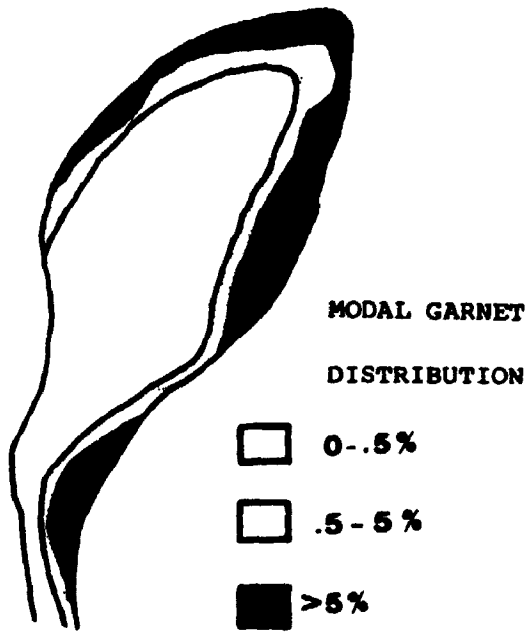
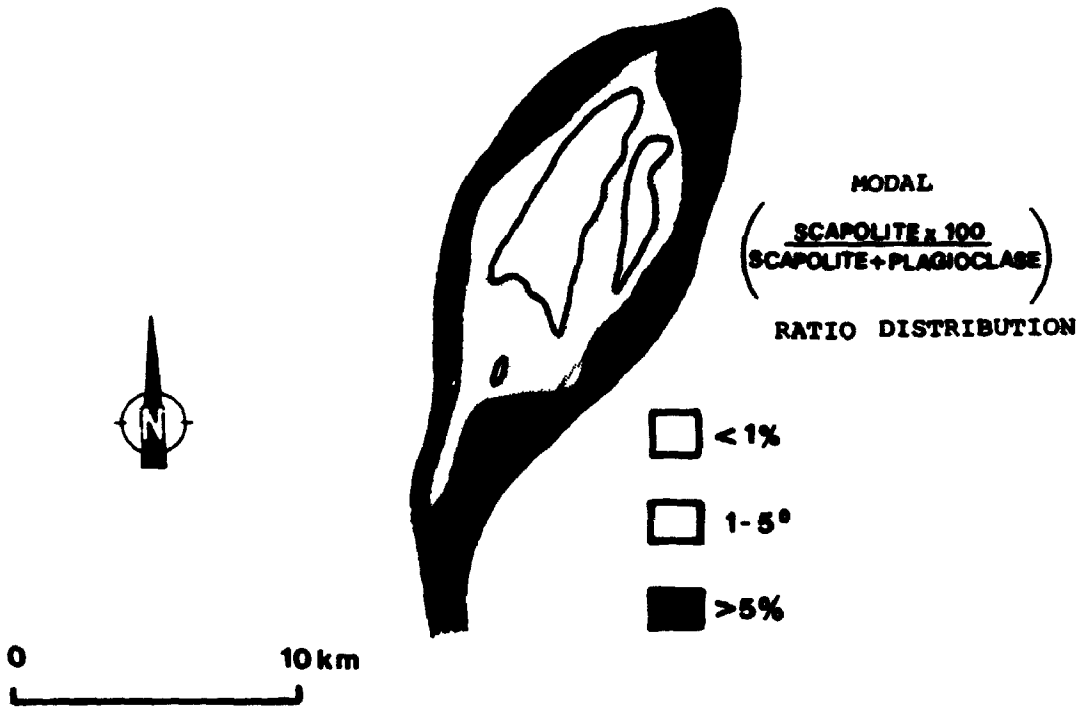
	1	2
Quartz	-	0.5
Plagioclase	83.2 (An56)	69.4 (An54)
Scapolite	13.4 (Me75)	14.5 (Me70)
Hornblende	3.1	9.7
Garnet	0.3	3.8
Titanite	-	1.9

On the basis of mineral assemblages observed in marble lenses in the surrounding metamorphic rocks, Lacy suggested a range of metamorphic conditions from amphibolite to granulite facies, and a retrogressive metamorphism along the eastern margin of the Whitestone Anorthosite. He interpreted the lack of reaction between metasedimentary units and the anorthosite to be evidence of either equilibrium between different rocks or metamorphic conditions not favoring reaction.

The Whitestone Anorthosite was later studied by Mason (1969) who described it as an igneous mass, composed of anorthosite and gabbroic anorthosite. He noted the occurrence of several "primary" facies: e.g. the glomeropoikilitic facies was characterized by a blotchy subhedral distribution of pyroxenes; the porphyritic facies was characterized by a homogeneous distribution of pyroxenes. The "primary" facies were explained by gravitational settling of crystals during slow cooling of the magma.

Mason reported the occurrence of chemical and mineralogical changes from the central core of the anorthosite toward the margin, and suggested that there are two different marginal subfacies (Fig. 2-3). One, an epidote-bearing marginal facies along the western margin in which garnet is a minor constituent or restricted to a narrow zone. The second, a garnet bearing marginal facies

Figure 2-3. Modal mineral distributions in the Whitestone Anorthosite (Reproduced from Mason, 1969).



along the eastern margin where epidote is minor. The mineralogical and compositional changes were attributed to alteration during late stage magmatic activity (Mason, 1969). Mason presented mineralogical and chemical data for 360 anorthosite samples and documented a spatial changes in the composition of the Whitestone Anorthosite as follows:

a) the eastern and western margins of the anorthosite display different chemical compositions;

b) the margins are enriched in TiO_2 , Fe_2O_3 , MgO , MnO , P_2O_5 , CO_2 , but depleted in Al_2O_3 , and CaO ;

c) the chemical composition of the southern "tail" of the anorthosite, which is the part with which this study is concerned, is more similar in composition to the eastern margin than to the core. Table 2-2 presents three average compositions of the anorthosite, computed from Mason's data by Thompson (1983). Each composition is based on several analyses from comparable locations within the Whitestone Anorthosite.

A textural and mineralogical study of opaque minerals of the marginal Whitestone Anorthosite at the Dunchurch area was conducted by Kretchmar (1968). He reported the formation of hemo-ilmenite, titanium-poor magnetite, almandine and hornblende during an episode of retrogressive metamorphism. On the basis of analyzed compositions of oxide assemblages observed in the marginal

8
8

Table 2-2 Average chemical compositions of the Whitestone Anorthosite, computed from Mason's chemical analyses by Thompson D.L. (1983). Other refers to apatite, quartz, carbonate, biotite, sphene, serpentine, muscovite and/or orthopyroxene.

	central core	eastern margin	western margin
SiO ₂	52.49	51.78	51.34
TiO ₂	0.19	1.14	0.49
Al ₂ O ₃	27.66	22.24	24.01
Fe ₂ O ₃	0.63	1.52	1.14
FeO	1.03	5.02	3.12
MnO	0.02	0.12	0.07
MgO	0.93	2.17	2.24
CaO	12.08	10.69	11.73
Na ₂ O	3.96	3.60	3.93
K ₂ O	0.47	0.62	0.52
P ₂ O ₅	0.02	0.11	0.04
H ₂ O	0.46	0.49	0.76
CO ₂	0.21	0.56	0.32
S	0.01	0.04	0.02
Cl	0.01	0.01	0.02
H ₂ O ⁻	0.08	0.08	0.08
total	100.25	100.19	99.83
Plg.	91.8	60.3	60.5
Pyx.	4.2	5.5	2.9
Amp.	2.4	11.4	14.6
Scp.	1.6	12.8	15.6
Gt.	tr	6.3	1.0
Ep.	-	-	3.9
Opq.	tr	1.5	0.2
Other	tr	2.2	1.3

anorthosite, he suggested oxygen fugacities between $\text{Fe}_3\text{O}_4 + \text{Fe}_2\text{O}_3$ and $\text{Ni} + \text{NiO}$ buffers. The value of $-\log f\text{O}_2$ was estimated to be 16.5 ± 2.5 for a metamorphic temperature of 700 C.

A petrographic study of coronite amphibolites at the western contact of the Whitestone Anorthosite was carried out by Mummery (1972) who reported that corona development resulted from contact metamorphism by the Whitestone Anorthosite. He suggested that the metamorphic conditions ranged from almandine to the clinopyroxene subfacies of granulite facies.

During a regional mapping program in the Ontario Gneiss segment by the Geological Survey of Canada, the Whitestone Anorthosite was described as a tectonic slice (Davidson and Morgan, 1981; Davidson et al., 1982b). Davidson et al. suggested that if any former intrusive relationship existed along the margin of the Whitestone Anorthosite, it was obliterated during the progressive development of mylonite from the gabbroic anorthosite. The authors also point out that pegmatites were involved at different stages of mylonitization.

In a related study, Nadeau (1984) investigated the deformation of the Mill Lake leucogabbro (anorthositic gabbro) in the southern extension of the Whitestone Anorthosite. He described it as a lenticular-shaped tectonic slice composed dominantly of leucogabbro and

gabbroic anorthosite, and, locally, quartz-bearing Fe-Ti rich rocks. He suggested that the lack of coherent internal structure and a uniform composition in the body could be attributed to the occurrence of several "syn-consolidational magma injections". The following conclusions in Nadeau's work bear on this study:

a) the amphibolite facies assemblage of the deformed Whitestone Anorthosite is $An_{(38-48)}$, hornblende, scapolite, garnet, biotite, epidote and titanite. Nadeau considered scapolite to be post-deformational, but presented no opinion about the significance of epidote distribution in the deformed rocks;

b) two tectonically distinct units are present in the southern extension of the Whitestone Anorthosite in which the present study area lies: Unit 16, massive, very slightly strained to moderately strained leuco-gabbro which retains primary structures, and Unit 17, highly strained equivalents of the rocks of unit 16 and gneissic and mylonitic quartz ferro-diorite, which was described as a fine to very fine grained rock with impure quartz veins. The intimate association of quartz ferro-dioritic and leucogabbroic rocks within the highly strained Unit 17 was considered to be the result of either tectonic mixing of originally distinct rock masses or a primary relationship. Observed large quartz grains were interpreted to be of primary origin. The occurrence of 10% quartz in some

meta-anorthositic rocks was assumed to have resulted from the break down of clinopyroxene;

c) the transformation from slightly strained (gneissic) to highly strained (mylonitic) meta-leucogabbro was essentially isovolumetric and isochemical.

Thompson (1983) investigated the eastern margin of the Whitestone Anorthosite where the anorthosite and country rocks have been subjected to granulite facies conditions. He described the outer margin of the Anorthosite as strongly deformed and metasomatized, and suggested that this was the result of mechanical mixing and absorption of mobile components (volatiles from the surrounding gneisses). During this process a reaction aureole formed in the country rocks. He suggested that the temperature of equilibrium was approximately 750 ± 70 C and speculated that it was 80 C higher than that of the western margin.

The nature of the tectonic slices recognized by Davidson et al. (1982a) has been disputed by Schwerdtner (1987). Based on an analysis of folding and gneissosity in the south-western Grenville Province, Schwerdtner has suggested that the tectonic units are bounded by low angle shear zones along which there has been later sinistral shear. He indicated that there is no necessity to assume large translations of crustal slices and proposed a

tectonic scenario in which discordances in regional gneissosity were accomplished by repeated folding.

The U-Pb zircon dating of the Whitestone Anorthosite and its mylonitized derivatives was carried out by van Breemen et al. (1986), who reported a crystallization age of 1350 ± 50 Ma for the southern extension of the Whitestone Anorthosite and a metamorphic age of 1160 Ma for sheared pegmatites in the mylonites. The dating of coronitic metagabbro bodies between the Parry Sound Domain and the Central Metasedimentary Belt Boundary Zone yielded metamorphic ages from 1060 Ma to 1030 Ma (van Breemen and Davidson, 1988). The authors suggested that this Grenvillian age for metamorphism coincides with tectonic displacement along the Central Metasedimentary Belt boundary zone, which occurred between 1020-1070 Ma.

In summary, previous studies have shown that the Whitestone Anorthosite displays, in the central part, the characteristic features of an igneous body. However, along the margins, it displays metamorphic/metasomatic assemblages and associated deformational structures. These features suggest that the Whitestone Anorthosite is bounded on both sides by tectonic contacts related to post-intrusion tectonic events dated about 1160 Ma.

CHAPTER 3

DEFORMATION OF THE WHITESTONE ANORTHOSITE IN THE PARRY SOUND SHEAR ZONE

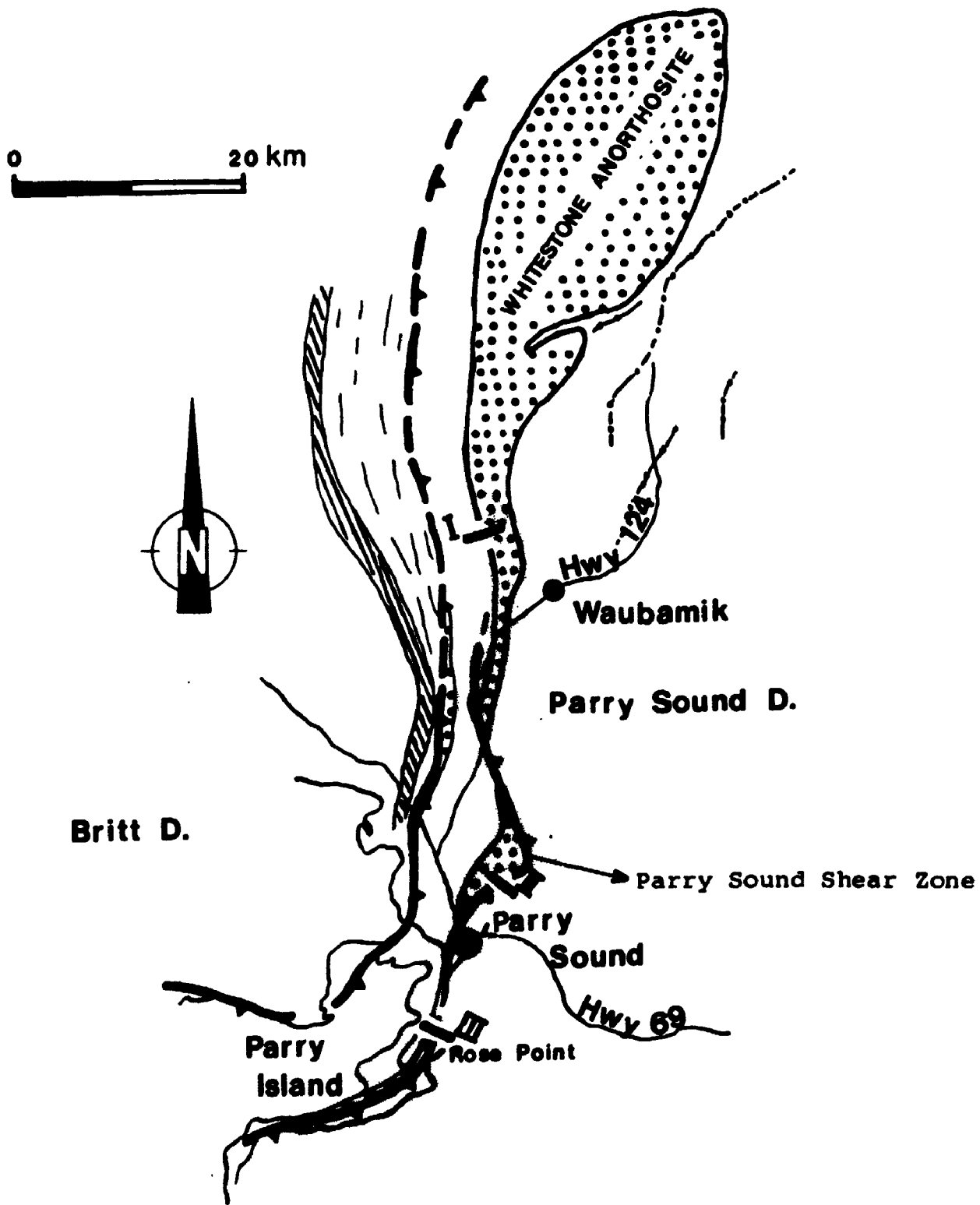
3.1 GENERAL STATEMENT

The Parry Sound Shear Zone transects the Whitestone Anorthosite, and produces progressive modification of the original anorthosite.

3.2 PROFILES OF THE WHITESTONE ANORTHOSITE AT THE INTERSECTION WITH THE PARRY SOUND SHEAR ZONE

Three traverses were made across the contact between the Parry Sound Shear Zone and the Whitestone Anorthosite. Traverse locations are shown in Figure 3-1, and each traverse is represented schematically and with specimen locations in Figures 3-2, 3-5, and 3-7. Traverse I is along a roadcut 3 km northwest of the village of Waubambik; the rocks exposed here provide a profile of the deformation across the western margin of the Whitestone Anorthosite where it is intersected by the Parry Sound Shear Zone. The next two traverses are within the shear zone. Traverse II is at a sand pit 2 km north of Parry Sound where garnet-rich porphyroblastic anorthosite, and its mylonitic derivatives are exposed. Traverse III is at

Figure 3-1 Location map of the Whitestone Anorthosite (solid circles) and the cross-cutting Parry Sound shear zone (lightly stippled area). The cross-sections studied in this thesis are indicated by roman numerals.



the Rose Point Marina, southeast of Parry Sound where similar rocks to those in traverse II are present.

Anorthositic gabbro occurs as a source material in all three traverses (Davidson et al., 1982b). Davidson et al. suggest that the mylonite protolith along traverse II is "foliated meta-anorthositic gabbro the same as that seen at the west end of the outcrop at stop 5" (traverse I). Further, the group of outcrops in traverse II is described as a superb illustration of "the progressive development of mylonite from anorthositic gabbro at several scales". Davidson et al. suggest that traverse III is "in the same mylonite zone that was examined at stop 6" (traverse II) and that "the mylonite lies structurally below and above a lens of anorthositic metagabbro identical to that at the last stop" (traverse II).

The similarity of the rocks exposed in these three traverses, and the progressive deformation which is apparent both from traverse to traverse and within each traverse, provides an opportunity to study the modifications which have occurred in the Whitestone Anorthosite in response to the deformation associated with the Parry Sound Shear Zone.

Traverse I is a 50-60 meter long roadcut at the western margin of the Whitestone Anorthosite. A characteristic feature of this traverse is the increasing state of deformation from rock with observable igneous

texture to fine grained mylonite which bears no textural resemblance to its source material.

Near the east end of the traverse, exposures display anastomosing shear zones in a relatively undeformed gabbroic anorthosite. In the central part of the traverse, sheared pegmatites are present in apparently more deformed anorthositic rocks. From here to the west end of the traverse, anorthositic gabbros occur with apparent deformation increasing to the west. Pegmatites are again observed in mylonites near the west end of the traverse.

Along this traverse, clinopyroxene occurs only in the least deformed rocks. Hornblende occurs either as aggregates or rims around altered edges of clinopyroxene. Plagioclase is recrystallized, but some original grains are present in less deformed rocks. Scapolite, epidote, biotite, and muscovite are present in small quantities (<3%) throughout, but they are more abundant (up to 5%) along the edges of local shear zones. Chlorite was observed along the edge of an anastomosing shear zone. Quartz and microcline are restricted to the central part of local shear zones. Garnet is present only in strongly deformed metagabbros at the west end of the traverse.

Traverse II crosses the eastern margin of the Parry Sound Shear Zone, and its location is indicated in Figures 3-3 and 3-4(a). Along this traverse the parent rock is anorthositic gabbro, similar to that in the western end of

67
81

Figure 3-2. Schematic cross-section of the Whitestone Anorthosite along traverse I.

1	PS-85-17	6	PS-85-10
2	PS-85-7, 7a, 7b, 7c	7	PS-85-6
3	PS-85-8, 8a, 8b	8	PS-86-14
4	PS-85-9	9	PS-86-15
5	PS-85-19	10	PS-86-23

TRAVERSE I

strongly modified anorthosite + weakly modified anorthosite + strong mod. anorth. + weakly modified anorthosite + original anorthosite
 + + + + +




NNW

SSE



Appx. scale: 0 10 m

legend:

-  anastomosing shear zones
-  feldspar augen
-  locations of samples referenced in this thesis

traverse I. The anorthositic gabbro occurs as a lens, and displays some relict texture although it is extensively folded and sheared as shown in the exposure illustrated in Figure 3-4(a). There is a well-developed, northwest-trending lineation defined by a preferred shape orientation of mafic grains and fold hinges. Figure 3-4(b) illustrates the orientation of the foliation and the lineation from this exposure. Mylonites derived from this gabbro occur above it and the contact is folded. There are progressive changes in the metagabbro toward the mylonite.

Two types of mylonites are present in area B, Figure 3-3. Those close to area A contain scapolite, plagioclase, amphibole and garnet while close to area C, the mylonites contain plagioclase, amphibole, garnet, disseminated quartz and K-feldspar augen. The latter shows complex isoclinal folds which suggest extreme ductility during their development.

A second lens of anorthositic meta-gabbro lies to the east, area C in Figure 3-3. The meta-gabbro is generally more deformed than that in area A, although there are pockets of less deformed anorthosite. The exposures illustrated in Figures 3-3 and 3-4(a) are combined in a schematic cross-section in Figure 3-5 on which the locations of specimens studied in this thesis are located.

Traverse III transects the southernmost extension of the Whitestone Anorthosite (Fig. 3-1). The anorthositic

Figure 3-3. Outcrop areas along traverse II. Area A is shown in more detail in Fig. 3-5 (Taken from Nadeau, 1984).

samples:

4 PS-86-5

5 PS-86-4

6 PS-86-2

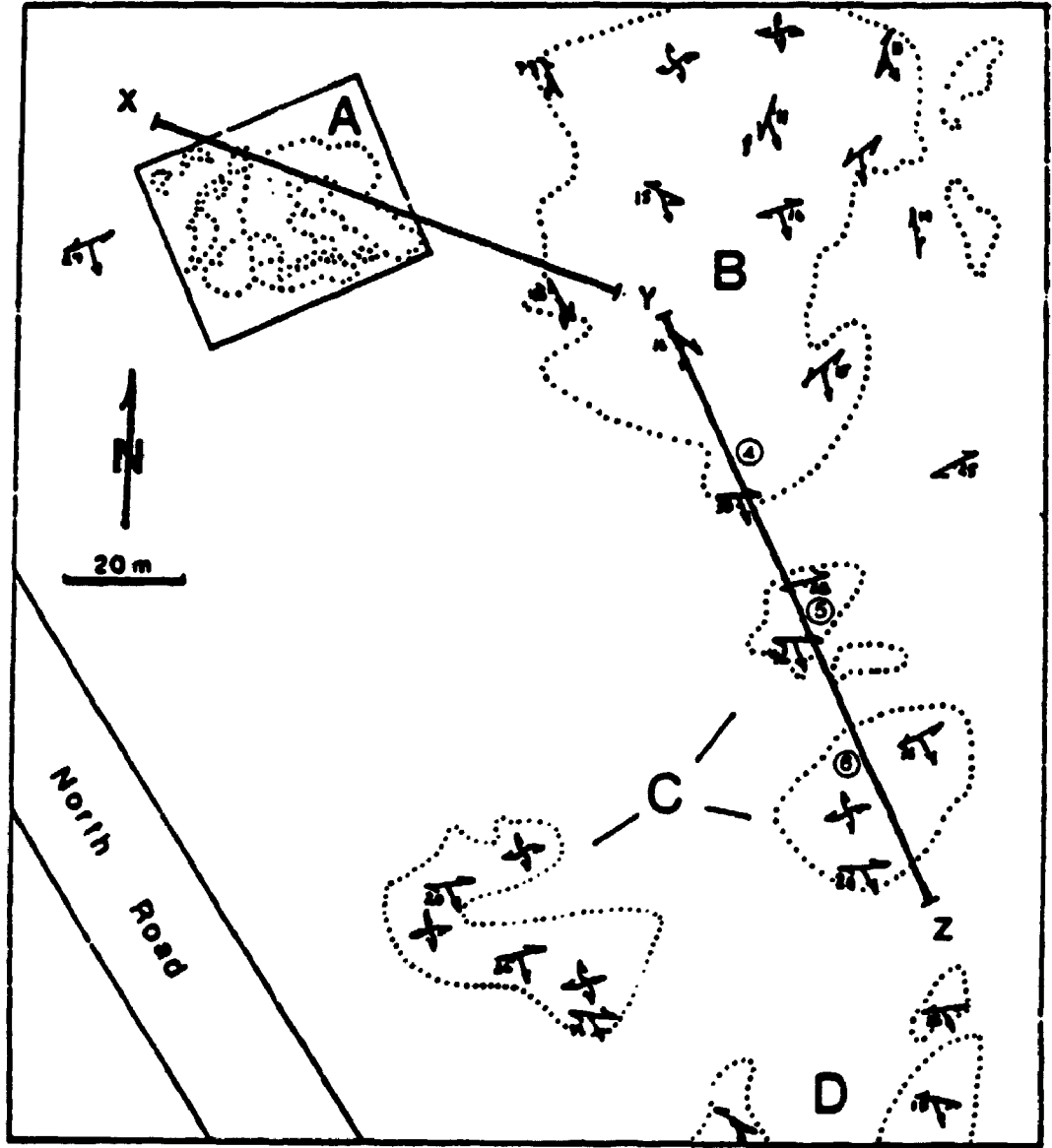
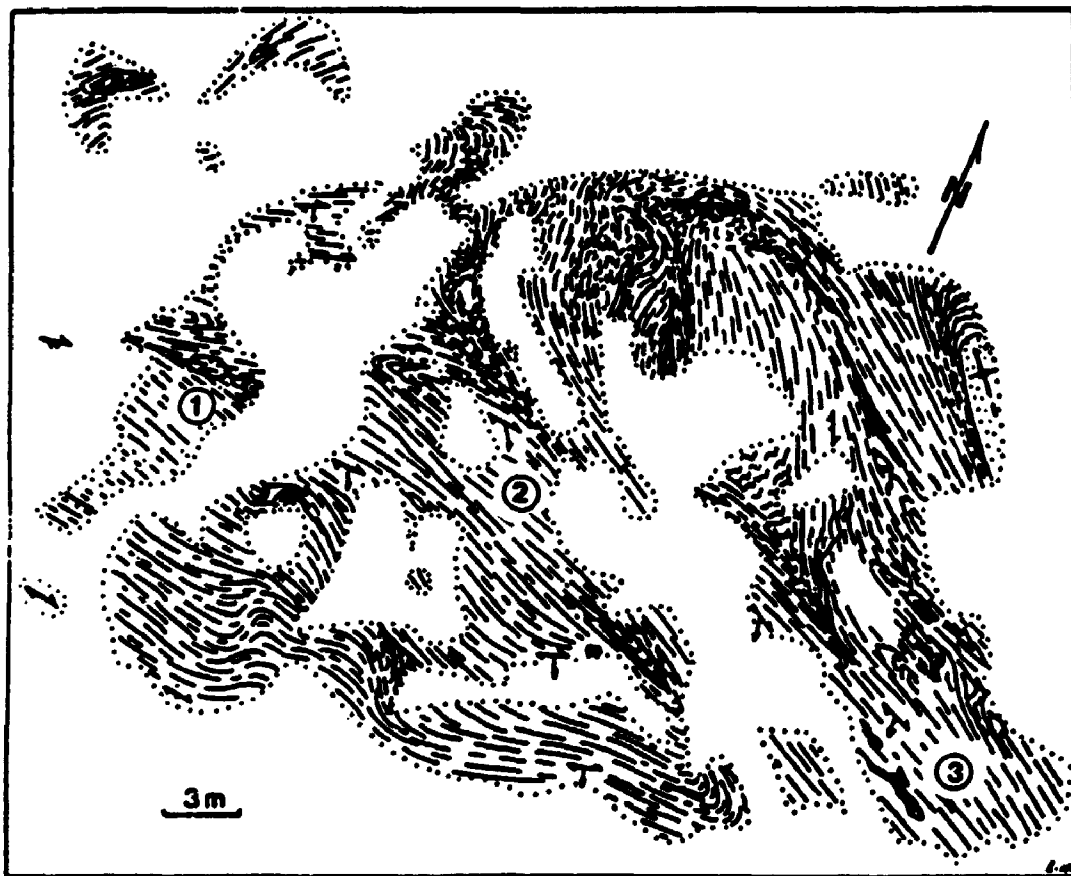


Figure 3-4. a) Anorthositic metagabbro at outcrop area A,
traverse II;

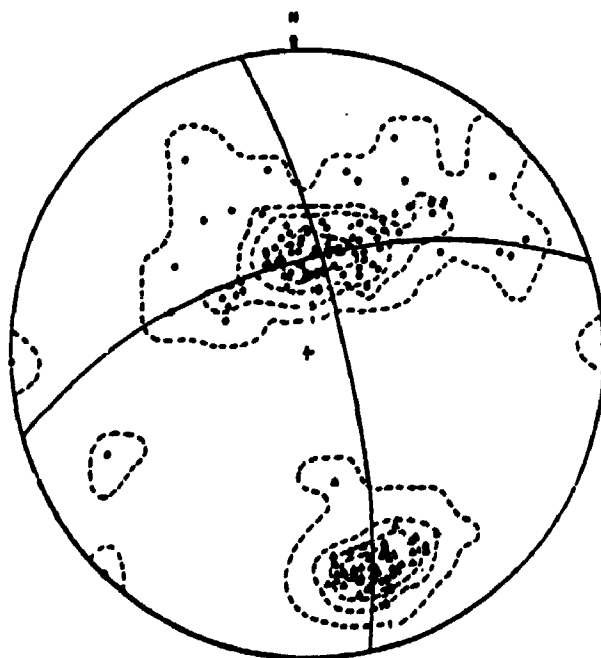
samples:

1: PS-85-1; 2: PS-85-2; 3: PS-85-18

b) Stereographic projection of 89 foliation poles (dots)
and lineations (triangles) from outcrop area A. (Taken from
Nadeau, 1984).



a)



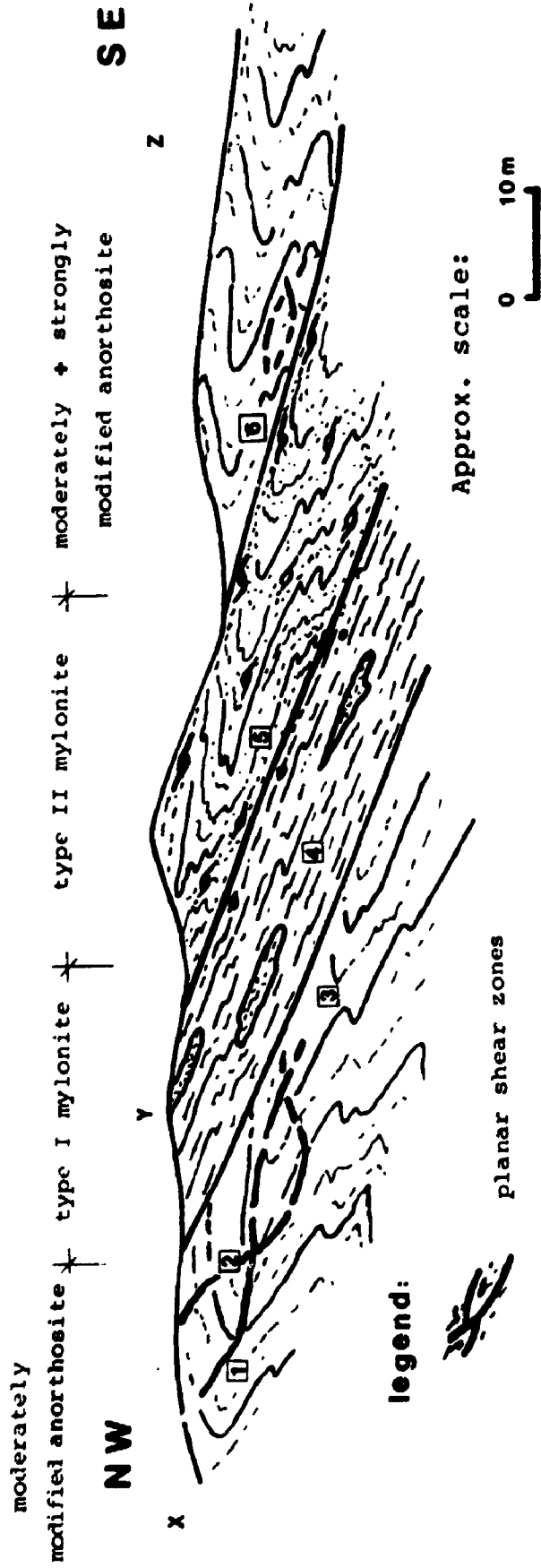
b)

Figure 3-5. Schematic cross-section of the Whitestone Anorthosite along the section line (X-Y-Z) of Fig. 3-3.

samples:

1	PS-85-1	4	PS-86-5
2	PS-85-2, 2a, 2b	5	PS-86-4
3	PS-85-18	6	PS-86-2

TRAVERSE II



legend:



Anorthosite boudin

[2] locations of samples referenced in this thesis



feldspar augen

metagabbro exposed in this traverse has a lenticular shape, and was described as "identical" to that at traverse II by Davidson et al. (1982b). Figure 3-6 is a geological map along the precise location of this traverse, and Figure 3-7 illustrates the general geological features of this traverse.

The anorthositic metagabbro contains a lens in which primary igneous texture is preserved. Elsewhere, the foliation is well-developed and large K-feldspar augen occur parallel to the foliation. The metagabbro contains the same minerals noted in traverse II, but quartz is more abundant. The quartz occurs in quartz ribbons along foliation planes defined by amphibole and garnet. Its abundance increases with increasing development of the foliation, while the abundance of scapolite decreases. Mylonites derived from the metagabbro near the road toward the lakeshore contain as much as 15 % quartz, and scapolite is rarely present. The very fine grained mylonite both above and below the metagabbro contains pegmatite veins that are flattened and stretched.

The orientation of the stretching lineation along this traverse is south-southeasterly. The sense of rotation in sigmoidal K-feldspar and amphibole augen suggest a northwesterly displacement of overlying rock mass.

Figure 3-6. Anorthositic metagabbro lens in mylonite. Section line of Fig. 3-7 marked (X-Y). (Taken from Davidson et al., 1982).

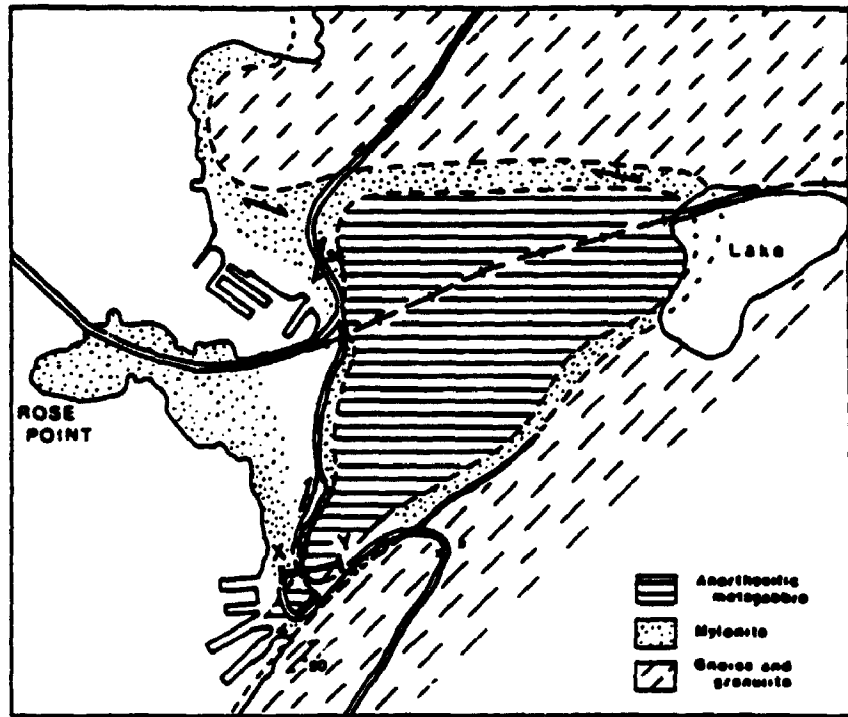


Figure 3-7. Schematic cross-section of the Whitestone Anorthosite along the section line (X-Y) of Fig. 3-6).

samples:

1 PS-86-17

5 PS-86-16b

2 PS-85-14

6 PS-85-13

3 PS-85-16

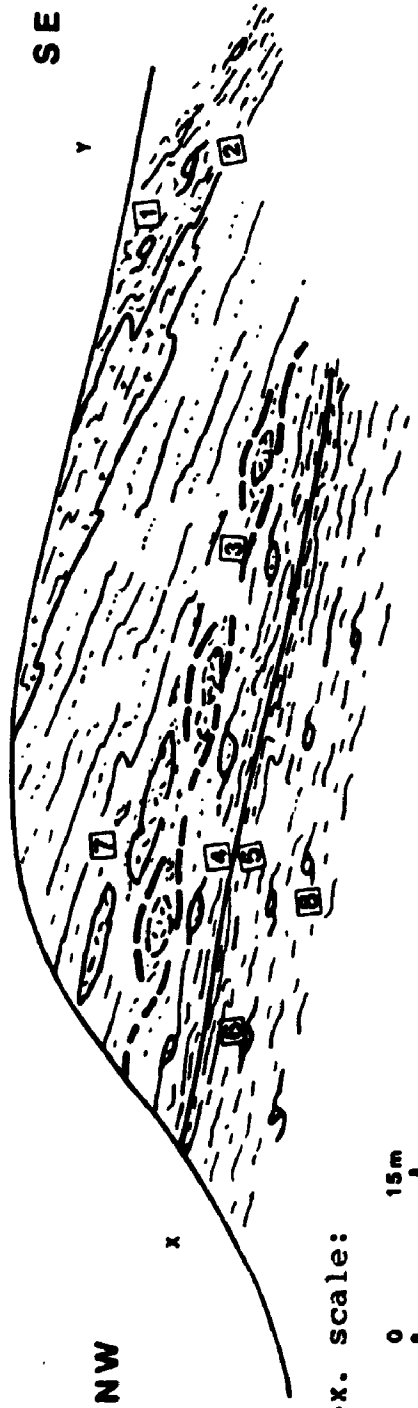
7 PS-86-9

4 PS-86-16

8 PS-85-12

TRAVERSE III

type II mylonite + strongly modified anorthosite + moderately modified anorthosite + orthogneiss + type II mylonite




Approx. scale:



legend:


 anastomosing shear zones


 feldspar augen


 locations of samples referenced in this thesis

3.3 COMPOSITE CROSS-SECTION OF THE WHITESTONE ANORTHOSITE AT THE INTERSECTION WITH THE PARRY SOUND SHEAR ZONE

Preliminary hand specimen and petrographic investigations of the anorthosite along the three traverses indicated that the deformational and the metamorphic states of the deformed anorthosite had to be considered in order to derive an accurate description of the rock type. A fourfold division into weakly modified, moderately modified, strongly modified anorthosites and mylonites is proposed here as the most suitable way to describe these rocks.

Figure 3-8 is a composite cross-section of the Whitestone Anorthosite at the contact with the Parry Sound Shear Zone, based on Figures 3-2, 3-5, and 3-7. It is proposed that Figure 3-8 represents, in a generalized way, the geology of the Whitestone Anorthosite where it is intersected by the Parry Sound Shear Zone. Relict igneous textures, crudely-defined foliation and quartz-bearing anastomosing shear zones characterize the weakly modified anorthosite which occurs in the main body of the anorthosite at a distance from the Parry Sound Shear Zone. Well-developed foliation and scapolite-rich, planar shear zones typify the moderately modified anorthosite which occurs in the anorthosite lenses within the Parry Sound Shear Zone. Mylonites and strongly modified anorthosite

Figure 3-8. Composite cross-section of the progressively modified Whitestone Anorthosite across the Parry Sound Shear Zone. Symbols are same as in Figs. 3-4 and 3-5.

occur along the contact between the Whitestone Anorthosite and the Parry Sound Shear Zone.

3.4 PRINCIPAL FEATURES OF THE WHITESTONE ANORTHOSITE AT THE INTERSECTION WITH THE PARRY SOUND SHEAR ZONE

3.4.1 DEFORMED ANORTHOSITE

3.4.1.1 WEAKLY MODIFIED ANORTHOSITE

Beyond a few 100 meters from the mylonites of the shear zone, the anorthosite is only weakly modified. An igneous texture is locally preserved and foliation is ill-defined (Plate 3-1a). A weakly developed stretching lineation is visible in the shape fabric of elongated mafic grains.

Weakly modified anorthosite exhibits inequant, subpolygonal texture with plagioclase, hornblende, scapolite and relicts of clinopyroxene as the main constituents. Clinopyroxene is often replaced by amphibole. Amphibole occurs as elongated grains with an average length about a centimeter. Plagioclase (An40-56) is recrystallized and zoned; the grain size averages a few millimeters.

3.4.1.2 MODERATELY MODIFIED ANORTHOSITE

Moderately modified anorthosite is characterized by the absence of relict igneous textures and the development of a pervasive foliation and lineation (Plate 3-1b). Isoclinal, refolded folds are common and unique to this anorthosite. Four different generations of folds are present (Nadeau, 1984). A northwest-trending mineral lineation, defined by a preferred shape orientation of mafic grains and fold hinges is well-developed (see Fig. 3-4b). A good exposure of moderately modified anorthosite can be seen in an old sand pit north-east of Parry Sound (see Davidson et al., 1982b, stop 7).

The moderately modified anorthosite displays a very different mineralogy to that of its less modified counterpart. Primary clinopyroxene is recrystallized, and the recrystallized pyroxene shows metamorphic corona structure with garnet. Primary plagioclase is rare. Recrystallized plagioclase (An49-58) has an average grain size of about 400 microns and an equant polygonal texture with equilibrium triple junctions is characteristic. Amphibole, with an average grain size of 500-600 microns, forms mafic rich layers interlayered with plagioclase. Almandine garnet is always present and there is a significant increase in the amount of ilmenite. The textural and mineralogical features of the moderately

modified anorthosite suggest a higher grade metamorphic environment than the weakly modified anorthosite.

3.4.1.3 STRONGLY MODIFIED ANORTHOSITE

The transition from moderately to strongly modified anorthosite is marked by the development of mineral differentiation into closely spaced macroscopic layers. There is a decrease in the hornblende content and the lineation seen in the moderately modified anorthosite is seldom present. Plate 3-1c illustrates the highly strained appearance of these rocks.

The strongly modified anorthosite is characterized by an inequant subpolygonal texture and a dark gray gneissic layering. The mineralogy varies from a scapolite-bearing assemblage to a quartz-bearing assemblage. Andesine (An₃₅₋₄₃), hornblende and garnet are the other mineral phases. The average grain size is usually less than that observed in the moderately modified anorthosite. It ranges from 200 to 500 microns. Plagioclase is strongly recrystallized and polysynthetic twinning is common. Garnet occurs as large augen.

3.4.1.4 MYLONITES

Mylonites occur at the intersection between the Whitestone Anorthosite and the Parry Sound Shear Zone, and

Plate 3-1.

a) Photograph of a sample of the weakly modified anorthosite, showing relict igneous texture in lower left corner. An anastomosing shear zone traverses the photograph from upper left corner to lower right corner. Sample PS-85-9. Scale bar = 1.0 cm.

b) Photograph of a sample of the moderately modified anorthosite in a section sub-normal to the foliation. A planar shear zone, trending sub-parallel to the long axis of the photograph, is indicated by a deflection in schistosity. Sample PS-85-2. Compass for scale is 8 cm across.

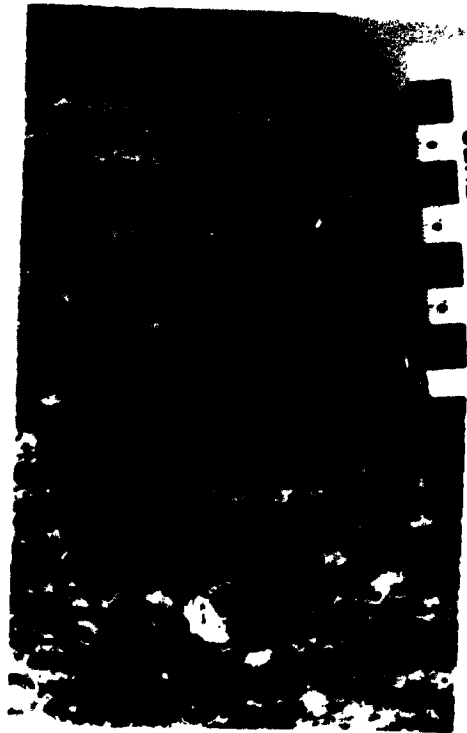
c) Handspecimen photograph of the strongly modified anorthosite. Plagioclase is mostly recrystallized. Gneissic fabric is well-developed. Sample PS-85-16. Scale bar = 1.0 cm.



a



b



c

PLATE 3-1

are of two distinct types. Both are readily recognizable by their dark-coloured matrix and fine grain size (Plate 3-2a). The mylonitic foliation is well-developed in both types and dips from 25 to 50 degrees to the southeast. The difference seen in the field is that type I mylonites contain relicts of the host anorthosite while type II mylonites commonly contain porphyroclasts of pegmatite and porphyroblasts of garnet. When viewed in the direction parallel to the NE-trending stretching lineation, the apparent rotations of porphyroclasts and porphyroblasts suggest a northwesterly thrusting of the Parry Sound Domain over the Britt Domain within the Parry Sound Shear Zone.

Type I mylonite has a mineralogy similar to that observed in moderately modified anorthosite with scapolite and plagioclase (An33-36) as the dominant phases and biotite as a minor phase. Garnet porphyroblasts are present. Equant polygonal texture with a grain size of approximately two hundred microns is characteristic (Plate 3-2b).

Type II mylonite contains porphyroclasts of K-feldspar, plagioclase and hornblende and large porphyroblasts of garnet (up to 4-6 cm in diameter) in a matrix composed of plagioclase (An18-21), hornblende, garnet, K-feldspar and quartz. In the matrix, plagioclase and hornblende have subpolygonal outlines and are

Plate 3-2.

a) Photograph of a contact between type I and type II mylonites. Type II mylonite is distinguished from type I mylonite by its darker coloured matrix and feldspar augen. Pencil for scale is 14 cm long.

b) Photomicrograph of type I mylonite. Plagioclase (plg), amphibole (amp), scapolite (scp) and garnet (gr) are the main constituents. Crossed nicols. Sample PS-86-5. Scale bar = 0.5 mm.

c) Photomicrograph of type II mylonite. Quartz (q) occurs as ribbons, or as isolated grains in the surrounding matrix. The matrix also contains Plagioclase (plg), amphibole (amp) and garnet (gr). Crossed nicols. Sample PS-86-16. Scale bar = 0.5 mm.



PLATE 3-2

extensively recrystallized. The mean grain size in the matrix is of the order of 50-150 microns. Undulose extinction and deformation lamellae are the most prominent deformational features of quartz and plagioclase. Quartz ribbons and amphibole grains define the mylonitic foliation (Plate 3-2c).

3.4.2 LOCAL SHEAR ZONES

Local shear zones are of two types. These are anastomosing shear zones and planar shear zones.

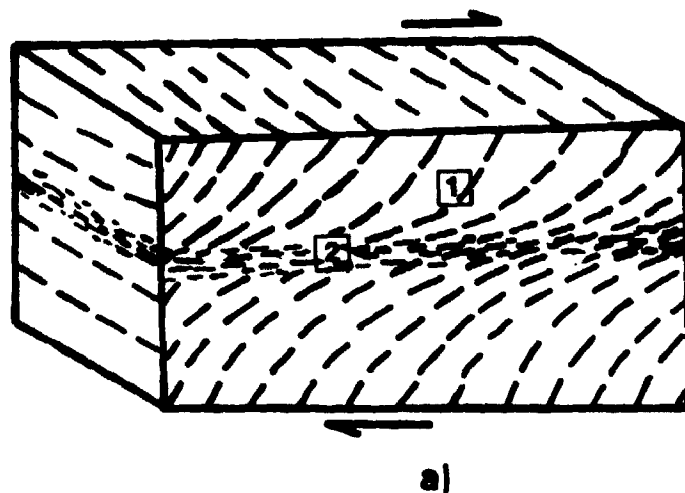
3.4.2.1 ANASTOMOSING SHEAR ZONES

Anastomosing shear zones are best observed in the weakly modified anorthosite although they are also occasionally noted in strongly modified anorthosites. They occur irregularly distributed and have a unique appearance in the field. There is a gradual change of colour from dark gray in the host rock through grayish-white at the boundaries to white in the central part of the shear zone. Plate 3-3a illustrates an example of an anastomosing shear zone in the weakly modified anorthosite.

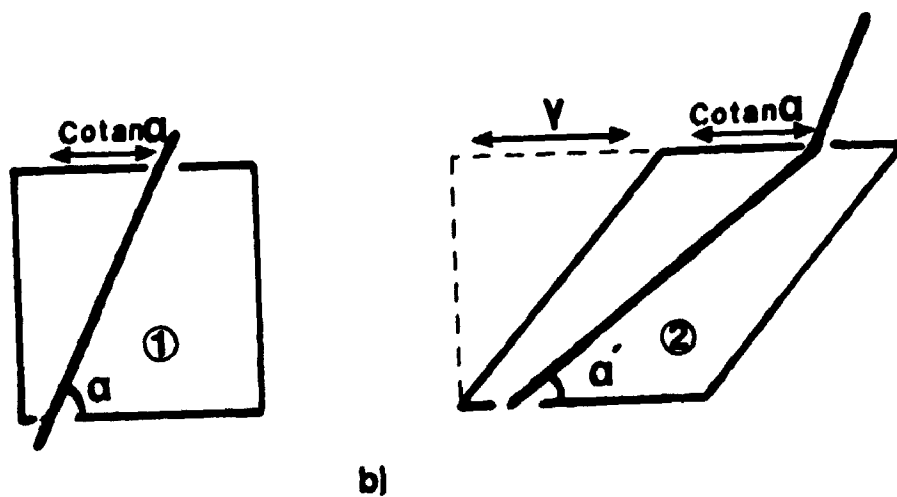
The shear strain in two anastomosing shear zones was quantified by measuring the angles between the schistosity and the boundary of the shear zone. The following relation was used:

Figure 3-9 . a) Diagram showing progressive rotation of the schistosity in a shear zone. The schistosity becomes progressively parallel to the shear zone boundary near the center of the shear zone.

b) Diagram showing the angles between the orientation of the schistosity and the shear zone boundary at locations 1 and 2 in Figure 3-9a. The equation characterizing this relationship is $\gamma = \cot \alpha' - \cot \alpha$.



$$Y = \text{Cotan } \alpha' - \text{Cotan } \alpha$$



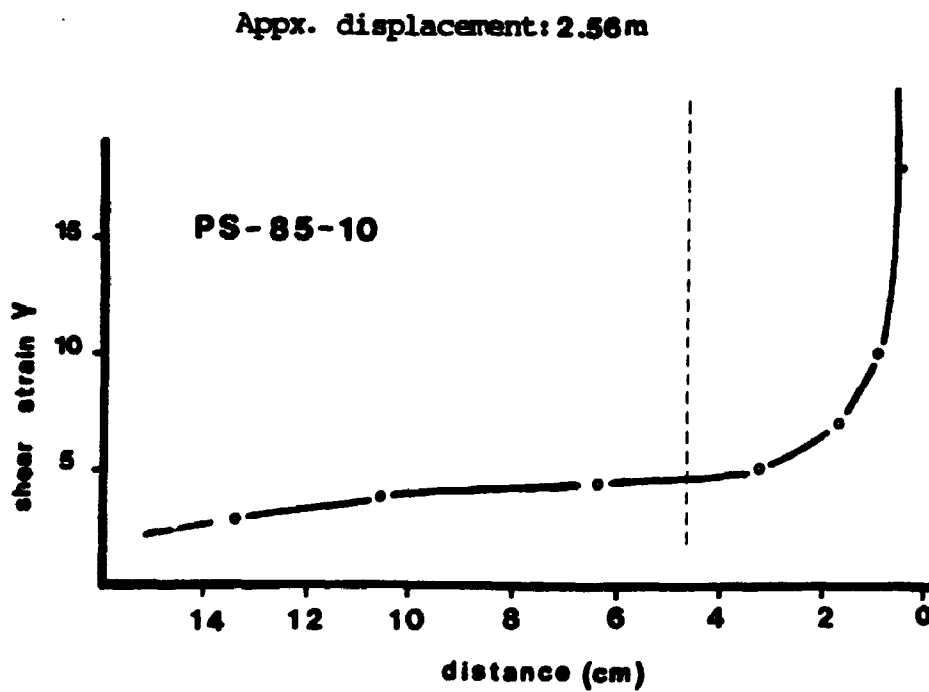
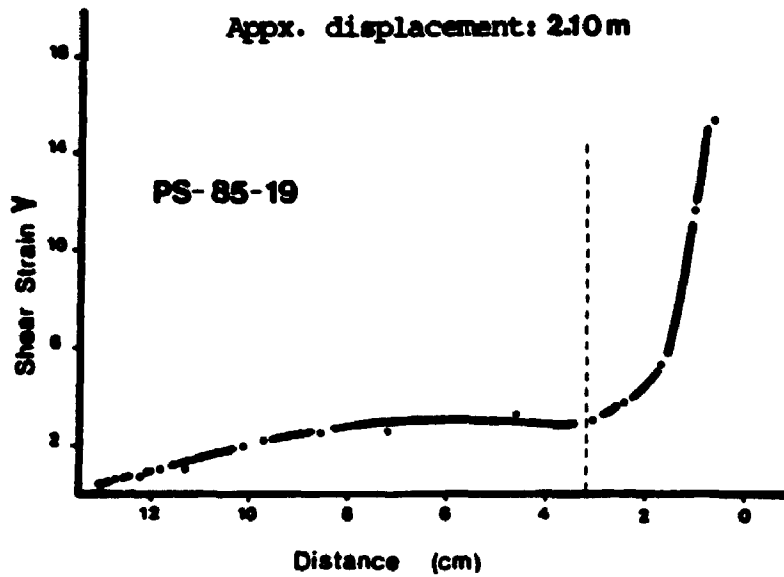
$$\text{Cot } \alpha' = \text{Cot } \alpha + V \quad (\text{Ramsay, 1967})$$

where α is the angle between the schistosity and the shear zone boundary measured outside the shear zone, which represents the original orientation and α' is measured inside the shear zone, where the schistosity has been rotated (Figure 3-9). Figure 3-10 illustrates the shear strain/distance curves derived from geometric analyses of schistosity across the two anastomosing shear zones (specimens PS-85-19 and PS-85-10). Dashed, vertical lines represent the boundary between the presence of biotite and amphibole. This is accompanied by an abrupt increase in the shear strain.

Although the application of this method to anastomosing shear zones is limited because simple shear cannot always be assumed at the shear zone boundaries (see Ramsay and Allison, 1977; Ramsay, 1980), the amount of displacement appears to be in the order of meters in anastomosing shear zones in the Parry Sound Shear Zone.

The mineralogy changes considerably across anastomosing shear zones. At the boundary, sodic plagioclase (An34-36), muscovite and biotite replace the more calcic plagioclase (An45-55), and the hornblende, and the scapolite content of the host decreases. In addition, iron-rich epidote commonly occurs as porphyroblasts. In the central part of the shear zone, abrupt changes in mineralogy take place. Scapolite and amphibole are

Figure 3-10. Shear strain-distance curves derived from geometric analyses of schistosity across two anastomosing shear zones. Dashed, vertical lines represent the approximate boundary of shear zones where the replacement of amphibole by biotite occurs.



replaced by quartz, muscovite, biotite, and microcline as the main mineral phases. The average grain size is 250 microns or more for quartz, plagioclase, and biotite and 1 millimeter or more for microcline, epidote, and muscovite.

PLANAR SHEAR ZONES

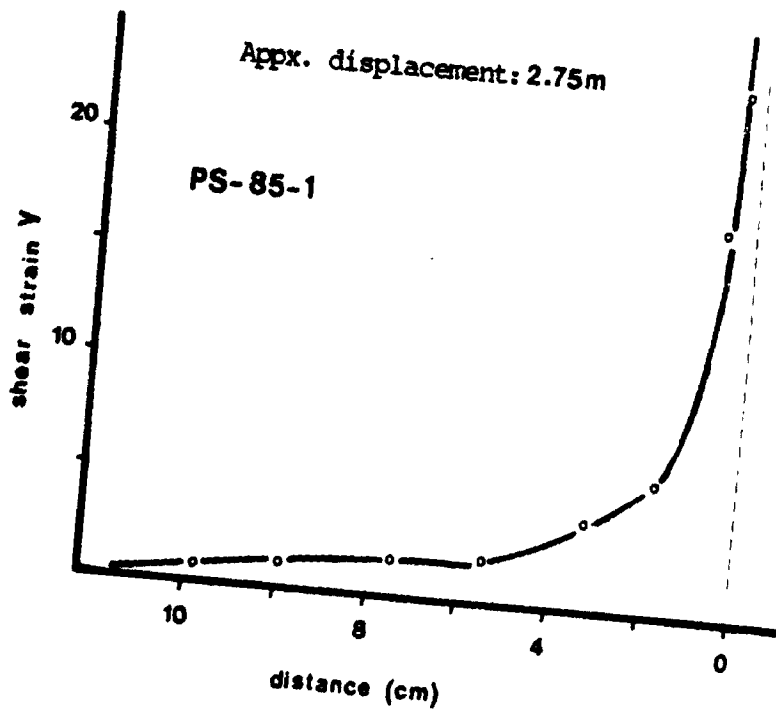
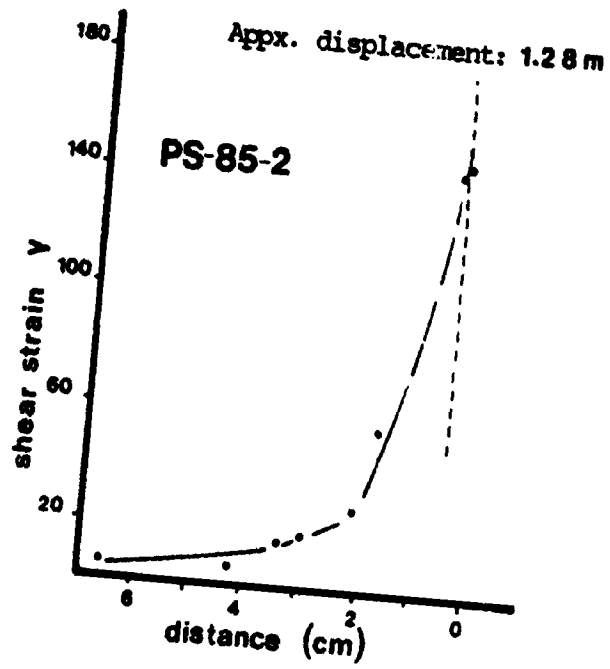
Planar shear zones are a structural feature of the moderately modified anorthosite. They cross-cut the foliation and, as a result, give a deceptive impression of an intruding dyke, especially when there is a small angle between the erosion surface and the plane of foliation. Plate 3-3b illustrates an example of a planar shear zone in a section perpendicular to the shear zone and parallel to the shear direction. This shear zone has a very different appearance to that of the shear zone illustrated in 3-1b which is viewed approximately perpendicular to the plane of foliation. The deflection of the schistosity at shear zone margins indicates a consistent NW-directed overthrusting which is also indicated by other indicators (e.g. tails developed from feldspar augen).

The shear zone illustrated in Plate 3-3b has a fairly uniform width and shows a curving alignment of mafic minerals (i.e. amphiboles). Where this fabric becomes visible, it has an angle of 35-40° to the shear direction, and it acquires an orientation increasingly parallel to

the shear direction nearer the shear zone boundary. Figure 3-11 illustrates the state of shear strain across this and one other planar shear zone using the progressive rotation of schistosity. There is no evidence of significant volume change along the length of the shear zone. This suggests that the boundary condition of simple shear may be satisfied. The increase in the intensity of schistosity with increasing strain indicates the contemporary development of schistosity from an initially isotropic rock.

The mineralogy of planar shear zones displays some differences from that of the moderately modified anorthosite in which they occur. However, the differences are small, and perhaps suggest that planar shear zones formed soon after the formation of the moderately modified anorthosite and under similar metamorphic conditions. Plagioclase, meionitic scapolite and biotite are the main minerals. The plagioclase is recrystallized and the anorthite content decreases from An49 in the host to An42 in the shear zone. Similarly, scapolite shows a decrease in both grain size and meionite content. Foam texture in the scapolite grains is characteristic and the average grain size is about one hundred and fifty microns. The appearance of biotite in the shear zone indicates potassium fixation during deformation.

Figure 3-11. Variation of shear strain (γ) across two planar shear zones. Shear strain values are derived from the geometric analysis of schistosity with respect to the shear direction. Dashed, vertical lines represent the boundary of shear zones marked by an abrupt change in microstructure and fabric.



3.5 SUMMARY

The increasingly modified original igneous texture of the Whitestone Anorthosite is interpreted to be the result of a strain gradient. Although good strain markers are absent, two lines of evidence are considered useful for the qualitative measure of strain. These are observed foliation spacing and reduction in grain size. The foliation becomes more closely spaced as the original texture of the Whitestone Anorthosite grades into mylonites. Similarly, the average grain size shows a progressive decrease.

The modified anorthosite displays evidence for varying conditions of deformation. The occurrence of two different mylonites suggests two different deformation events. Similarly, the two different kinds of local shear zones suggest two different deformation events. Further, the presence of different mineral assemblages indicate different metamorphic conditions of deformation. On the basis of these differences, moderately modified anorthosite, type I mylonite and planar shear zones are attributed to an early event, while weakly modified anorthosite, type II mylonite and anastomosing shear zones are attributed to a late event.

Plate 3-3.

a) Photograph of a handspecimen of an anastomosing shear zone cross-cutting weakly modified anorthosite. Sample PS-85-9. Scale bar = 1.0 cm

b) Photograph of a handspecimen of a planar shear zone viewed normal to the shear direction. Arrows point to the boundary of the shear zone. Scale bar = 1.0 cm.



a



b

PLATE 3-3

CHAPTER 4

MINERAL ASSEMBLAGES OF THE WHITESTONE ANORTHOSITE IN THE PARRY SOUND SHEAR ZONE

4.1 GENERAL STATEMENT

The Whitestone Anorthosite contains a variety of mineral assemblages. Plagioclase (An60) and magnesium-rich clinopyroxene are primary constituents of the undeformed Whitestone Anorthosite (Mason, 1969). Clinopyroxene, plagioclase (An 54-56), scapolite (Me70-75), garnet and amphibole is the mineral assemblage of the eastern margin (Fig. 2-1) (Lacy, 1960; Thompson, 1983). Plagioclase, hornblende and epidote is the mineral assemblage of the western margin (Fig. 2-1) (Mason, 1969). Plagioclase (An47-38), scapolite, hornblende, garnet, epidote and quartz is the mineral assemblage of the southern extension of the Whitestone Anorthosite (Nadeau, 1984). These mineral assemblages and those noted in Chapter 3 indicate more than one metamorphic facies, and an understanding of the relationship between these mineral assemblages is necessary to evaluate the deformation history. This chapter details the mineral assemblages of the Whitestone Anorthosite at the contact with the Parry Sound Shear Zone.

The samples of anorthosite were investigated by transmitted- and reflected-light microscopy, and by electron-microprobe analysis of selected mineral grains. Mineral analyses from rocks representing each type of increasingly modified anorthosite are assembled in tables which are presented at the end of each subsection. Additional analyses of many mineral species are presented in Appendix C. Leake (1978) was followed for amphibole classification.

4.2 INCREASINGLY MODIFIED ANORTHOSITES

4.2.1 ORIGINAL ANORTHOSITE

In the field, the Whitestone Anorthosite away from the Parry Sound Shear Zone has a massive to glomeropoikilitic texture; however, in thin section, it displays evidence of dynamic metamorphism. The mineral assemblage consists of primary pyroxene and plagioclase (An52-57), metamorphic hornblende, clinozoisite, and, locally, recrystallized plagioclase (An52-57).

The augite is the most common pyroxene and mafic component of the Whitestone Anorthosite. Weakly pleochroic, pale green to colorless in thin section, the augite shows high relief and moderate birefringence. It exhibits a prismatic habit, and cleavages are usually present. Table 4-1 lists the average composition of augite

Table 4-1. Chemical analysis of primary pyroxene from the unmodified Whitestone Anorthosite (Reproduced from Mason, 1969).

Structural formula
on the basis of 6 oxygens

SiO ₂	48.79	Si	1.84
TiO ₂	0.68	Ti	0.02
Al ₂ O ₃	5.76	Al	0.10
Fe ₂ O ₃	3.51	Fe ³⁺	0.10
FeO	8.05	Fe ²⁺	0.25
MnO	0.23	Mn	0.01
MgO	10.61	Mg	0.60
CaO	21.57	Ca	0.87
K ₂ O	0.01	K	0.00
Na ₂ O	0.79	Na	0.06
Total	100.00		

from the Whitestone Anorthosite reported by Mason (1969).

Plagioclase is usually myrmekitic and has lobate boundaries. Some plagioclase displays polysynthetic twins, which are sometimes bent. The anorthite content of primary plagioclase is greater than An57 and shows surprisingly little change over the body (Mason, 1969). Table 4-2 column 1 lists the analysis of a primary plagioclase from specimen PS-85-17.

The original anorthosite displays a high temperature igneous assemblage. Martignole (1986) has suggested that a temperature in excess of 1000 C and a pressure of 4-5 kb existed during the crystallization of the anorthosites in the eastern Grenville Province.

4.2.2 WEAKLY MODIFIED ANORTHOSITE

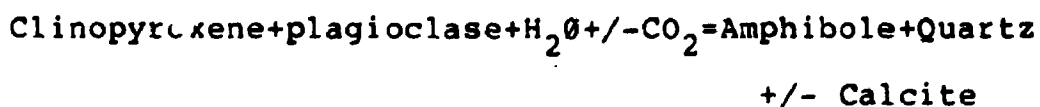
The stable mineralogical assemblage of the weakly modified anorthosite consists of plagioclase (An40-56), ferromagnesian hornblende, scapolite (Me57-63), biotite, minor quartz, titanite and sulphides. Clinopyroxene is present as relict grains in some samples of weakly modified anorthosite. Epidote occurs as porphyroblasts in weakly modified anorthosite near anastomosing shear zones.

The augite shows signs of disequilibrium in the weakly modified anorthosite. Its discolouration and the formation of dark green coloured, strongly pleochroic

amphibole rims are indications of the incipient disequilibrium. Near shear zones, the disequilibrium is increased, and the augite is replaced by blue-green hornblende.

Plagioclase is recrystallized, and has a composition of An 40-56. Table 4-2 lists the analysis of a plagioclase from specimen PS-85-8, additional analyses are presented in Appendix C. The average grain size varies from 2 mm to 4mm.

Amphibole has a deep green-blue colour, and shows strong pleochroism from dark to olive green which often masks the interference colours. Grain size ranges from 600 to 2000 microns. It has a ferroan pargasite core and magnesian hornblende rim, Table 4-3, column 2. The amphibole usually occurs with oxides as a rim around augite which suggest that it is derived from augite by a reaction such as the following:

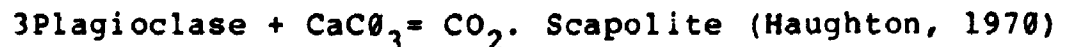


Laird and Albee (1981) suggested that the composition of amphibole varies with metamorphic facies. They illustrated the variation of amphibole composition by a plot of atomic ratios. Similar plots are used here. Figure 4-1 illustrates the ratios of $({}^{\text{iv}}\text{Al}) : ({}^{\text{vi}}\text{Al})$ and $(100 \text{ Na} / \text{Na} + \text{Ca}) : (100 \text{ Al} / \text{Si} + \text{Al})$ and Figure 4-2 illustrates the ratios of the $({}^{\text{vi}}\text{Al} + \text{Fe}^{3+} + \text{Ti}) : ({}^{\text{iv}}\text{Al})$ and $(100$

Na/(Na+Ca):(100 Al/Si+Al) in amphiboles compared with data for reference metamorphic terranes of Laird and Albee (1981). The data for the increasingly modified anorthosite, including the weakly modified anorthosite, are represented on these figures.

Scapolite is a minor constituent of the weakly modified anorthosite. Electron microprobe analyses of scapolite show it to be a calcium-rich member of the scapolite solid-solution series with a composition of Me57-63. The analysis of a scapolite is listed in Table 4-4, column 1.

Scapolite forms from transformation of plagioclase (Plate 4-2c). The degree of completion of the transformation appears to be a function of the grain size of the plagioclase. The smaller the grains, the more complete the scapolitization. Scapolitization takes place according to the following reaction:



Epidote grows with biotite (Plate 4-3a). Epidote formation involves a reaction between plagioclase, hornblende and a fluid phase which is analogous to the garnet-forming reaction.

The composition of plagioclase (An40-46) and the ratios of (^{iv}Al):(^{vi}Al) and (100 Na/(Na+Ca):(Al/Si+Al) in amphiboles (Fig. 4-1) suggest lower amphibolite facies conditions (Goldsmith, 1982; Laird and Albee, 1981). The

occurrence of epidote also suggests intermediate pressure lower amphibolite facies (Miyashiro, 1961; Apter and Liou, 1983). Thus, the metamorphic mineral assemblage of the weakly modified anorthosite suggests moderate pressure type, lower amphibolite facies conditions.

4.2.3 MODERATELY MODIFIED ANORTHOSITE

The equilibrium mineral assemblage of the moderately modified anorthosite consists of clinopyroxene, plagioclase (An48-58), amphibole (pargasite, hastingsite), garnet (Alm 63), scapolite (Me69-75), minor ilmenite, sphene and quartz.

Clinopyroxene is recrystallized, it is green, slightly pleochroic and has well-developed basal parting. In contrast to the primary pyroxene, it lacks oriented inclusions of oxide and silica exsolution (Mason, 1969). Metamorphic corona structures--a discontinuous garnet rim, amphibole corona and quartz symplectites--occur at grain boundaries with plagioclase and iron oxides occur along cleavage planes (Nadeau, 1984).

Plagioclase has a composition of An48-58, and the representative analysis of plagioclase, specimen PS-85-2, is listed in Table 4-2, column 3. Polysynthetic twins are thick, continuous and simple. Albite twins are common, but pericline twins are rare. Plagioclase is 60-70%

recrystallized and the grain size is about 400 microns. Recovery related features are also present; mechanical twinning and undulose extinction are most pronounced. Minute grains of oxides occur in some plagioclase megacrysts, giving them a netted appearance. Plate 4-1b shows the style of twinning both in the relict and recrystallized plagioclase.

Amphibole has a mean grain size from 400 to 600 microns. It occurs as aggregates and shows symplectic corona texture with clinopyroxene grains. It is commonly associated with garnet, sphene and ilmenite (see Plate 4-2b). The composition varies from a hastingsite at the center to a ferroan pargasite composition at the rims of the grains. Table 4-3, column 3 lists the analysis of an amphibole. Additional analyses are presented in Appendix C.

Scapolite is an important constituent (Plate 4-2c). Its formation postdates the crystallization of primary igneous plagioclase, and forms by transformation from plagioclase. It has a composition of Me69-75 (Appendix C). Table 4-4 column 2 lists a representative composition of the scapolite.

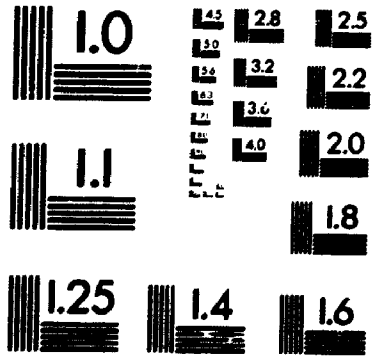
Garnet is a prominent constituent of the moderately modified anorthosite. It is pink in thin section, and occurs as aggregates. It has an almandine-rich composition, and is associated with ilmenite and iron

oxides in myrmekitic-graphitic intergrowths with sphene forming a rim between the phases (see plate 4-2b). Its association with pyroxene and amphibole suggests a reaction involving these two constituents.

Ilmenite occurs as anhedral blebs. It is frequently rimmed by amphibole or garnet, suggesting a genetic relationship. Hematite exsolution is characteristic, and up to 50% hematite has been reported in ilmenite from the anorthosite along the eastern margin of the anorthosite (Kretschmar, 1968). The average bulk composition of ilmenite, Hem₄₄ Ilm₅₆, suggests the oxidising conditions of Ni + NO through Fe₂O₃ + FeO buffers (Kretschmar, 1968). Plate 4-4a is a photomicrograph of ilmenite in the moderately modified anorthosite.

The occurrence of clinopyroxene with plagioclase (An₄₈₋₅₈) suggests granulite and upper amphibolite facies (Miyashiro, 1961; Fyfe et al., 1978). The ratios of (^{iv}Al):(^{vi}Al) and (100 Na/(Na+Ca)):(100 Al/(Si+Al)) in amphiboles (Fig. 4-1) also suggest granulite to upper amphibolite facies conditions (Laird and Albee, 1981). The comparison of the (^{vi}Al+Fe³⁺+Ti):(^{iv}Al) and (100 Na/(Na+Ca)):(100 Al/(Si+Al)) ratios with those reported from a variety of metamorphic terranes (Fig. 4-2) indicates metamorphic conditions similar to those of Haas River, New Zealand, and the Abukuma terrane, Japan (Laird and Albee, 1981) (Fig. 4-2). The occurrence of almandine-rich garnet

2



with a high grossularite component suggests amphibolite facies. The composition of scapolites also suggests metamorphic conditions higher than sillimanite-muscovite grade (Hietanen, 1967; La Tour, 1974). The occurrence of scapolite and ilmenite with a significant hematite component in the assemblages of the moderately modified anorthosite indicates CO_2 metasomatism during the oxidising conditions of upper-middle amphibolite facies.

In summary, the assemblage of recrystallized augite, titanium rich, aluminous green-brown amphibole (hastingsite, ferroan pargasite), andesine (An55-46) and almandine garnet in the moderately modified anorthosite indicates CO_2 dominated, moderate-pressure type upper-middle amphibolite facies conditions (Miyashiro, 1961; Ernst, 1976; Fyfe et al., 1978).

4.2.4 STRONGLY MODIFIED ANORTHOSITE

Strongly modified anorthosite displays some variation in mineral assemblage. Plagioclase, almandine garnet, biotite, ilmenite, quartz (<3%), epidote and minor sphene are the dominant phases.

The plagioclase composition is An 42-35, analyses of plagioclase are presented in Appendix C. The grain size ranges between 200 and 500 microns (Table 4-2, column 4). Mechanical twinning is characteristic (see plate 3-1c).

Amphibole has a smaller grain size than that of moderately modified anorthosite. The colour is brownish-green. It occurs as anhedral, single grains with poorly developed cleavages (Plate 3-2b). An electron microprobe analysis of the amphibole yields a ferroan pargasite-hastingsite composition, Table 4-3, column 4, additional amphibole analyses are presented in Appendix C.

Scapolite occurs as small grains and scapolitization is not always complete. It has a composition of Me₆₅₋₇₅ (see Appendix C).

Garnet shows a sieved texture containing all other constituents. The sieved texture suggests repeated involvement of the garnet during deformation.

Titanite, ilmenite and quartz occurs in small quantities, less than 3%.

The strongly modified anorthosite frequently displays disequilibrium mineral assemblages. In samples where the mineral assemblage approaches equilibrium, the plagioclase, scapolite and amphibole compositions suggest metamorphic conditions lower than those in the moderately modified anorthosite and the weakly modified anorthosite.

4.2.5 MYLONITES

Type I mylonites display the following stable mineral assemblage: plagioclase (An33-36), amphibole (pargasite), scapolite (Me68-70), garnet (Alm 65), biotite, minor sphene, and sulphides.

Plagioclase is strongly recrystallized (see Plate 3-2b), and the grain size has an average grain diameter of the order of 200 microns. The plagioclase has a composition of An 33-36. The representative analysis of plagioclase is listed in Table 4-2, column 5. Mechanical twinning and subgrain development are present, but are not as abundant as in the strongly modified anorthosite. The lack of any marked recovery is consistent with mylonitization during an amphibolite facies metamorphism.

Amphibole has a small mean grain size of 200 microns. The colour is brownish-green. It occurs as anhedral, single grains with poorly developed cleavages. An electron microprobe analysis of the amphibole shows a pargasite composition, Table 4-3, column 5. Additional analyses of amphiboles are presented in Appendix C.

Scapolite is a major constituent of type I mylonites. It occurs as single, isolated grains, and has a meionite-rich composition, Table 4-4 column 4.

Garnet occurs as anhedral grains. It is an impure almandine and poorer in grossularite compared to the

moderately modified anorthosite, Table 4-5 column 2.

Pyrite and ilmenite occur as anhedral, interstitial grains. They are frequently rimmed by amphibole and garnet.

Titanite and zircon occur as additional accessory minerals.

The assemblage of the type I mylonite suggests upper amphibolite to granulite facies metamorphic conditions. The anorthite content of plagioclase and the ratios of (^{iv}Al):(^{vi}Al) and (100 Na/Ca+Na):(100 Al/Si+Al) (Fig. 4-1) suggest granulite to upper amphibolite facies (Laird and Albee, 1981). The occurrence of almandine garnet and scapolite are consistent with these conditions.

The mineral assemblage of the type II mylonites differs from that of the type I mylonite. It consists of plagioclase (An18-21), amphibole (pargasite), garnet, quartz, both in ribbons and isolated grains, biotite, minor oxides and sulphides and porphyroclasts of K-feldspar and amphibole.

Plagioclase is extensively recrystallized and has a composition of An18-21. Table 4-2, column 6 lists an analysis of plagioclase. The grain size ranges between 60-100 microns. Polysynthetic twinning is present in some grains.

Amphibole occurs as anhedral, single grains with

poorly developed cleavages (Plate 3-2c). The grain size is 60-150 microns and has the composition of hastingsite, Table 4-3, column 6.

Garnet shows a sieved texture. It is richer in almandine and spessartine and poorer in grossularite and pyrope compared to type I mylonite, Table 4-5 column 3.

Quartz occurs as isolated grains in a matrix of other minerals, or as ribbon-like aggregates. The ratio of major to minor axis of the grains is usually greater than 3:1. Plate 4-3d illustrates quartz in a ribbon. Quartz displays little evidence for relict intracrystalline strain. In the quartz in ribbons, signs of recovery such as deformation lamellae and undulose extinction and recrystallization are locally present. In the quartz surrounded by matrix, signs of deformation are small grain size (70-100 microns) and occasionally undulose extinction.

The abundance of sulphides is higher in type II mylonites compared to the increasingly modified anorthosite. This preferential occurrence suggests that sulphides are related to the late episode of deformation within the Parry Sound Shear Zone.

Pyrite and chalcopyrite are the most commonly occurring sulphides, but pyrrhotite also occurs. Pyrite often displays euhedral to subhedral habit and constitutes 60-70% of all sulphides (Plate 4-4c). Chalcopyrite and pyrrhotite show anhedral habits.

Table 4-2. Chemical analyses and mean grain sizes of plagioclase grains in the Whitestone Anorthosite sampled across the Parry Sound Shear Zone. PS-85-17, unmodified anorthosite; PS-85-8, weakly modified anorthosite; PS-85-2, moderately modified anorthosite; PS-86-16, strongly modified anorthosite; PS-86-5, type I mylonite; PS-86-4, type II mylonite.

	1	2	3		5	6
SAMPLE #	PS-85-17	PS-85-8	PS-85-2	PS-86-16	PS-86-5	PS-86-4
Grain Size	4-5mm	2-4mm	400 μ	200-500 μ	200 μ	60-100 μ

Weight % oxides

SiO ₂	53.66	55.99	55.00	57.79	59.33	63.29
Al ₂ O ₃	29.12	27.70	27.69	27.41	26.07	22.11
CaO	12.48	9.38	11.40	8.92	7.22	4.23
K ₂ O	0.01	0.15	0.18	0.30	0.30	0.19
Na ₂ O	4.61	6.05	4.80	6.86	7.46	9.25
Total	99.88	99.27	99.07	101.28	100.38	99.07

Numbers of cations on the basis of 32 oxygens

Si	9.72	10.12	10.00	10.25	10.55	11.29
Al	6.22	5.90	5.93	5.73	5.47	4.65
Ca	2.42	1.82	2.22	1.70	1.37	0.81
K	0.00	0.03	0.04	0.07	0.07	0.04
Na	1.62	2.12	1.69	2.36	2.57	3.20
Total	19.98	20.00	19.89	20.10	20.00	20.00

An content %	60	46	56	41	34	20
--------------	----	----	----	----	----	----

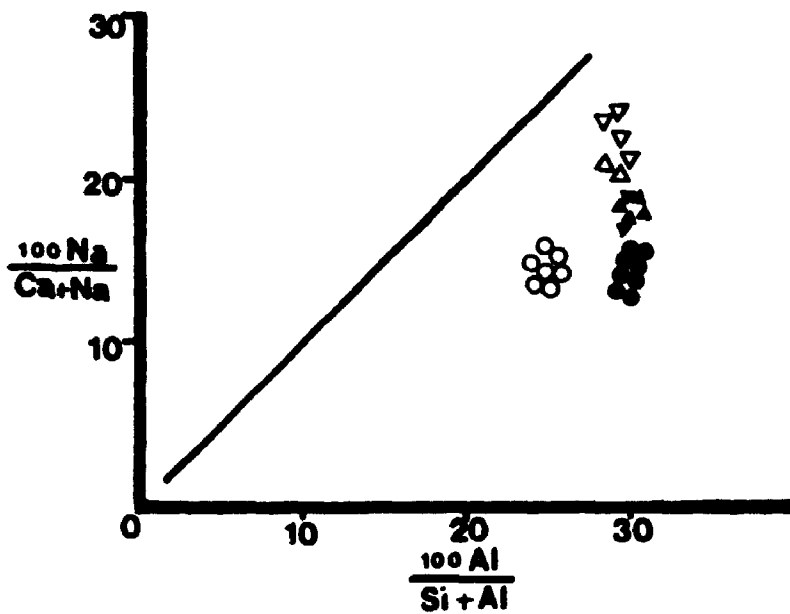
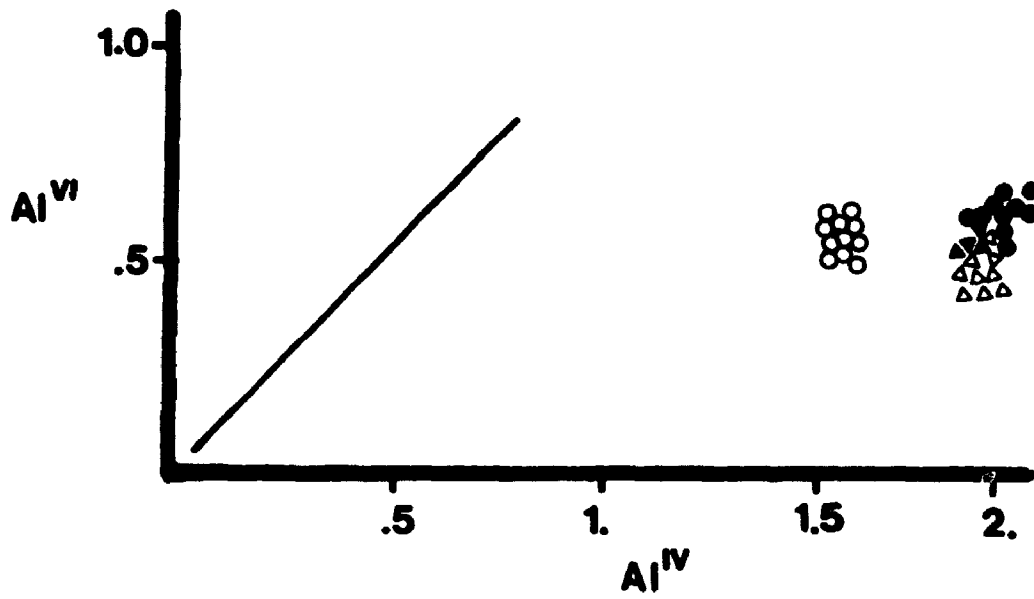
Table 4-3. Chemical analyses and mean grain sizes of amphibole grains in the Whitestone Anorthosite sampled across the Parry Sound Shear Zone. PS-85-17, unmodified anorthosite; PS-85-7, weakly modified anorthosite; PS-85-2, moderately modified anorthosite; PS-86-5, type I mylonite; PS-86-16, strongly modified anorthosite; PS-86-4, type II mylonite.

	1	2	3	4	5	6
SAMPLE #	PS-85-17	PS-85-7	PS-85-2	PS-86-16	PS-86-5	PS-86-4
	Weight % oxides					
Grain Size	4-5mm	0.6-2mm	500 μ	200-500 μ	200 μ	60-100 μ
SiO ₂	43.94	43.29	38.93	39.15	38.02	37.45
TiO ₂	0.82	0.28	1.04	1.16	1.12	1.34
Al ₂ O ₃	12.31	12.44	14.14	14.09	13.79	13.21
Fe O	14.59	13.80	21.27	20.85	23.24	25.97
MgO	11.68	12.42	6.91	6.80	5.35	4.23
MnO	0.22	0.36	0.22	0.60	0.22	0.15
CaO	11.51	12.27	12.29	11.91	11.61	11.17
K ₂ O	0.85	0.80	1.70	1.62	1.74	1.59
Na ₂ O	1.48	1.33	1.08	1.23	1.29	1.60
Total	97.40	96.99	97.58	96.87	96.28	96.71

Numbers of cations on the basis of 23 oxygens

Si	6.46	6.37	5.96	6.04	5.99	5.94
Ti	0.09	0.03	0.12	0.13	0.13	0.16
^{iv} Al	1.54	1.62	2.03	1.95	2.00	2.05
^{vi} Al	0.74	0.53	0.52	0.61	0.55	0.41
Fe ²⁺	1.39	1.12	2.11	2.27	2.55	2.83
Fe ³⁺	0.37	0.57	0.61	0.41	0.49	0.60
Mg	2.56	2.72	1.58	1.56	1.25	1.00
Mn	0.02	0.04	0.03	0.01	0.03	0.02
Ca	1.81	1.93	2.01	1.97	1.96	1.90
K	0.16	0.15	0.33	0.31	0.35	0.32
NaM4	0.04	0.03	0.00	0.01	0.02	0.05
Na-A	0.39	0.34	0.32	0.35	0.37	0.43
Comp.	Pargasitic Hornbld.	Mg Hast. Hornbld.	Mg Hast.	Ferroan Pargst.	Ferroan Pargst.	Hasting.

Figure 4-1. The $({}^{\text{vi}}\text{Al}):({}^{\text{iv}}\text{Al})$ ratio and the $(100 \text{ Na}/\text{Ca}+\text{Na}):(100 \text{ Al}/\text{Si}+\text{Al})$ ratio in amphiboles from progressively modified anorthosite in the Parry Sound Shear Zone.



- Δ type II mylonite (An_{18-21})
- \blacktriangle type I mylonite (An_{33-36})
- \bullet moderately modified anorthosite (An_{40-58})
- \circ weakly modified anorthosite (An_{40-46})

Figure 4-2. The $(^{vi}Al + Fe + Ti):(^{iv}Al)$ ratio and the $(100 Na/Ca+Na):(100 Al/Si+Al)$ in amphiboles from progressively modified Whitestone Anorthosite, compared with data from various occurrences of mafic schists in the world. The Sanbagawa terrane in Japan and the Franciscan terrane in California represents the high pressure facies. The Dalradian terrane in Southwestern Scotland and the Haast River schist in New Zealand represents the medium pressure facies. The Abukuma Terrane in Japan represents the low pressure facies.

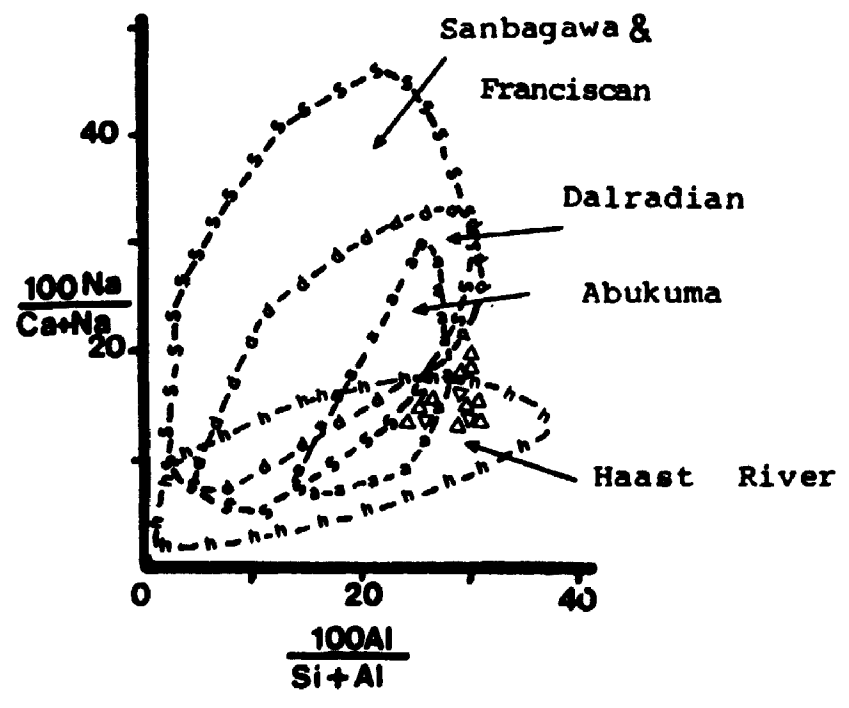
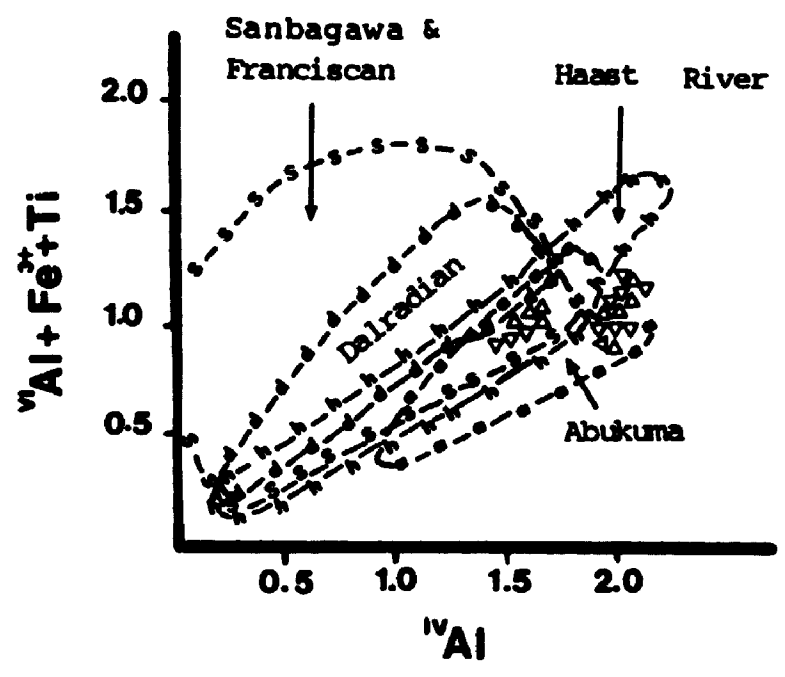


Table 4-4. Analyses of scapolite in the Whitestone
Anorthosite sampled across the Parry Sound Shear Zone.
PS-85-17, unmodified anorthosite; PS-85-2, moderately
modified anorthosite; PS-86-5, type I mylonite; PS-86-16,
strongly modified anorthosite; PS-86-5, type I mylonite.

	1	2	3	4
SAMPLE #	PS-85-8	PS-85-2	PS-86-16	PS-86-5
Weight % oxides				
SiO ₂	47.54	45.33	46.17	46.79
Al ₂ O ₃	26.98	27.84	28.23	27.84
CaO	16.19	17.78	17.84	16.56
K ₂ O	0.40	0.14	0.24	0.41
Na ₂ O	4.27	3.25	3.65	4.00
SO ₃	0.06	0.77	0.06	0.49
Cl	0.51	0.05	0.15	0.39
Total	95.95	95.16	96.34	96.48

Numbers of ions on the basis of 12 (Si, Al)

Si	7.23	6.97	6.96	7.05
Al	4.76	5.02	5.03	4.94
Ca	2.64	2.94	2.91	2.70
K	0.07	0.02	0.04	0.07
Na	1.26	0.97	1.07	1.18
S	0.00	0.08	0.00	0.05
Cl	0.13	0.01	0.03	0.10
Me content %	66	74	72	70

Table 4-5. Analyses of garnet in the Whitestone
Anorthosite sampled across the Parry Sound Shear Zone.
PS-85-2, moderately modified anorthosite; PS-86-5, type I
mylonite; PS-86-4, type II mylonite.

	1	2	3
SAMPLE #	PS-85-2	PS-86-5	PS-85-4
Weight % oxides			
SiO ₂	36.97	37.32	37.42
Al ₂ O ₃	20.23	21.11	22.37
Fe ₂ O ₃	27.34	26.75	29.50
MnO	0.78	0.74	1.55
MgO	1.88	2.89	1.55
CaO	12.06	10.45	9.45
Total	99.29	99.26	101.84

Numbers of cations on the basis of 24 (O)

Si	5.96	5.95	6.02
Al	3.84	3.97	3.86
Fe	3.68	3.57	3.97
Mn	0.11	0.1	0.21
Mg	0.45	0.69	0.37
Ca	2.08	1.79	1.63
Alm.	62.78	65.42	68.32
Gross.	35.45	32.74	28.04
Pyrp. content %	7.14	11.19	6.01
Spess.	1.18	1.83	3.64

Magnetite displays a euhedral habit (Plate 4-4b). Its pink-tinted colour suggests a titanium-rich composition. In specimens of the present study, magnetite seems to reflect reduction in the oxidation state of the fluid interacted with the type II mylonite.

Titanite and zircon are present in small quantities.

Comparison of the ratios of $(^{iv}Al):(^{vi}Al)$ and $(100 Na/Ca+Na):(100 Al/Si+Al)$ (Fig. 4-1) with the ratios from mafic schists in Vermont suggests lower amphibolite facies (Laird and Albee, 1981). Also, the anorthite content of plagioclase and the occurrence of almandine garnet with a low grossularite component indicates middle-lower amphibolite facies. Thus, the metamorphic mineral assemblage of the type II mylonite indicates the conditions of lower amphibolite facies.

4.3 LOCAL SHEAR ZONES

4.3.1 ANASTOMOSING SHEAR ZONES

The stable mineral assemblage of the anorthosite near the edge of the anastomosing shear zone is plagioclase (An35-40), hornblende, scapolite (Me 59-62), epidote, biotite, muscovite and quartz.

Plagioclase is recrystallized. Some relict grains display a mortar texture. It has a grain size of 200 microns and a composition of An35-40. The analysis of a

plagioclase is listed in Table 4-6, column 5.

Hornblende also occurs as recrystallized grains with a grain size ranging from 150 to 500 microns. It has the composition of ferroan hornblende.

Epidote is a prominent constituent of the anastomosing shear zones. It grows with biotite (Plate 4-2d), and when it is present garnet is absent. Epidote formation involves a reaction between plagioclase, hornblende and a fluid phase, analogous to that of garnet. The presence of 8% Fe₂O₃ in the mineral composition of epidote (Mason, 1969) suggests that the fluid present during the reaction was ferric iron-rich.

Biotite has a small grain size (60-100 microns), light colour and ill-defined preferred shape orientation (Plate 4-3a). The occurrence of biotite is accompanied by the appearance of quartz and a decrease in scapolite content.

Muscovite is restricted to anastomosing shear zones in the Whitestone Anorthosite (Plate 4-3b). It replaces plagioclase and is in equilibrium with biotite.

Chlorite occurs in an anastomosing shear near toward the west end of traverse I. It occurs with plagioclase, altered hornblende, scapolite, epidote and quartz. The grain size is 150-200 microns. In the center of this anastomosing shear zone, the mineral assemblage consists of microcline and quartz.

Microcline occurs in the central part of well-developed, anastomosing shear zones (Plate 4-3c), and its association with plagioclase, quartz, calcite and biotite suggests some combination of these minerals may be involved in its formation.

The compositions of plagioclase and coexisting hornblende suggest lower amphibolite facies conditions (Spear, 1980). The occurrence of epidote and, locally, chlorite also suggests the conditions of lower amphibolite facies (Miyashiro, 1961; Moody et al., 1983; Apter and Liou, 1983). Thus, the mineral assemblage of the anastomosing shear suggest lower amphibolite facies conditions.

The occurrence of muscovite, microcline, quartz and sulphide minerals in the weakly modified anorthosite and anastomosing shear zones indicate K and SiO_2 metasomatism.

4.3.2 PLANAR SHEAR ZONE

The stable mineral assemblage in planar shear zones is plagioclase (An39-42), scapolite, amphibole (pargasite), garnet, and trace amount sulphides. It is similar to the mineral assemblages of moderately modified anorthosite and type I mylonites.

The plagioclase is strongly recrystallized, and the grain size is approximately 250 microns (Plate 4-1c). Its

grain size is approximately 250 microns (Plate 4-1c). Its composition is An39-42. The analysis of a plagioclase is listed in Table 4-6, column 3. Additional analyses of the plagioclase are presented in Appendix C.

Scapolite is abundant in planar shear zones, 30%. The composition is Me69-71. The very common association with minor shear zones suggest a history of growth contemporary with deformation.

Garnet usually occurs as small euhedra. It is Almandine.

Biotite occurs as a major constituent. It replaces hornblende and is in equilibrium with other mineral phases. It is orientated with the cleavage parallel to the shear plane and is, therefore, useful for determining the orientation of planar shear zones in thin section (Plate 4-3a). Biotite shows strong pleochroism in dark shades of brown. This may be due to high Ti (Robbins and Strens, 1972). It replaces hornblende and the reaction releases calcium along with magnesium, iron and sodium. Na reacts with plagioclase to produce a more sodic plagioclase while Ca is incorporated into melonitic scapolite and apatite. Iron may form iron oxides. Silica is removed.

The mineral assemblage of the planar shear zones resembles the mineral assemblages of the moderately modified anorthosite and the type I mylonite, but some differences are observed. For example, the anorthite

Table 4-6. Chemical analyses and mean grain sizes of plagioclase grains from a planar shear zone and an anastomosing shear zone. PS-85-2, moderately modified anorthosite outside the planar shear; zone; PS-85-2a, less deformed edge of the planar shear zone; PS-85-2b, strongly deformed center of the planar shear zone; PS-85-8a, weakly modified anorthosite near the anastomosing shear zone; PS-85-8b, less deformed edge of the anastomosing shear zone.

	1	2	3	4	5
SAMPLE #	PS-85-2	PS-85-2a	PS-85-2b	PS-85-2a	PS-85-2b

Weight % oxides

Grain Size	400 μ	250-300 μ	150 μ	2-4mm	250 μ
SiO ₂	55.00	55.96	57.46	55.99	60.33
Al ₂ O ₃	27.69	29.03	27.28	27.70	24.85
CaO	11.40	10.45	8.77	9.38	7.38
K ₂ O	0.18	0.22	0.20	0.15	0.07
Na ₂ O	4.80	5.70	6.54	6.05	7.67
Total	99.07	101.36	100.25	99.27	100.30

Numbers of cations on the basis of 32 oxygens

Si	10.00	9.94	10.27	10.12	10.72
Al	5.93	6.08	5.75	5.90	5.20
Ca	2.22	1.99	1.68	1.82	1.40
K	0.04	0.05	0.05	0.03	0.01
Na	1.69	1.96	2.27	2.12	2.64
Total	19.89	20.00	20.01	20.00	20.00

An content %	56	50	42	46	35
--------------	----	----	----	----	----

Table 4-7. Analyses of scapolite from a planar shear zone. PS-85-2, moderately modified anorthosite outside the planar shear zone; PS-85-2a, less deformed edge of the shear zone; PS-85-2b, strongly deformed center of the shear zone.

	1	2	3
SAMPLE #	PS-85-2	PS-85-2a	PS-85-2b
	Weight % oxides		
SiO ₂	45.33	46.51	46.92
Al ₂ O ₃	27.84	27.59	27.59
CaO	17.78	17.25	16.87
K ₂ O	0.14	0.34	0.39
Na ₂ O	3.25	3.58	3.93
SO ₃	0.77	0.32	0.45
Cl	0.05	0.37	0.36
Total	95.16	95.96	96.15

Numbers of ions on the basis of 12 (Si, Al)

Si	6.97	7.06	7.09
Al	5.02	4.93	4.90
Ca	2.97	2.80	2.73
K	0.02	0.06	0.07
Na	0.97	1.05	1.14
S	0.08	0.03	0.05
Cl	0.01	0.09	0.02

Me content %	75	71	69
--------------	----	----	----

content of plagioclase indicates lower grade metamorphism than that of the moderately modified anorthosite, but higher than that of the type I mylonite. Similar differences are indicated by the mineral composition of the scapolite, which suggests metamorphism lower than that of the moderately modified anorthosite, but higher than that of type I mylonite. The occurrence of garnet indicates amphibolite facies metamorphic conditions (Miyashiro, 1961). Thus, the mineral assemblage of the planar shear zone suggest upper-middle amphibolite facies conditions.

4.4 SUMMARY

The mineralogy of the moderately modified anorthosite differs from that of the weakly deformed anorthosite. There are, also, mineralogical differences between the type I and type II mylonites, as well as between planar shear zones and anastomosing shear zones. These differences indicate different metamorphic conditions.

Generally, the mineral assemblages characterize two different metamorphic facies. Moderate pressure upper-middle amphibolite facies assemblages occur in moderately modified anorthosite, type I mylonite and planar shear zones. Lower amphibolite or epidote-amphibolite facies assemblages occur in weakly

planar shear zones. Lower amphibolite or epidote-amphibolite facies assemblages occur in weakly modified anorthosite, type II mylonites and anastomosing shear zones. Upper-middle amphibolite facies assemblages indicate CO_2 metasomatism during oxidizing conditions. Lower amphibolite facies assemblages indicate K_2O and SiO_2 metasomatism (related to pegmatite formation) under reducing conditions.

Plate 4-1.

a) An example of recrystallized and relict plagioclase (plg) grains with albite twinning, in moderately modified anorthosite. Crossed nicols. Sample PS-85-2. Scale bar = 0.5 mm.

b) A large grain of plagioclase (plg) in a matrix of recrystallized plagioclase in strongly modified anorthosite. An aggregate of garnet (gr) and amphibole (amp) is visible from lower left to lower right. Crossed nicols. Sample PS-86-16. Scale bar = 0.5 mm.

c) Plagioclase (plg) at the boundary of a planar shear zone in moderately modified anorthosite. Arrows point to the shear zone boundary which traverses the photograph subparallel to the long dimension. The shear zone occupies the upper third of the photograph. A decrease in grain size and an increase in scapolite content are noted within the shear zone. Crossed nicols. Sample PS-85-2. Scale bar = 0.5 mm.

d) Plagioclase at the boundary of an anastomosing shear zone, transecting weakly modified anorthosite. Arrows point to the curving boundary of the shear zone, which traverses the photograph diagonally from upper right corner towards lower left corner. Plagioclase (plg), quartz (q) and biotite are the main constituents of the anastomosing shear zone. Crossed nicols. Sample PS-85-9. Scale bar = 0.5 mm.



b



d



a



c

PLATE 4-1

Plate 4-2.

a) Photomicrograph of amphiboles (amp) in weakly modified anorthosite. Note slight elongation of the grains. Coexisting plagioclase often has twinning. Crossed nicols. Sample PS-85-9. Scale bar = 0.5 mm.

b) Photomicrograph showing the usual association of garnet (gr) with amphibole (amp) in moderately modified anorthosite. Ilmenite occurs in the central portion of the garnet (gr), sphene (sp) forms a rim between the two phases. Plane polarized light. Sample PS-85-2. Scale bar = 0.5 mm.

c) Photomicrograph of scapolite showing the replacement of plagioclase. Crossed nicols. PS-85-1. Scale bar = 0.01 mm.



b



a



c

PLATE 4-2

R
800

Plate 4-3.

a) Photomicrograph showing epidote (ep) at the weakly deformed edge of an anastomosing shear zone. Scapolite (scp) and biotite (bt) are also present. Plagioclase (plg) exhibits zoning, developed contemporaneously with deformation. Crossed nicols. Sample PS-85-8. Scale bar = 0.5 mm.

b) Photomicrograph showing muscovite (mus) in an anastomosing shear zone. A late biotite (bt) replaces the muscovite (mus). A portion of a large quartz ribbon (q) is visible near the upper edge of the photograph. Crossed nicols. Sample PS-85-19. Scale bar = 0.1 mm.

c) Large microcline grains (mic) in the strongly deformed center of an anastomosing shear zone. Crossed nicols. Sample PS-85-7c. Scale bar = 0.1 mm.

d) Photomicrograph showing a portion of a quartz ribbon (q) and isolated quartz grains in the matrix of type II mylonite. Also visible are elongated amphibole grains (amp). Crossed nicols. Sample PS-86-16. Scale bar = 0.1 mm.



b



d



a



c

PLATE 4-3

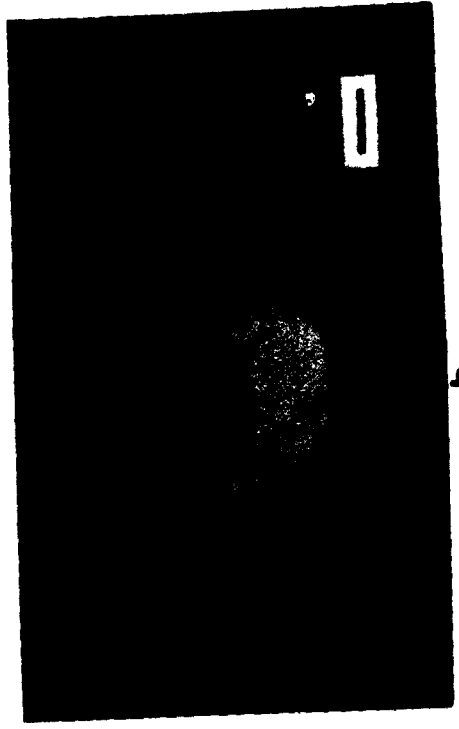
Plate 4-4.

a) An ilmenite grain with hematite exsolution in moderately modified anorthosite. The ilmenite is located within a garnet crystal. Reflected light. Sample PS-85-2. Scale bar = 0.03 mm.

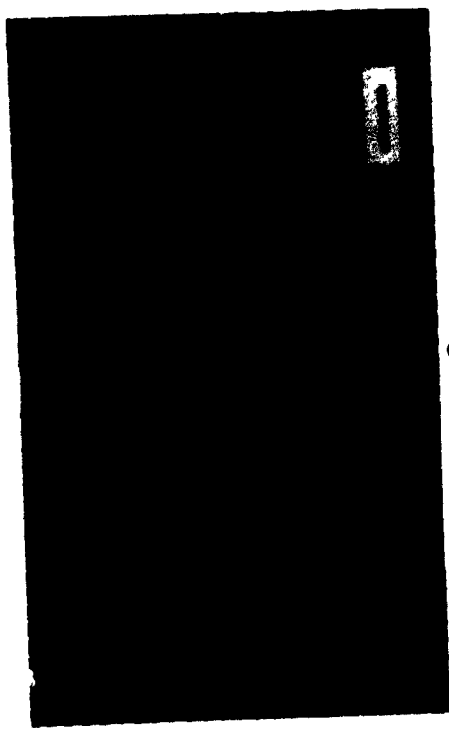
b) A euhedral magnetite crystal in the matrix of type II mylonite. It has a pinkish colour, suggesting a Ti rich composition. Reflected light. Sample PS-86-4. Scale bar = 0.03 mm.

c) Photomicrograph of pyrite crystals in type I mylonite. A light blue alteration rim surrounds pyrite grains. Reflected light. Sample PS-86-5. Scale bar = 0.03 mm.

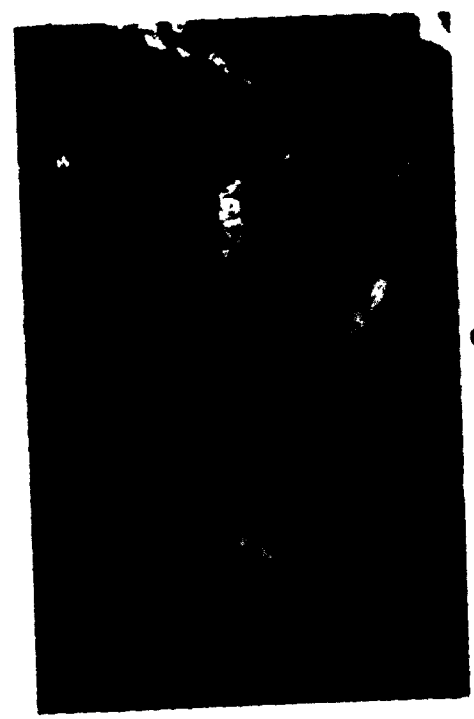
PLATE 4-4



b



a



c

CHAPTER 5

GEOCHEMISTRY OF THE WHITESTONE ANORTHOSITE AT THE INTERSECTION WITH THE PARRY SOUND SHEAR ZONE

5.1 GENERAL STATEMENT

The deformed Whitestone Anorthosite exhibits extensive mineralogical and microstructural modifications. These modifications were sufficient to suggest a geochemical study of the anorthosite in order to gain information about:

i) the scope of chemical changes in the deformed anorthosite at its contact with the Parry Sound Shear Zone; and

ii) the nature of fluid participation at different stages of progressive modification.

5.2 ANALYTICAL METHODS

The geochemical study of the anorthosite was two fold. First, analyses of major and minor whole rock chemistry and associated mass balance calculations were performed. Second, the oxidation states of iron were determined. Major and trace element analyses were made on a X-ray fluorescence spectrometer (XRF). Rare earth analyses were made by instrumental neutron activation

analysis (INAA). Details of analytical procedures are presented in Appendix D. Data are recorded in Tables 5-1, 5-3, 5-4, 5-6, 5-7, 5-9 and in Appendix D.

Chemical changes in rock compositions can result from either material transport into or out of the anorthosite with or without volumetric changes. Thus, there are a large number of possible equations that can describe the mass balance and the selection of a particular equation must accord with the volumetric and chemical character of the process by which transformation from the reactant (i.e. unaltered sample) to the product (i.e. altered sample) took place.

Gresens (1967) has introduced a method for selecting the appropriate equation. This method involves a graphical solution to equations relating gains and losses of each element to the chemical analyses and specific gravities of the reactant and the product. The general composition-volume equation is as follows:

$$(fv * (gb/ga) * C_b - C_a) * 100 = X_n$$

where

X_n = gain or loss (in grams per 100 grams unaltered rock);

fv = volume factor;

ga = specific gravity of unaltered sample;

gb = specific gravity of altered sample;

C_a = weight fraction of the component in unaltered

sample;

C_b = weight fraction of the component in altered sample;
The volume factor is the ratio of the rock volumes before and after the reactions. For example, $fv=1$ means an isovolumetric process, while $fv>1$ indicates a net volume increase. Substituting the values of the chemical analyses (C_a , C_b) and specific gravities of the rocks (g_a , g_b) into the above equation, the gains or losses of each element (X_n) are computed as a function of variation in volume factor (fv). These values are plotted to obtain lines on a composition-volume diagram for a specific transformation (e.g. Fig. 5-2).

The slope of each line in the composition-volume diagrams is a function of the elements' abundance in the product rock. The Y intercept is a negative function of the elements' abundance in the reactant rock. If the intersection of lines representing presumed immobile elements (e.g. Al, Ti, P) occurs near a common volume factor, this is assumed to indicate an isovolumetric transformation. If the intersection of these lines occurs at different volume factors, this indicates an allovolumetric reaction. Published studies on chemical changes associated with shear zones have shown the usefulness of this method in investigating the nature of chemical variation between two rock specimens from a shear zone (Vocke et al., 1987; Kerrich et al, 1977).

Gresens' method is employed in a sample series when each sample is assumed to be derived from the same rock type. This is best considered on a component ratio diagram where the abundances of chemical components in a sample is normalized to one of the elements from that sample (see Fig. 5-1). If the analyzed samples were originally identical, and have not been changed, then the component ratios show no significant change across the series. If there were original variations, or if there has been addition or subtraction of an element, the component ratios will vary between the altered and the unaltered sample.

5.3 RESULTS

Fourteen specimens were chosen from a sample suite that represents the increasing degrees of microstructural and mineralogical modifications in the deformed Whitestone Anorthosite discussed above. Results are presented in relation to the structure of the anorthosite at the contact with the Parry Sound Shear Zone, and in the local shear zones.

5.3.1 DEFORMED ANORTHOSITE

The chemical investigation of the deformed anorthosite involved the analysis of samples chosen as representative of the observed modifications. The source rock for all analyzed samples is anorthositic gabbro, and a detailed discussion of relations between each sample and their source rock is available in Chapter 3.

Table 5-1 lists the major element compositions and specific gravities of representative specimens of unmodified anorthosite, weakly modified anorthosite, moderately modified anorthosite, type I mylonite and type II mylonite from traverses I and II. Chemical compositions of additional specimens including a mylonite specimen from traverse III, PS-86-16b, are presented in Appendix D. The selected specimens represent the increasing apparent modification of the Whitestone Anorthosite. Chemical changes are most pronounced between the modified anorthosites and the mylonites. The changes in SiO_2 , TiO_2 , Fe_2O_3 , MgO , CaO , P_2O_5 and Na_2O are prominent. Minor and trace element concentrations were obtained from selected samples primarily for determining volume factors. These are presented in Appendix D.

Table 5-1 lists the major element compositions and specific gravities of representative specimens of unmodified anorthosite, weakly modified anorthosite,

moderately modified anorthosite, type I mylonite and type II mylonite from traverses I and II. Chemical compositions of additional specimens including a mylonite specimen from traverse III, PS-86-16b, are presented in Appendix D. The selected specimens represent the increasing apparent modification of the Whitestone Anorthosite. Chemical changes are most pronounced between the modified anorthosites and the mylonites. The changes in SiO_2 , TiO_2 , Fe_2O_3 , MgO , CaO , P_2O_5 and Na_2O are prominent. Minor and trace element concentrations were obtained from selected samples primarily for determining volume factors. These are presented in Appendix D.

Figure 5-1 is a component ratio diagram for the representative suite of increasingly modified anorthosite samples listed in Table 5-1. Components are normalized to the Al_2O_3 content in each sample because of its presumed immobility under metamorphic conditions. The normalized values of Na_2O and CaO are approximately constant, while SiO_2 , TiO_2 , Fe_2O_3 , MnO , MgO and K_2O values generally increase. The nearly constant component ratios of Na_2O and CaO with respect to Al_2O_3 support the proposition that the relative abundances of these elements have remained approximately unchanged.

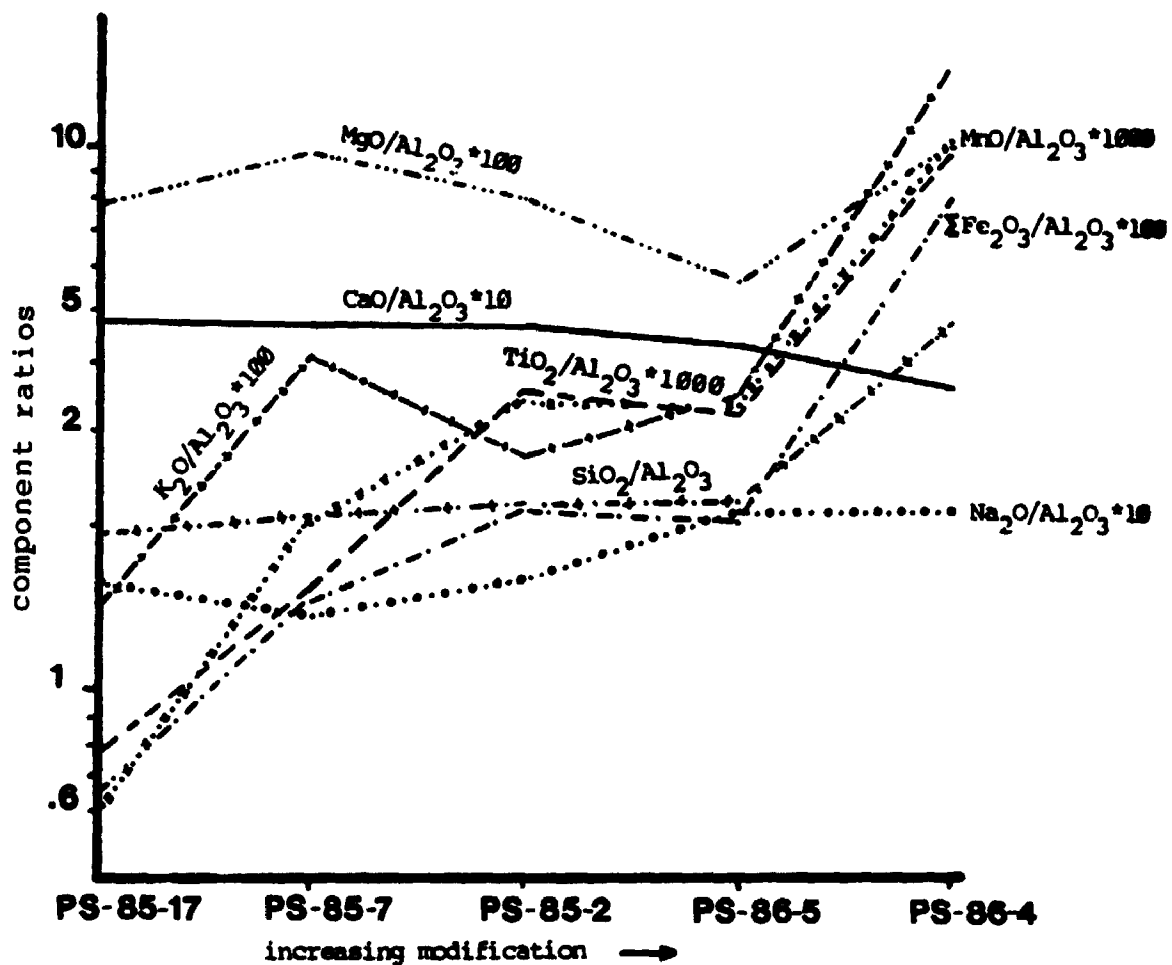
Figures 5-2, 5-3, 5-4 and 5-5 are composition-volume diagrams derived from the specimens selected as representing the transformation of unmodified anorthosite

Table 5-1. Abundances of major elements, expressed as oxides, in increasingly modified Whitestone Anorthosite in the Parry Sound Shear Zone. PS-85-17, unmodified anorthosite; PS-85-7, weakly modified anorthosite; PS-85-2, moderately modified anorthosite; PS-86-5, type I mylonite; PS-86-4, type II mylonite. Total Fe expressed as Fe_2O_3 ; Loss on ignition at 1000°C (LOI) adjusted for oxidation of FeO; Specific gravity (S.G.) in gm/cm^3 .

SAMPLE #	PS-85-17	PS-85-7	PS-85-2	PS-86-5	PS-86-4
SiO ₂	51.74	51.85	51.83	53.32	62.65
TiO ₂	0.15	0.38	0.83	0.76	1.29
Al ₂ O ₃	26.70	24.42	22.98	23.23	12.85
Fe ₂ O ₃	1.70	3.60	5.58	5.08	10.78
MnO	0.02	0.05	0.08	0.08	0.20
MgO	2.08	2.44	1.88	1.35	1.42
CaO	12.71	11.55	11.10	10.16	4.71
K ₂ O	0.37	1.01	0.63	0.83	1.90
P ₂ O ₅	0.00	0.03	0.35	0.13	0.31
Na ₂ O	4.46	3.40	3.95	5.07	2.81
LOI	0.58	0.77	0.48	0.40	0.63
Total	100.51	99.50	99.69	100.41	99.55
S.G.	2.81	2.82	2.86	2.78	2.90

0 2 1
0 1 1

Figure 5-1. Component ratio diagram for modified anorthosite from the Parry Sound Shear Zone. PS-85-17, unmodified Whitestone Anorthosite; PS-85-7, weakly modified anorthosite; PS-85-2, moderately modified anorthosite; PS-86-5, type I mylonite; PS-86-4, type II mylonite.



to modified anorthosites and mylonites. Figure 5-2 illustrates the composition/volume change from unmodified anorthosite to weakly modified anorthosite. Lines representing presumed immobile elements such as Al_2O_3 , MnO and Ni intersect near a volume factor of 1.15. Lines representing the trace elements intersect different values of volume factors. Elements such as Pb, Sr, and Zn are off scale on this diagram, indicating extreme depletion or enrichment.

The composition/volume change associated with the transformation of unmodified anorthosite to moderately modified anorthosite is illustrated by Figure 5-3 which resembles Figure 5-2. There is a coincidence of SiO_2 , Al_2O_3 , CaO and Y around a volume factor 1.1.

Figure 5-4 illustrates the composition/volume change from moderately modified anorthosite to type I mylonite. The intersection of presumed immobile components occur around a volume factor of 1.0. Elements showing large gains are Cr, Pb, Zn, Nb, and Rb while Ni shows a large loss.

The data in Figures 5-2 through 5-4 suggest that reactions associated with the modification of weakly, moderately modified anorthosites and type I mylonites were essentially isovolumetric.

In Figure 5-5, the composition/volume change accompanying the transformation of moderately modified

anorthosite to type II mylonite is illustrated. There is much variation in both major and minor components. Components showing enrichment are K_2O , Fe_2O_3 , and Na_2O . The components showing losses are mostly those presumed to be immobile such as P_2O_5 , TiO_2 , Al_2O_3 , Ni, Ga, and V. This suggests that a volume increase accompanied the transformation to type II mylonite since depletion in the presumed immobile components is highly unlikely. A volume change of 75% is indicated during transformation to PS-86-4 if Al_2O_3 is presumed immobile (Fig. 5-5).

Table 5-2 summarizes the suggested compositional changes at different increments of observed mineralogical and textural modification in the Whitestone Anorthosite. Specimens PS-85-7, PS-85-2, PS-86-5 representing weakly modified and moderately modified anorthosite, and type I mylonite respectively, undergo small chemical changes relative to their less deformed counterparts. Increases in SiO_2 and Fe_2O_3 and a decrease in CaO are the most notable changes. An increase in CO_2 has also been reported (Nadeau, 1984) and this is consistent with the appearance of scapolite in these rocks. Specimen PS-86-4, type II mylonite, has significant chemical differences from its parent. The most prominent changes are increases in SiO_2 , Fe_2O_3 , K_2O and depletion in CaO. Increases in TiO_2 , Fe_2O_3 , MnO, and P_2O_5 are considered to indicate some process where the rock was enriched in relatively immobile

Figure 5-2. Composition-volume diagram showing the transformation of unmodified anorthosite (PS-85-17) to weakly modified anorthosite (PS-85-7). The gains and losses, shown along the ordinate, are in grams per 100 grams of parent rock for major elements, and μ grams per gram for trace elements. The vertical dashed line represents an isovolumetric transformation. The arrow indicates the value of volume factor derived from the intersections of lines representing presumed immobile components.

Sample PS-85-17 → PS-85-7

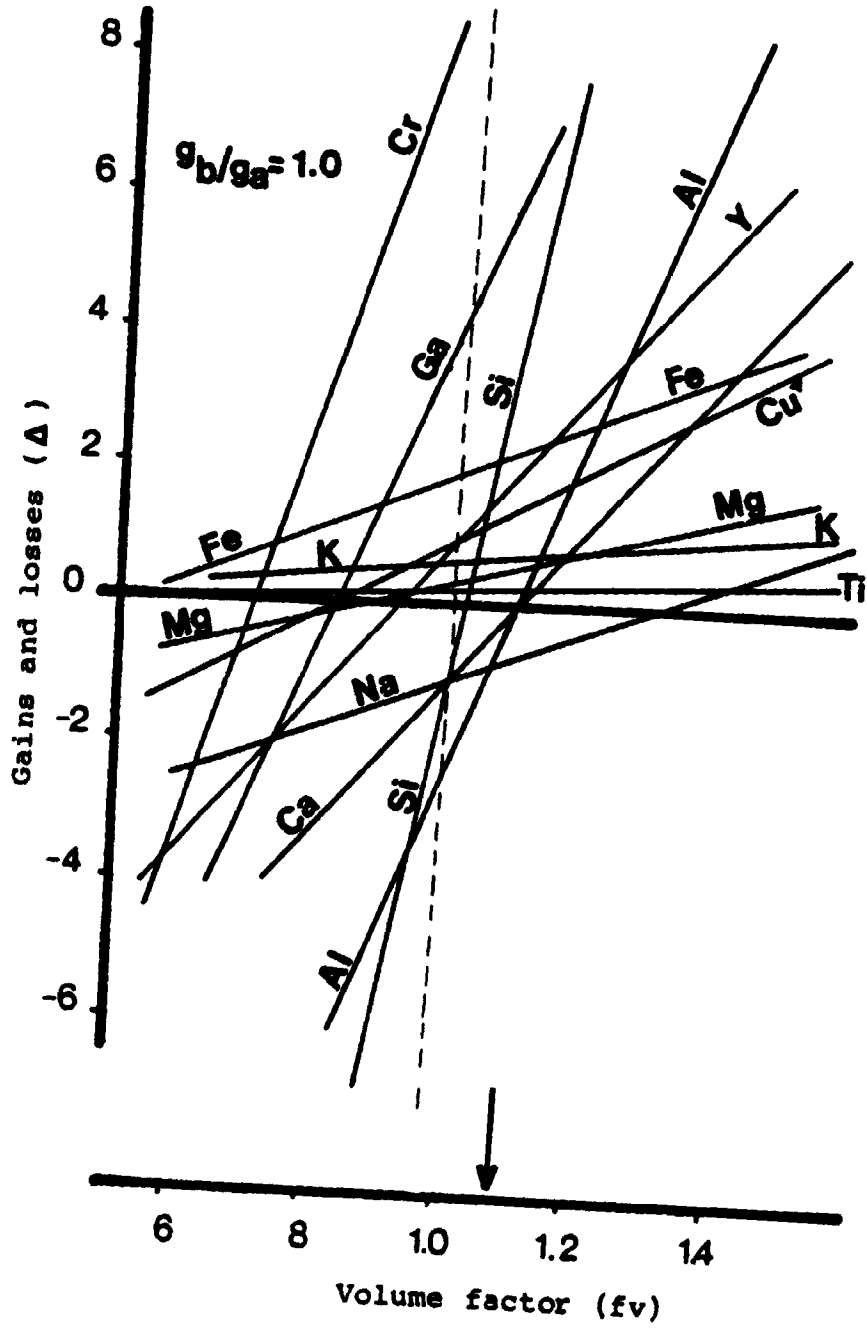


Figure 5-3. Composition-volume diagram showing the transformation of unmodified anorthosite (PS-85-17) to moderately modified anorthosite (PS-85-2). The gains and losses, shown along the ordinate, are in grams per 100 grams of parent rock for major elements, and μ grams per gram for trace elements. The vertical dashed line represents an isovolumetric transformation. The horizontal line represents an isochemical transformation. The arrow indicates the value of volume factor derived from the intersections of lines representing presumed immobile components.

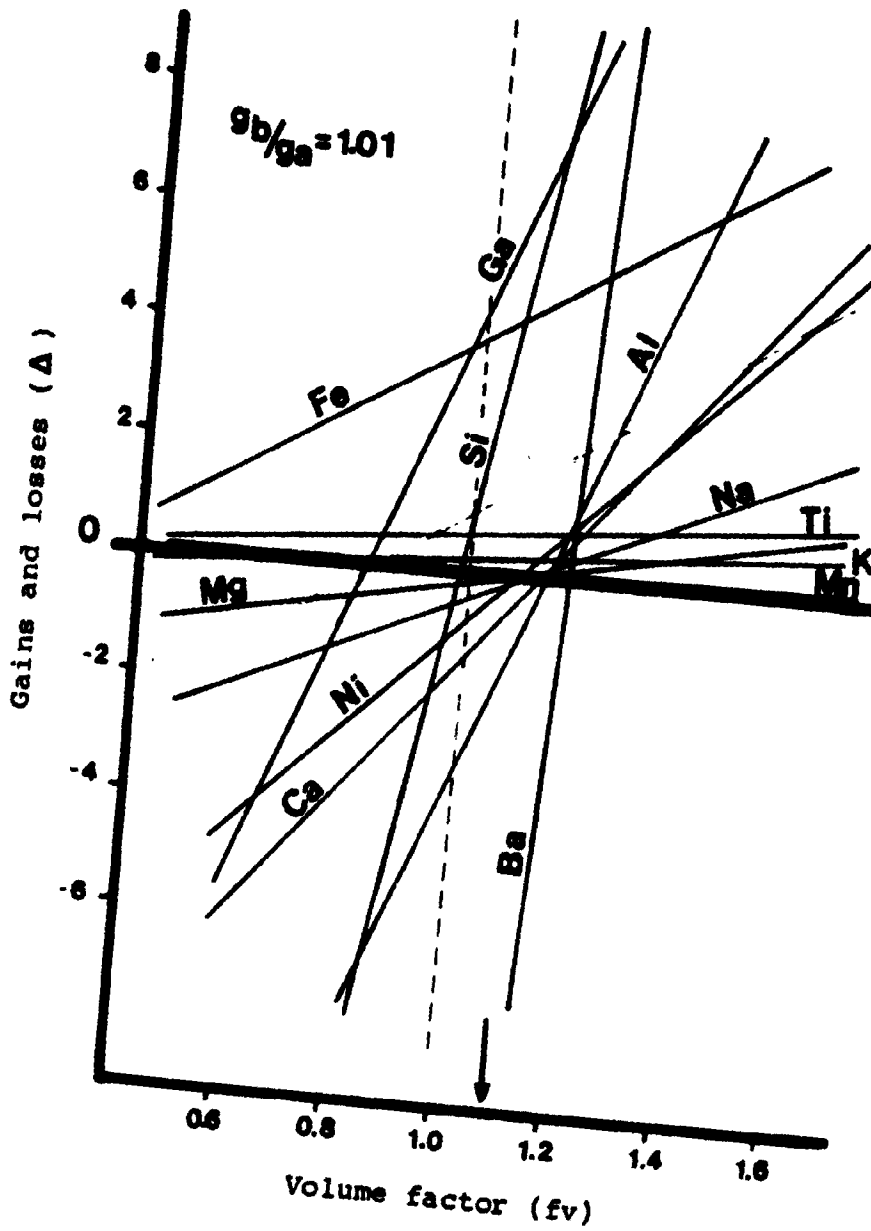
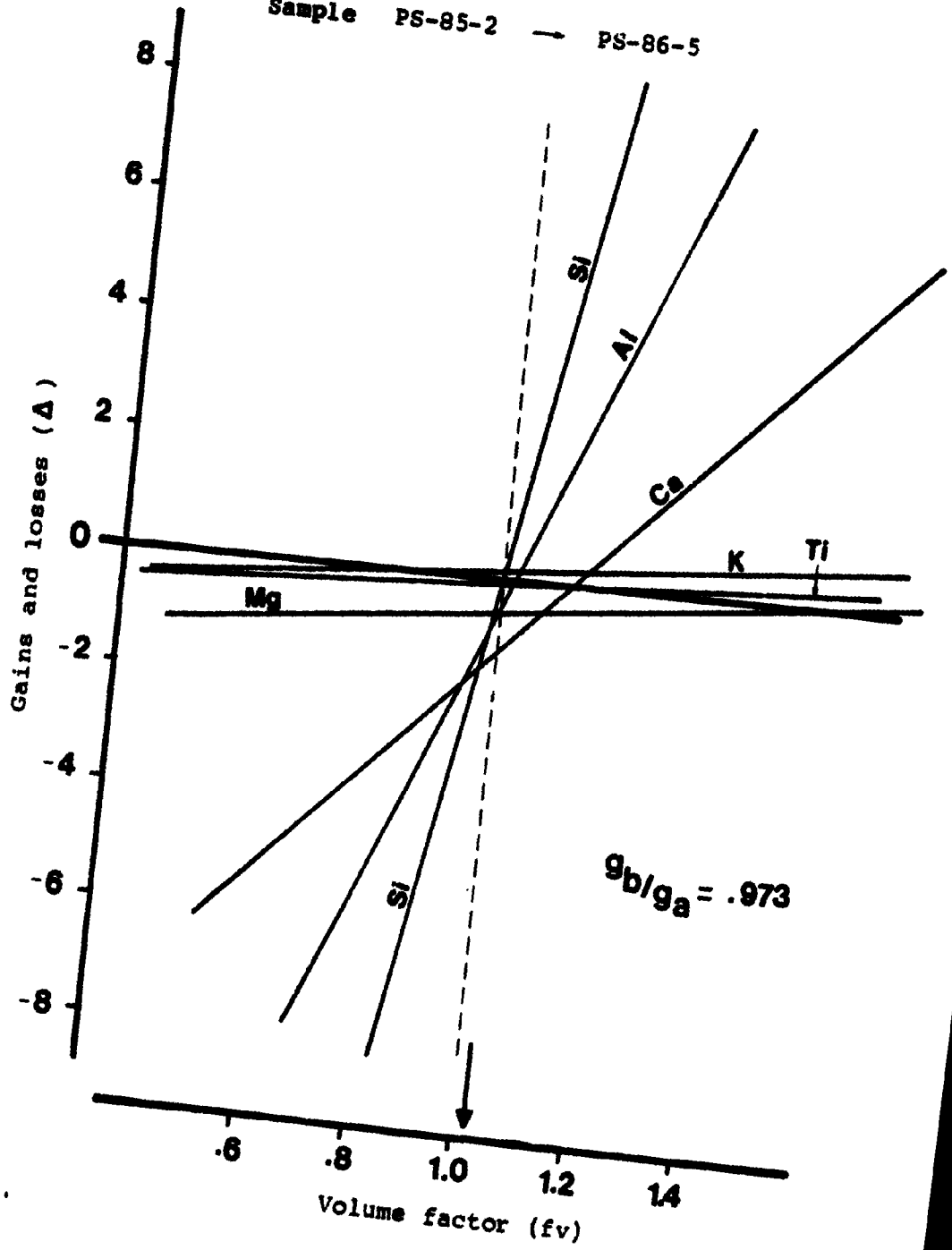


Figure 5-4 a&b. Composition-volume diagram showing the transformation of moderately modified anorthosite (PS-85-2) to type I mylonite (PS-86-5). The gains and losses, shown along the ordinate, are in grams per 100 grams of parent rock for major elements, and μ grams per gram for trace elements. The vertical dashed line represents the isovolumetric transformation. The horizontal line represents the isochemical transformation. The arrow indicates the value of volume factor derived from the intersections of lines representing presumed immobile components.

si major oxides

Sample PS-85-2 → PS-86-5



b) minor and trace elements

Sample PS-85-2 → PS-86-5

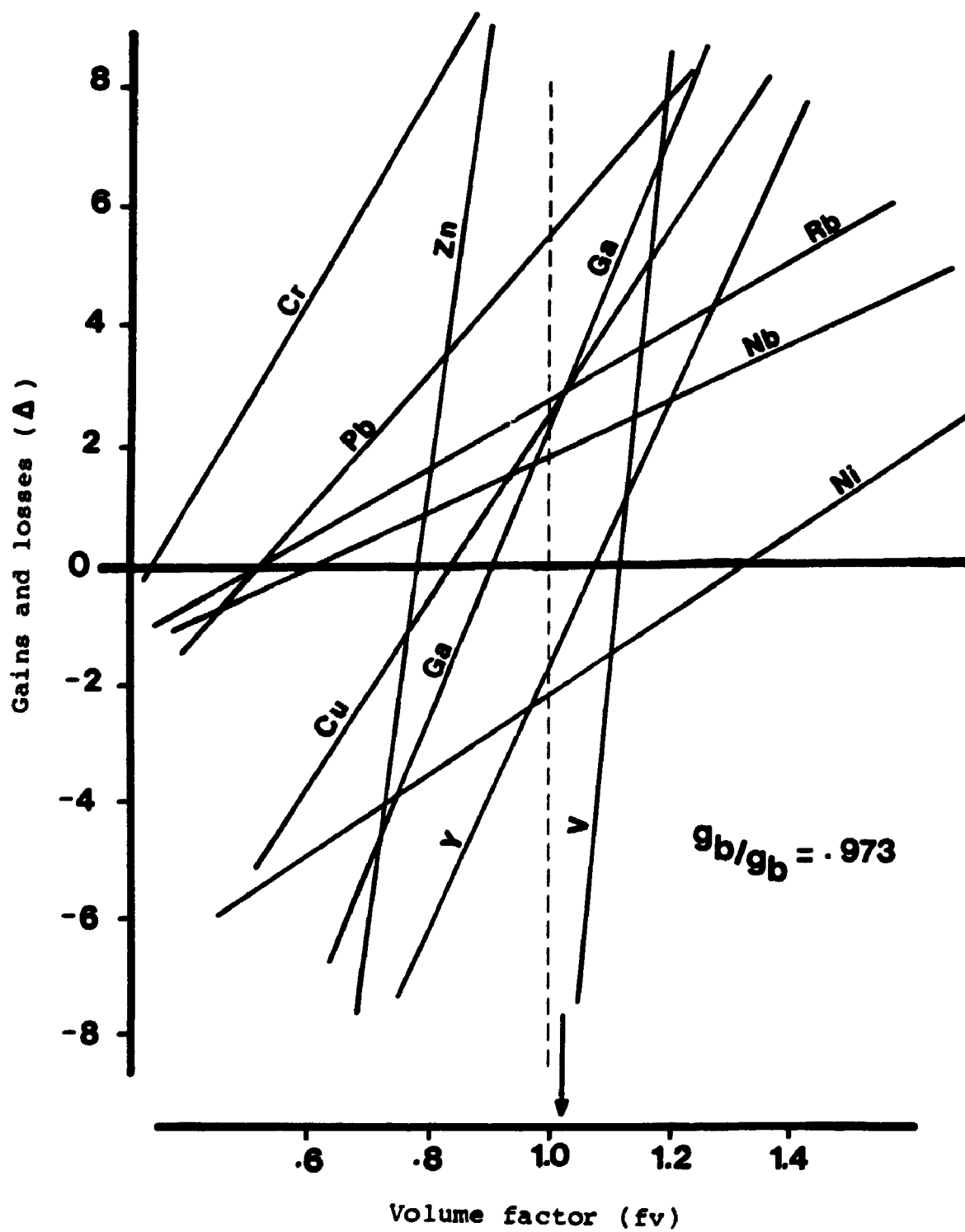


Figure 5-5. Composition-volume diagram showing the transformation of moderately modified anorthosite (PS-85-2) to type II mylonite (PS-86-4). The gains and losses, shown along the ordinate, are in grams per 100 grams of parent rock for major elements, and μ grams per gram for trace elements. The vertical dashed line represents the isovolumetric transformation. The horizontal line represents the isochemical transformation. The arrow indicates the value of volume factor derived from the intersections of lines representing presumed immobile components.

Sample PS-85-2 → PS-86-4

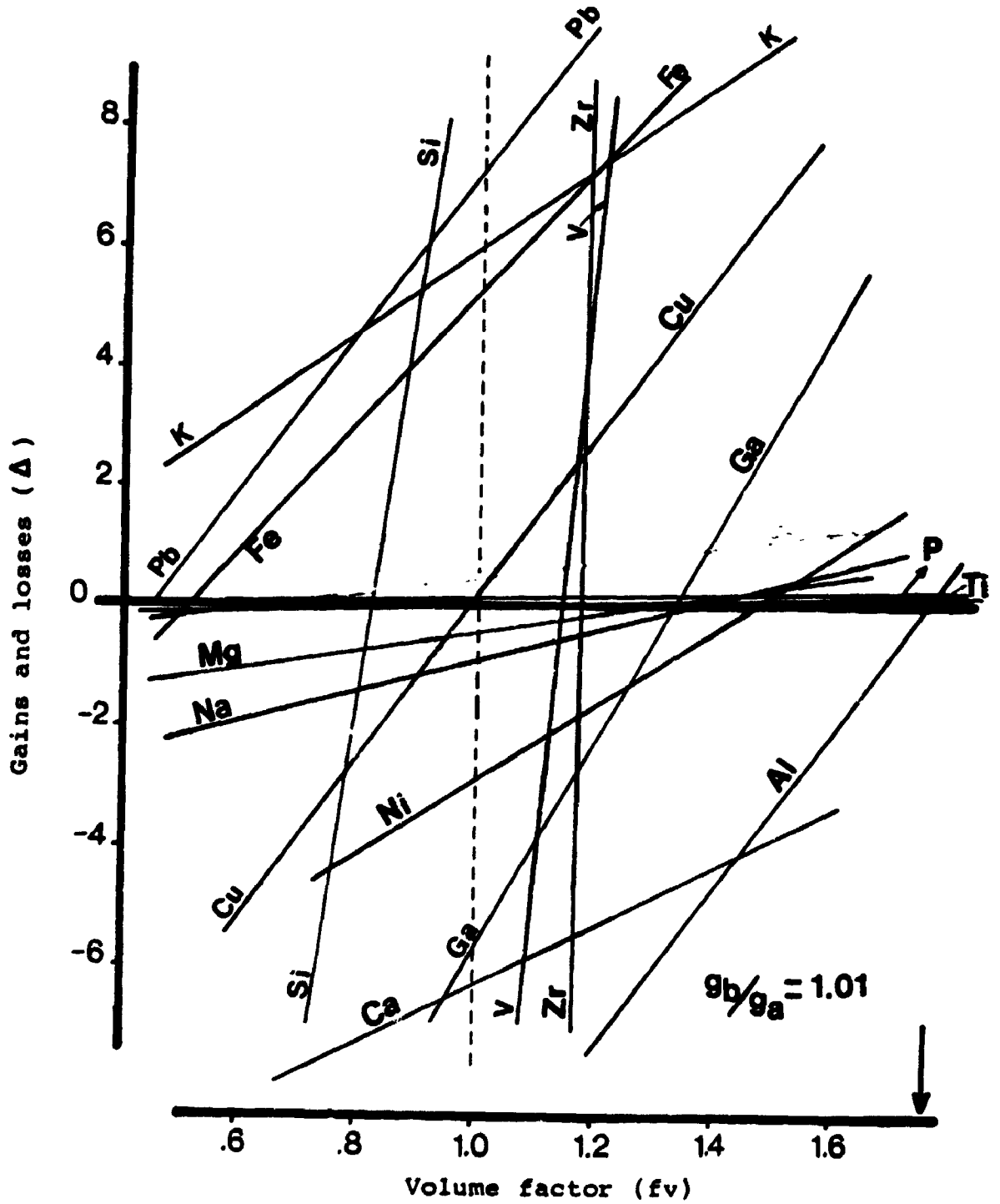


Table 5-2. Compositional changes in increasingly modified
Whitestone Anorthosite in the Parry Sound Shear Zone.
PS-85-17, unmodified anorthosite; PS-85-7, weakly modified
anorthosite; PS-85-2, moderately modified anorthosite;
PS-86-5, type I mylonite; PS-86-4, type II mylonite. Total
Fe expressed as Fe_2O_3 ; Loss on ignition at $1000^\circ C$ (LOI)
adjusted for oxidation of FeO; Volume factors are derived
from composition-volume diagrams in Figs. 5-2 to 5-5.

	from: PS-85-17	PS-85-17	PS-85-2	PS-85-2
	to: PS-85-7	PS-85-2	PS-86-5	PS-86-4
Volume fact.	1.1	1.09	1.02	1.75
SiO ₂	+3.88	+6.26	+1.12	+57.88
TiO ₂	+0.26	+0.78	-0.07	+1.46
Al ₂ O ₃	+0.01	-0.98	+0.09	+0.17
Fe ₂ O ₃	+2.23	+4.54	-0.53	+13.40
MnO	+0.03	-0.07	0.00	+0.27
MgO	+0.59	+0.02	-0.54	+0.64
CaO	-0.07	-0.29	-1.01	-2.73
K ₂ O	+0.73	+0.33	+0.19	+2.74
P ₂ O ₅	+0.00	+0.39	-0.22	+0.20
Na ₂ O	-0.74	-0.04	+1.08	+1.04
LOI	+0.26	-0.04	-0.08	+0.64

Table 5-3. Oxidation state of iron in increasingly modified Whitestone Anorthosite in the Parry Sound Shear Zone. PS-85-17, unmodified anorthosite; PS-85-7, weakly modified anorthosite; PS-85-2, moderately modified anorthosite; PS-86-5, type I mylonite; PS-86-4, type II mylonite.

SAMPLE #	Total Fe	FeO	Fe ₂ O ₃	Ox. Index
PS-85-17	1.70	1.00	0.59	53.95
PS-85-7	3.60	2.25	1.10	49.46
PS-85-2	5.58	3.42	1.78	51.01
PS-86-5	5.08	3.40	1.31	43.66
PS-86-4	10.70	7.60	2.27	37.42

components (Thompson, 1983). However, increases in SiO_2 and K_2O reflect the flux of fluid through the shear zone.

Table 5-3 lists the oxidation indices of iron in the Whitestone Anorthosite. A gradual decrease in the oxidation index between the undeformed anorthosite and the modified anorthosites and the mylonites, and evidence of different $^{18}\text{O}/^{16}\text{O}$ ratios of the original anorthosite and their deformed counterparts (Shieh and Schwarcz, 1974; Personal communication with Shieh, 1987) suggest a change in the character of the fluid. Thus, the large changes noted above for PS-86-4 in Figure 5-5 and Table 5-2 may in part be related to a change in the character of the fluid.

5.3.2 LOCAL SHEAR ZONES

The chemical investigation of local shear zones involved the analysis of suites consisting of specimens from the strongly deformed centre of the shear zone, from the less deformed edge of the shear zone, and from the host rock adjacent to the shear zone. These specimens are expected to show the chemical modification of the host rock with increasing deformation within the shear zone. Analyses were conducted on representative suites of samples from both an anastomosing and a planar shear zone.

Table 5-4 lists the chemical compositions of the anorthosite with increasing deformation in an anastomosing

shear zone from traverse I. The locations of analyzed specimens are shown in Figure 5-6. Changes in SiO_2 , Fe_2O_3 , K_2O , CaO and Na_2O are most notable. The increases in SiO_2 , and K_2O and decreases in Na_2O and CaO are similar to those observed in type II mylonites (compare with Table 5-1, PS-86-4).

Figure 5-7 is a component-ratio diagram for the data in Table 5-4 normalized to the Al_2O_3 content of each sample. The normalized values of Na_2O , CaO and MgO show least variation which suggests that these elements were relatively unaffected by deformation and that the anorthosite was initially homogeneous. The normalized values of SiO_2 , and K_2O increase with increasing deformation while the normalized values of TiO_2 , Fe_2O_3 and MgO increase near the less deformed edge of the shear zone, but decrease towards the center of the shear zone. The pattern of increase in these elements is similar to the enrichment of immobile elements around marginal zones of the Whitestone Anorthosite (Thompson, 1983).

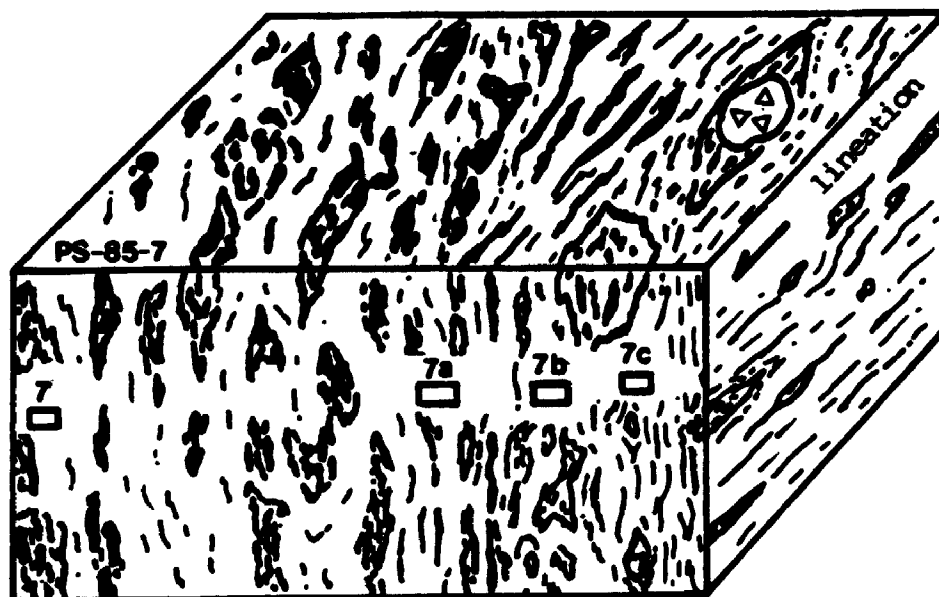
The composition/volume changes accompanying the transformation of weakly modified anorthosite by the anastomosing shear zone are illustrated in Figures 5-8, 5-9, and 5-10. The composition/volume change associated with the transformation of weakly modified anorthosite in the proximity of the shear zone is illustrated by Figure 5-8, which shows considerable separation between lines

Table 5-4. Abundances of major elements expressed as oxides in samples from an anastomosing shear zone.

PS-85-7, weakly modified anorthosite; PS-85-7a, weakly modified anorthosite near the anastomosing shear zone; PS-85-7b, anorthosite from the less deformed edge of the shear zone; PS-85-7c, anorthosite from the strongly deformed center of the shear zone. Loss on ignition at 1000°C (LOI) adjusted for oxidation of FeO; Total Fe expressed as Fe₂O₃. Specific gravity (S.G.) in gm/cm³.

SAMPLE #	PS-85-7	PS-85-7a	PS-86-7b	PS--86-7c
SiO ₂	51.85	64.39	66.34	74.50
TiO ₂	0.38	0.64	0.26	0.11
Al ₂ O ₃	24.42	17.32	16.98	14.05
Fe ₂ O ₃	3.60	3.49	2.17	0.72
MnO	0.05	0.03	0.02	0.01
MgO	2.44	2.43	1.67	1.20
CaO	11.55	5.27	4.61	3.12
K ₂ O	1.01	1.90	2.43	2.81
P ₂ O ₅	0.03	0.05	0.00	0.00
Na ₂ O	3.40	3.48	4.10	2.01
LOI	0.77	0.60	0.67	0.44
Total	99.50	99.60	99.25	98.97
S.G.	2.82	2.73	2.64	2.62

Figure 5-6. Block-diagram of an anastomosing shear zone in weakly modified anorthosite indicating the locations of analyzed samples.



† shear zone

Scale:

0 7 cm

legend:



schistosity indicated
by amphibole clots

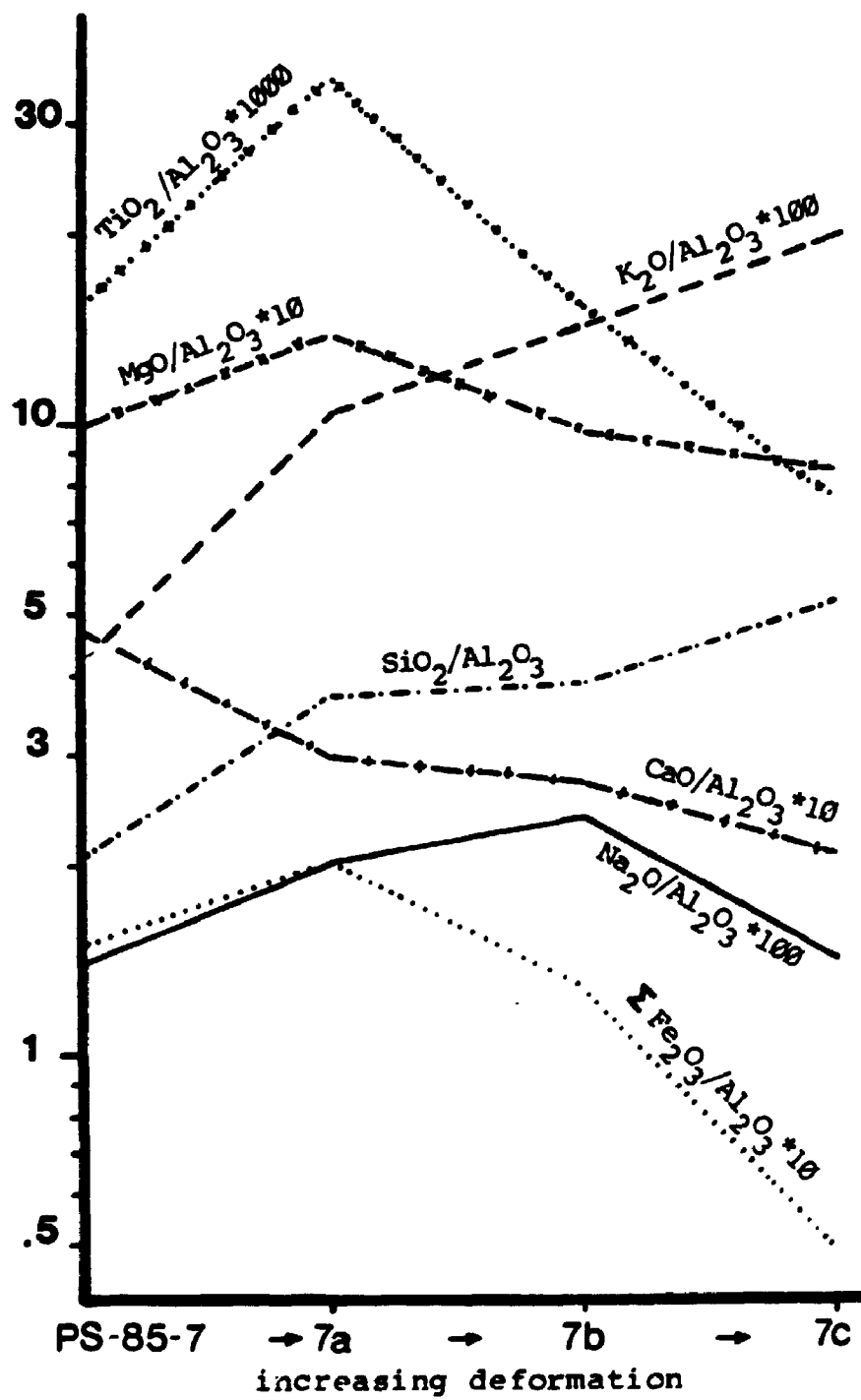


locations of
analyzed specimens



feldspar augen

Figure 5-7. Component ratio diagram for specimens from an anastomosing shear zone. PS-85-7, weakly modified anorthosite; PS-85-7a, weakly modified anorthosite near the anastomosing shear zone; PS-85-7b, less deformed edge of the shear zone; PS-85-7c, strongly deformed center of the shear zone.



representing presumed immobile elements. Al_2O_3 , Ga, and V are lost, while Ni, K_2O , SiO_2 are gained. Figure 5-9 illustrates the composition/volume change associated with the transformation of weakly modified anorthosite near the shear zone to the less deformed edge of the shear zone. Al_2O_3 , SiO_2 , and Rb intersect near a volume factor of 1.06. Components for which gains are indicated are K_2O , MgO, and Na_2O ; components for which losses are indicated are CaO, Fe_2O_3 , Sr, Y and Ga. The composition/volume change associated with the transformation of anorthosite from the less deformed edge to the strongly deformed center of the shear zone is illustrated by Figure 5-10. Lines representing presumed immobile components such as Al_2O_3 , Ga, and Ni intersect different values of volume factors. Lines representing rare earth elements and mobile elements such as CaO, Na_2O , MgO and K_2O also intersect different values of volume factors.

The variation in the intersections of the lines representing presumed immobile components Al, Ni, Ga and V on the X axis in Figures 5-8, 5-9 and 5-10 suggests allovolumetric reactions for the anastomosing shear zone. A volume increase of more than 70% is indicated if Al_2O_3 is presumed immobile (see Table 5-5). This increase is similar to that suggested above for the type II mylonite (compare with Table 5-2, PS-86-4).

Table 5-5 lists suggested chemical changes at

Figure 5-8. Composition-volume diagram showing the transformation of weakly modified anorthosite (PS-85-7) to weakly modified anorthosite near the anastomosing shear zone (PS-85-7a). The gains and losses, shown along the ordinate, are in grams per 100 grams of parent rock for major elements, and μ grams per gram for trace elements. The vertical dashed line represents the isovolumetric transformation. The horizontal line represents the isochemical transformation. The arrow indicates the value of volume factor derived from the intersection of lines representing presumed immobile components.

Sample PS-85-7 → PS-85-7a

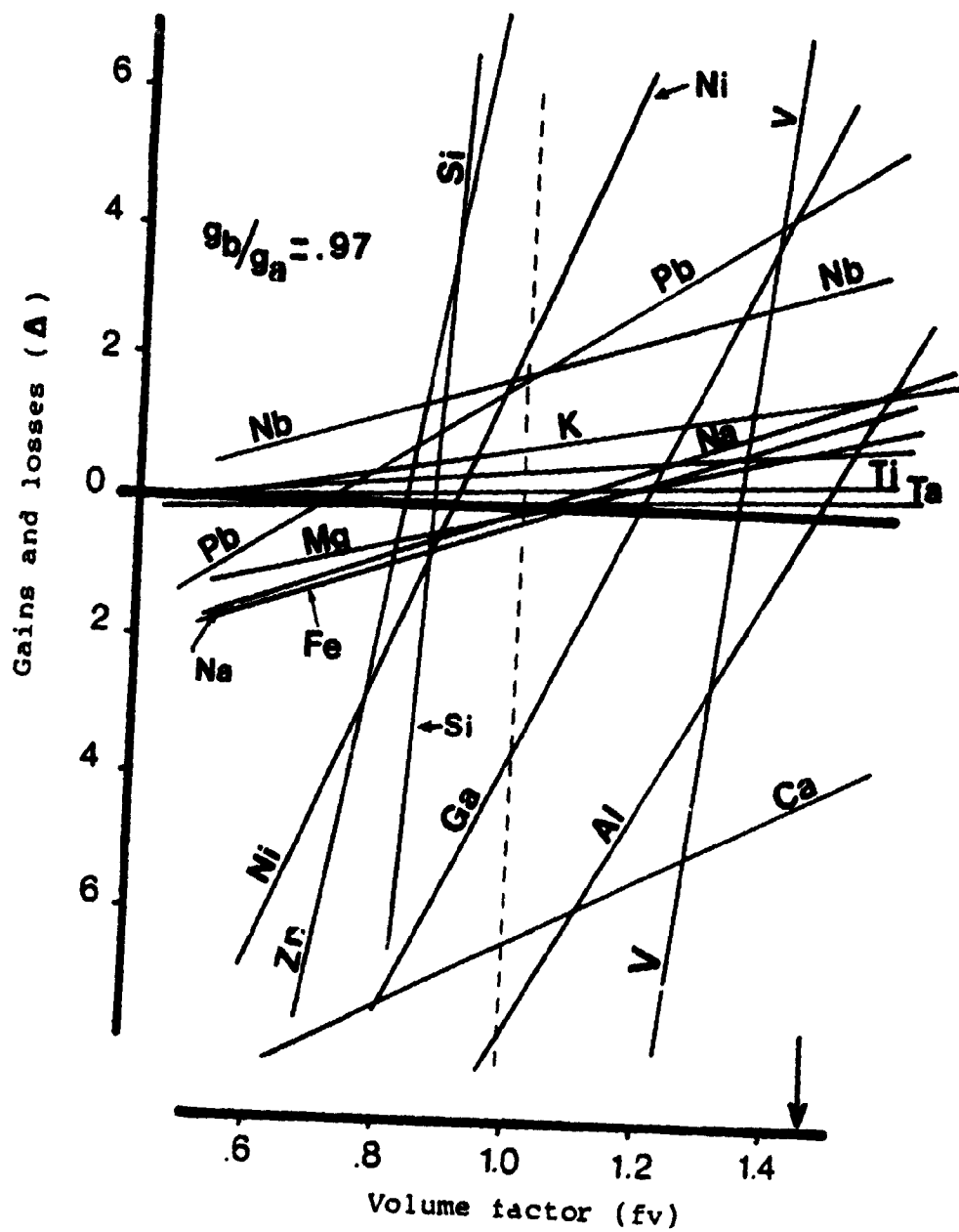
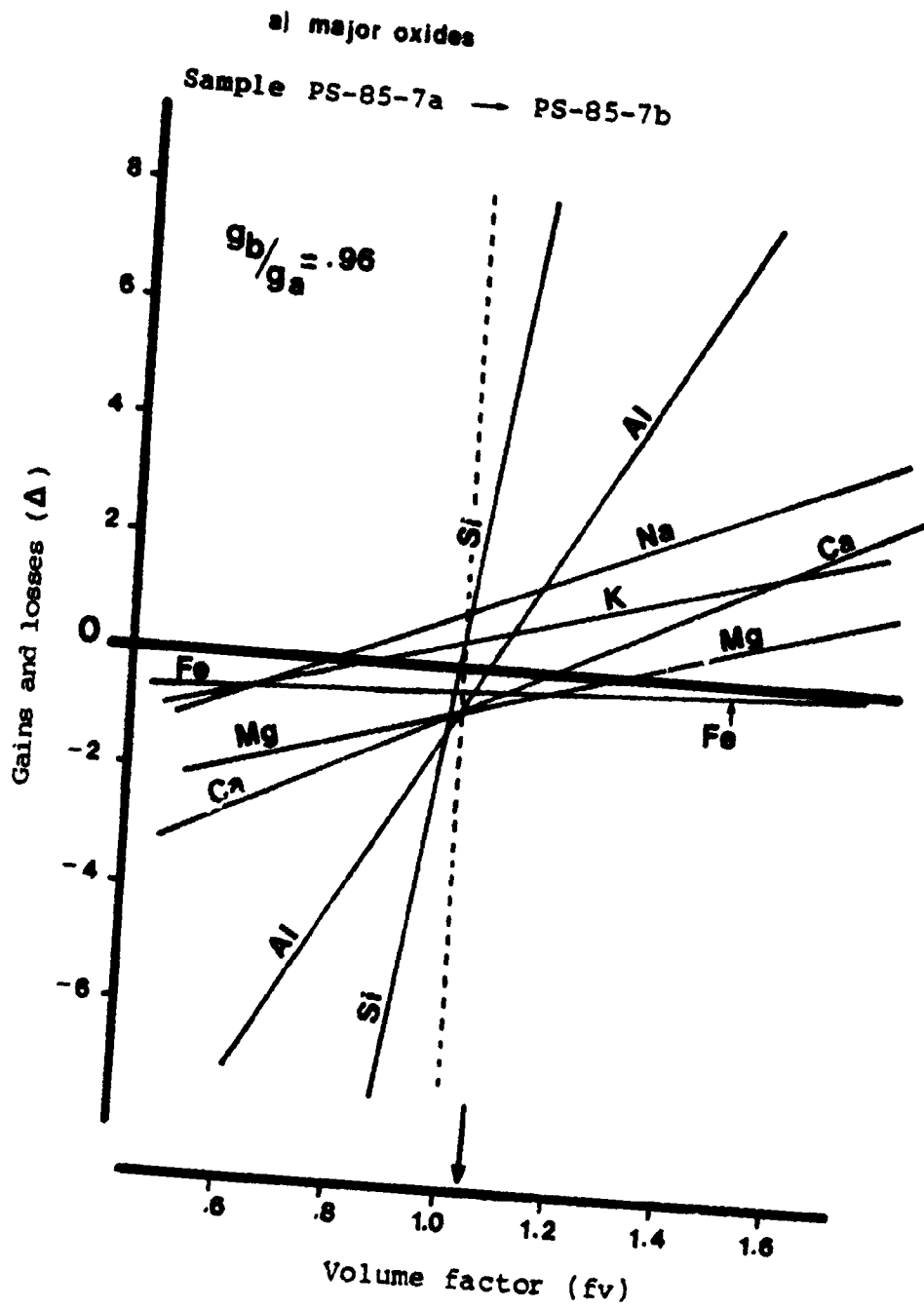


Figure 5-9 a&b. Composition-volume diagram showing the transformation of weakly modified anorthosite near the anastomosing shear zone (PS-85-7a) to anorthosite at less deformed edge of the shear zone (PS-85-7b). The gains and losses, shown along the ordinate, are in grams per 100 grams of parent rock for major elements, and μ grams per gram for trace elements. The vertical dashed line represents the isovolumetric transformation. The horizontal line represents the isochemical transformation. The arrow indicates the value of volume factor derived from the intersection of lines representing presumed immobile components.



b) minor and trace elements

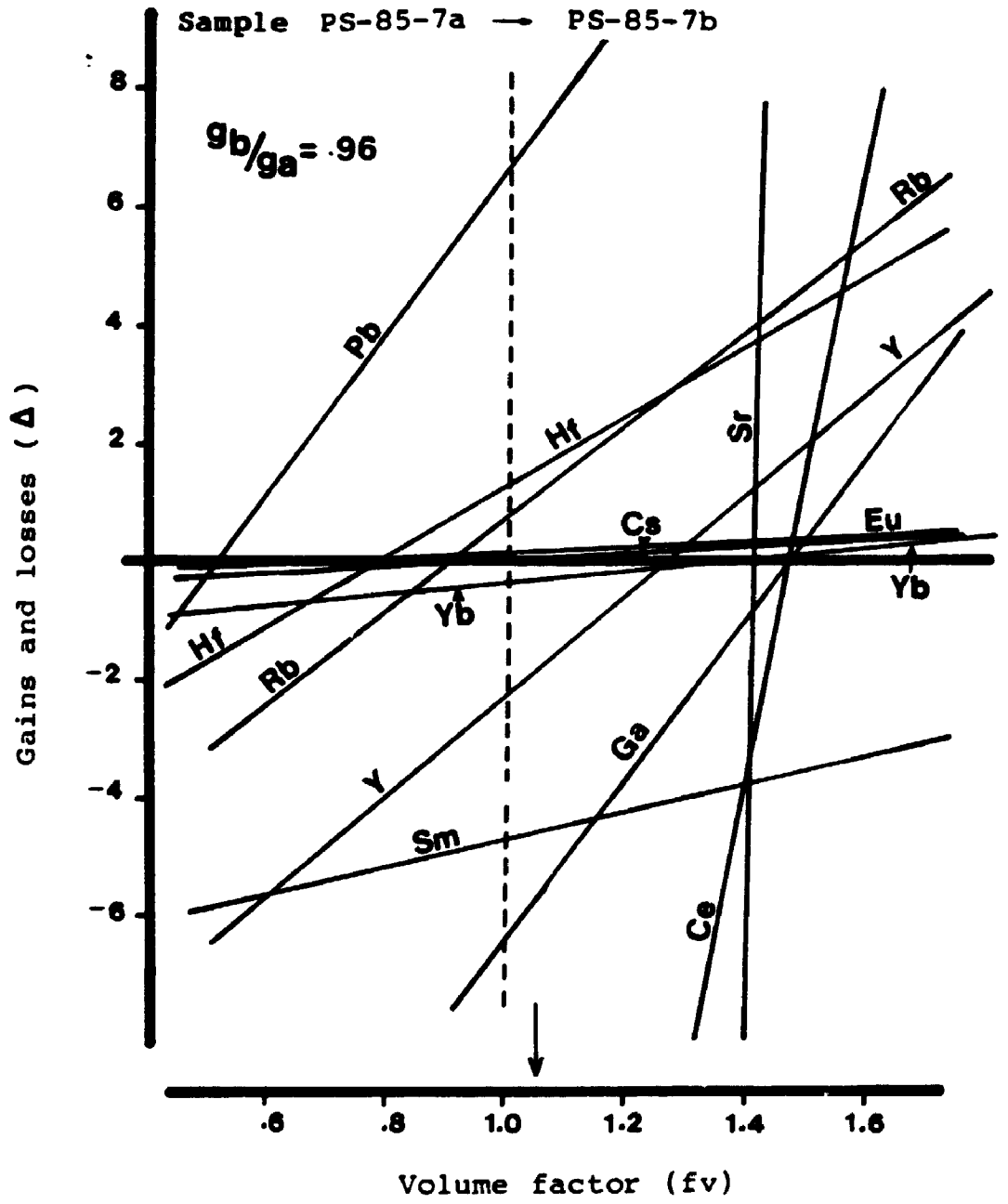
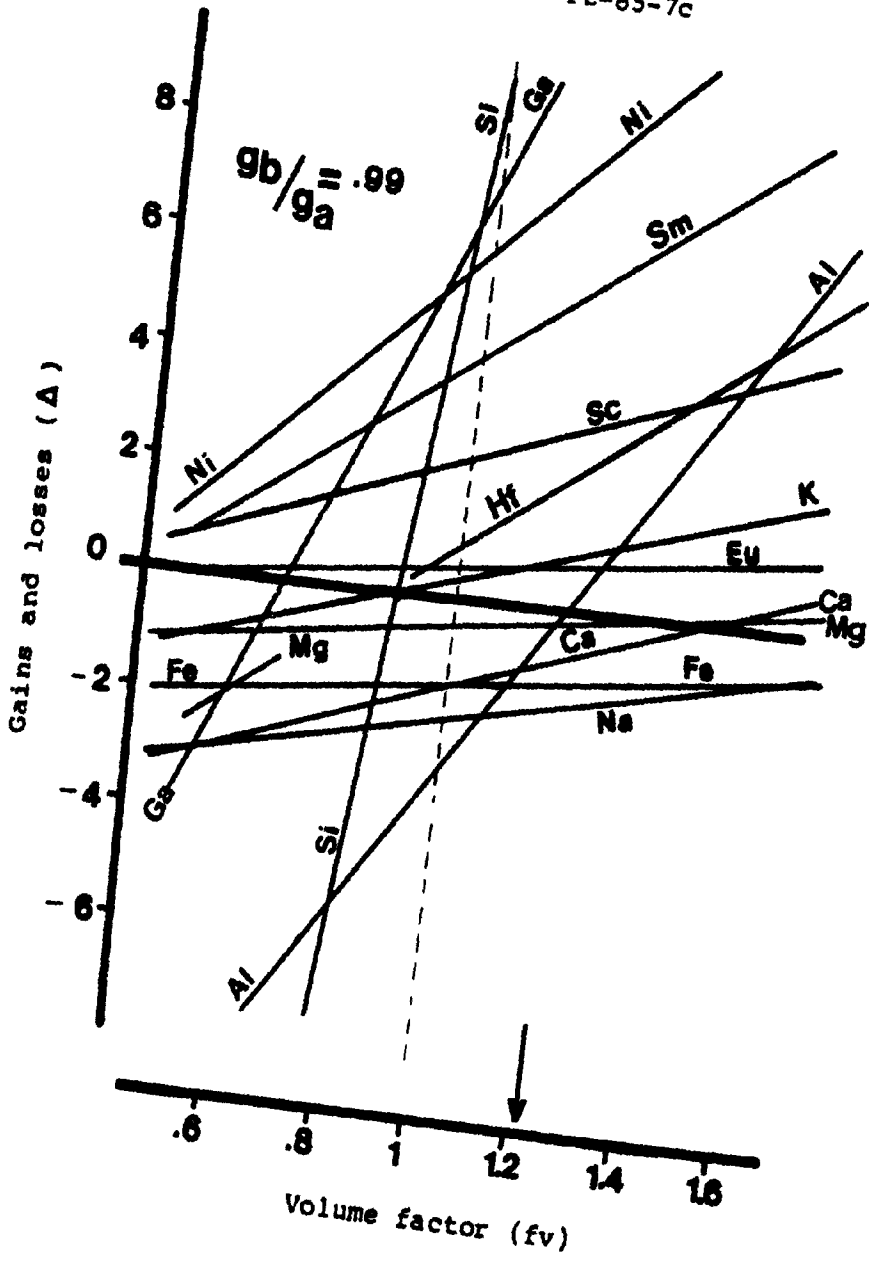


Figure 5-10. Composition-volume diagram showing the transformation of anorthosite from the less deformed edge of the anastomosing shear zone (PS-85-7b) to the strongly deformed center of the shear zone (PS-85-7c). The gains and losses, shown along the ordinate, are in grams per 100 grams of parent rock for major elements, and μ grams per gram for trace elements. The vertical dashed line represents the isovolumetric transformation. The horizontal line represents the isochemical transformation. The arrow indicates the value of volume factor derived from the intersection of lines representing presumed immobile components.

Sample PS-85-7b → PS-85-7c



increasing increments of deformation in the anastomosing shear zone. Specimen PS-85-7b, representing weakly modified anorthosite near the anastomosing shear zone, differs significantly from its weakly modified anorthosite host. Increases in SiO_2 , Fe_2O_3 , MgO and K_2O , and decreases in CaO and Na_2O are most notable. Specimens PS-85-7b and PS-85-7c, representing anorthosite from the less deformed edge of the shear zone and anorthosite from the strongly deformed center of the shear zone respectively, undergo chemical changes relative to less deformed counterparts. The most prominent changes are increases in SiO_2 and K_2O , and decreases in Fe_2O_3 , CaO and Na_2O . In summary, the data in Table 5-5 indicate that large losses in CaO and Na_2O , and significant increases in K_2O and SiO_2 accompanied the anastomosing shear zone development. These chemical changes are similar to those observed in type II mylonite noted above (specimen PS-86-4). Figure 5-11 illustrates these compositional changes associated with the transformations across the anastomosing shear zone.

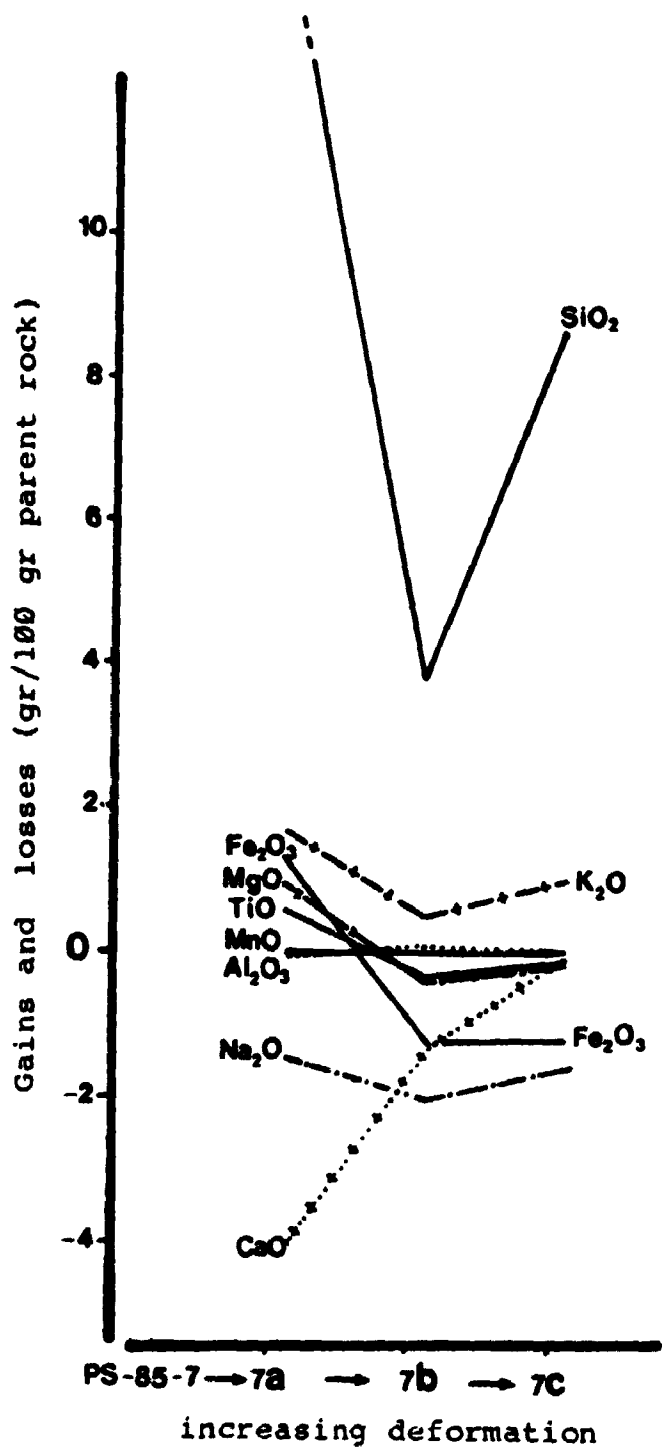
The oxidation state of iron in the anastomosing shear zone shows significant decreases relative to the oxidation state of its host (i.e. weakly modified anorthosite), Table 5-6.

A detailed chemical analysis was conducted on a planar shear zone from area A, Traverse II. Figure 5-12 illustrates the locations of the analyzed specimens.

Table 5-5. Compositional changes associated with an anastomosing shear zone. PS-85-7, weakly modified anorthosite; PS-85-7a, weakly modified anorthosite near the anastomosing shear zone; PS-85-7b, anorthosite from the less deformed edge of the shear zone; PS-85-7c, anorthosite from the strongly deformed center of the shear zone. Loss on ignition at 1000° C (LOI) adjusted for oxidation of FeO; Total Fe expressed as Fe₂O₃; Specific gravity (S.G.) in gm/cm³. Volume factors are derived from compositon-volume diagrams in Figs. 5-7 to 5-9.

	from: PS-85-7	PS-85-7a	PS-85-7b
	to: PS-85-7a	PS-85-7b	PS-86-7c
Volume fact.	1.45	1.06	1.22
SiO ₂	+39.60	+3.74	+23.70
TiO ₂	+0.52	-0.37	-0.15
Al ₂ O ₃	-0.09	+0.12	+0.00
Fe ₂ O ₃	+1.30	-1.26	-1.30
MnO	0.00	-0.01	0.00
MgO	+0.97	-0.48	-0.22
CaO	-4.14	-1.40	-0.22
K ₂ O	+1.65	+0.45	+0.96
P ₂ O ₅	+0.04	+0.00	-0.00
Na ₂ O	-1.49	-2.03	-1.67
LOI	+0.07	-0.22	-0.14

Figure 5-11. Compositional variation of the Whitestone Anorthosite across an anastomosing shear zone. PS-85-7, weakly modified anorthosite; PS-85-7a, weakly modified anorthosite near the anastomosing shear zone; PS-85-7b, less deformed edge of the shear zone; PS-85-7c, strongly deformed center of the shear zone.



97

Table 5-6. Oxidation state of iron in an anastomosing shear zone. PS-85-7, weakly modified anorthosite; PS-85-7a, weakly modified anorthosite near the anastomosing shear zone; PS-85-7b, less deformed edge of the anastomosing shear zone; PS-85-7c, strongly deformed center of the anastomosing shear zone.

SAMPLE #	Total Fe ₂ O ₃	FeO	Fe ₂ O ₃	Ox. Index
PS-85-7	3.60	2.25	1.10	49.46
PS-85-7a	3.49	2.68	0.51	27.83
PS-85-7b	2.17	1.64	0.89	29.76
PS-85-7c	0.72	0.63	0.02	5.36

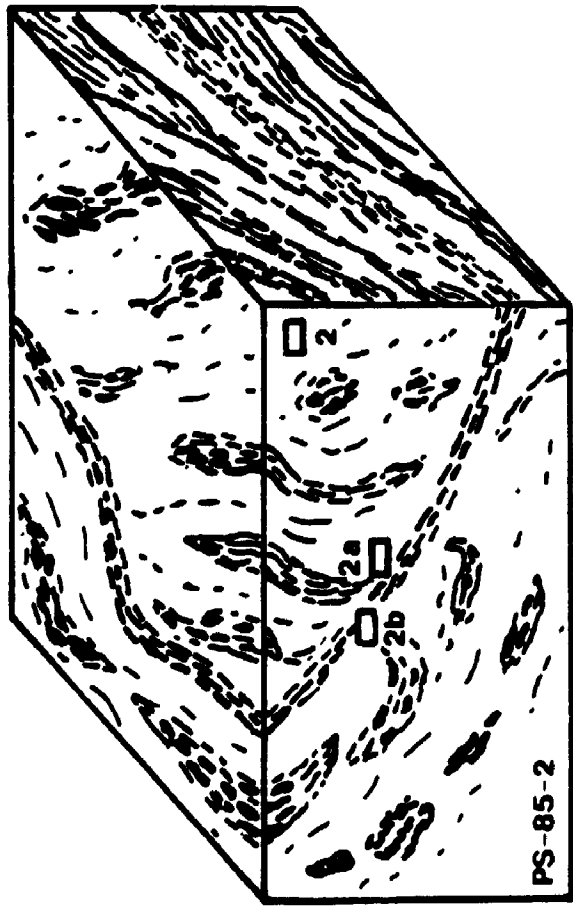
Table 5-7 lists the compositions of the anorthosites with increasing deformation in the planar shear zone sample. Small apparent changes in K_2O , CaO and Na_2O are most notable, and the changes are different from those recorded in the anastomosing shear zone (Table 5-4).

Figure 5-13 illustrates the composition/volume changes associated with the transformation of moderately modified anorthosite in the center of the planar shear zone. The intersection of the lines representing relatively immobile elements such as Al, Ni and V on the X axis near $fv=1$ suggests a nearly isovolumetric process for the chemical changes associated with the planar shear zone. Components for which gains are indicated are Pb, Ga and Zn. Components for which losses are indicated are Na and Y.




Table 5-8 summarizes the suggested compositional changes accompanying the transformation of the moderately modified anorthosite by the strong deformation at the center of the planar shear zone. The most prominent changes are increases in MgO , K_2O and volatiles and losses in CaO and Na_2O , which are less than 1%. The chemical changes are similar to those observed in moderately deformed anorthosite and type I mylonites (specimens PS-85-2 and PS-86-5, respectively in Table 5-2), but rather different to those noted for the anastomosing shear zone, Table 5-6.

Table 5-9 lists the oxidation state of iron outside

Figure 5-12. Block-diagram of a planar shear zone in moderately modified anorthosite indicating the locations of analyzed samples.



legend :

-  schistosity indicated by amphibole clots
-  planar shear zone
-  locations of analyzed specimens

Scale:  7 cm

Table 5-7. Abundances of major elements, expressed as oxides, in samples from a planar shear zone. PS-85-2, moderately modified anorthosite outside the shear zone; PS-85-2a, less deformed edge of the shear zone; PS-85-2b, strongly deformed center of the shear zone. Loss on ignition at 1000°C (LOI) adjusted for oxidation of FeO; Total Fe expressed as Fe₂O₃; Specific gravity (S.G.) in gm/cm³.

SAMPLE #	PS-85-2	PS-85-2a	PS-85-2b
SiO ₂	51.83	51.74	51.36
TiO ₂	0.83	1.11	0.73
Al ₂ O ₃	22.98	23.59	22.60
Fe ₂ O ₃	5.58	6.38	5.34
MnO	0.08	0.08	0.06
MgO	1.88	1.76	2.03
CaO	11.10	10.57	10.64
K ₂ O	0.63	0.69	1.54
P ₂ O ₅	0.35	0.11	0.13
Na ₂ O	3.95	3.86	3.17
LOI	0.48	0.30	1.39
Total	99.59	100.19	98.99
S.G.	2.86	n.d.	2.84

Figure 5-13. Composition-volume diagram showing the transformation of moderately modified anorthosite (PS-85-2) to the strongly deformed center of a planar shear zone (PS-85-2b). The gains and losses, shown along the ordinate, are in grams per 100 grams of parent rock for major elements, and μ grams per gram for trace elements. The vertical dashed line represents the isovolumetric transformation. The horizontal line represents the isochemical transformation. The arrow indicates the value of volume factor derived from the intersection of lines representing presumed immobile components.

Sample PS-85-2 → PS-85-2b

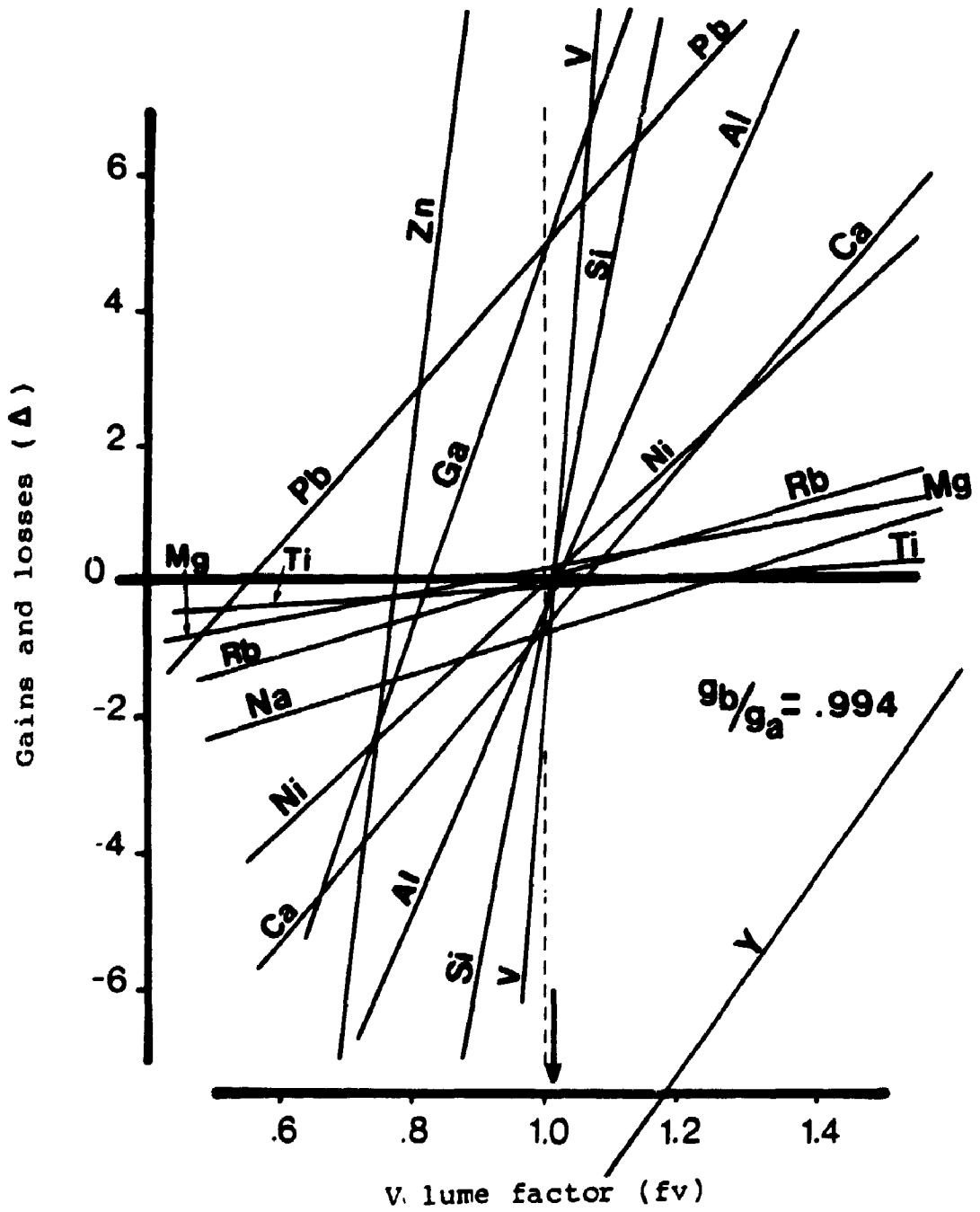


Table 5-8. Compositional changes associated with a planar shear zone. PS-85-2, moderately modified anorthosite outside the shear zone. PS-85-2a, less deformed edge of the shear zone; PS-85-2b, strongly deformed center of the shear zone. Loss on ignition at 1000° C (LOI) adjusted for oxidation of FeO; Total Fe expressed as Fe₂O₃; Volume changes accompanying increasing modification are determined from compositional volume diagrams in Fig. 5-11.

from: PS-85-2

to: PS-85-2b

Volume fact.	1.01
SiO ₂	+0.31
TiO ₂	-0.09
Al ₂ O ₃	-0.04
Fe ₂ O ₃	-0.16
MnO	-0.02
MgO	+0.14
CaO	-0.30
K ₂ O	+0.93
P ₂ O ₅	-0.22
Na ₂ O	-0.73
LOI	+0.93

12
6 .

Table 5-9. Oxidation state of iron in a planar shear zone.
PS-85-2, moderately modified anorthosite outside the
shear zone; PS-85-2b, strongly deformed center of the shear
zone.

SAMPLE #	Total Fe ₂ O ₃	FeO	Fe ₂ O ₃	Ox. Index
PS-85-2	5.58	3.42	1.78	51.01
PS-85-2b	5.34	3.93	0.98	33.20

and within the planar shear zone. The oxidation state of iron within the planar shear zone is similar to that in its host and is consistent with the observed small compositional changes (Table 5-8).

5.4 SUMMARY

Chemical analyses were performed on fourteen samples selected as representing the modified anorthosites. The results of the chemical analyses suggest that there are two distinct modified anorthosite compositions present in the Parry Sound shear zone. The first is enriched predominantly in CO_2 , and to some degree in Fe_2O_3 , and SiO_2 , it occurs in moderately modified anorthosite, type I mylonite and in planar shear zones. Isovolumetric transformations and nearly constant oxidation states of iron characterize these anorthosites. The second anorthosite composition is richer in SiO_2 , K_2O and occurs in weakly modified anorthosite, type II mylonite and in anastomosing shear zones. Allovolumetric transformations and decreasing oxidation states of iron typify anorthosites of the second set. The presence of two chemically distinct modified anorthosites leads the author to suggest that there were at least two different metasomatic events associated with different metamorphic conditions during the deformation history of the Parry

Sound Shear Zone.

CHAPTER 6

QUARTZ AND FELDSPAR FABRICS IN THE WHITESTONE ANORTHO SITE

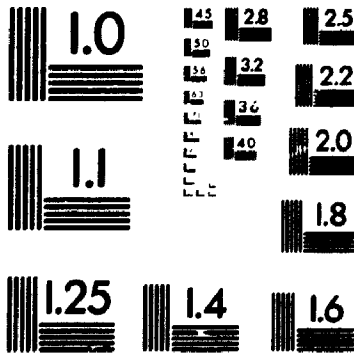
6.1 GENERAL STATEMENT

This chapter presents results of analyses of the crystallographic orientation of quartz and plagioclase feldspar in the deformed anorthosite. The objective is to contribute to the understanding of deformation of the Whitestone Anorthosite in the Parry Sound Shear Zone.

6.2 METHOD

Petrofabric analyses were carried out by a technique similar to that described by Starkey and Cutford (1978). First, the optical orientations were measured in thin sections cut normal to the foliation in orientations both normal and parallel to the lineation. In addition, X-ray diffraction has been used to obtain crystallographic orientation data for quartz in some of the samples (see Starkey, 1964). Orientation diagrams were prepared by contouring the data on an equal area, upper hemisphere, spherical projection.

3



6.3 RESULTS

6.3.1 QUARTZ FABRIC

Petrofabric analyses were carried out separately for quartz in ribbons and isolated quartz grains in the matrix of type II mylonites and anastomosing shear zones.

Orientation diagrams have been prepared from the optically determined orientations of quartz c-axes using an interactive version of a computer program in which the statistical distribution is independent of the sample size (Starkey, 1970). In order to compare the orientation patterns in different samples, all orientation patterns were rotated so that in the figures the foliation is vertical and N-S and the lineation is horizontal.

Figures 6-1 and 6-2 show quartz c-axis orientation diagrams for mylonites and anastomosing shear zones of the Whitestone Anorthosite. The computer program used to prepare the orientation diagrams also calculates the mean areas occupied by the different point concentrations of quartz c-axes, and their standard deviations, by sampling the data in intervals of $n/10$, where n is the total sample size. The statistical data obtained from this program are presented in Appendix E. Orientation patterns are considered not to differ significantly from random when the mean area occupied by empty space is within one

standard deviation of 36.8 % (see Starkey, 1977). On this basis, isolated quartz grains in the matrix of the type II mylonites and the anastomosing shear zones have random or near random patterns. The quartz in quartz ribbons in the same specimens have non-random patterns (Figs. 6-1 and 6-2).

Two different preferred orientation patterns are observed. In the quartz in quartz ribbons in both of the specimens from the anastomosing shear zone (PS-85-19 and PS-85-16, Fig. 6-2) and in one of the type II mylonites (PS-86-4, Fig. 6-1), a single maximum occurs in the plane of foliation, normal to the lineation, while in the remaining specimens of the type II mylonites (PS-85-12, PS-85-13, PS-85-14, Figs. 6-1), the c-axes are distributed in a great circle girdle at a high angle to the lineation. The girdles contain more than two maxima. The girdle in specimen PS-85-12 differs from the girdles in PS-85-13 and PS-85-14 in that it is normal to the lineation.

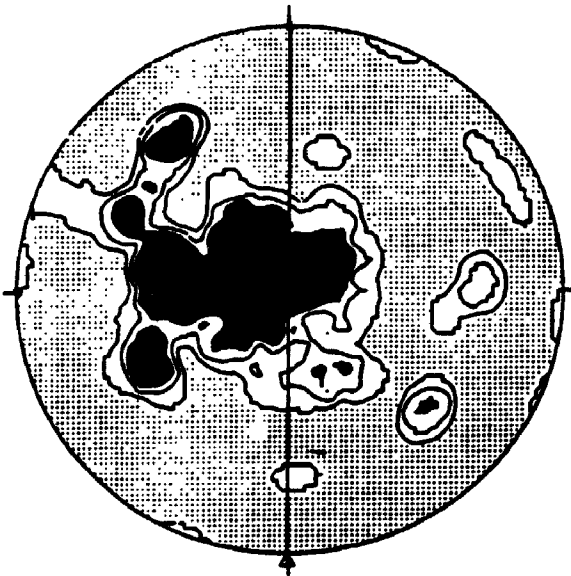
The orientation of quartz in a mylonite and an anastomosing shear zone specimen investigated optically was also investigated by X-ray diffraction. The crystal orientation of quartz grains in the ribbons could not be determined because of the difficulty of isolating a suitable quartz ribbon. The results indicate that the isolated grains in the matrix do not have a detectable preferred crystal orientation of $\{10\bar{1}1\}$ which is

Figure 6-1. Quartz c-axis orientation patterns in type II mylonites. For each specimen except PS-85-14, separate diagrams are presented for quartz in quartz ribbons and for isolated quartz grains in the matrix between the ribbons. In specimen PS-85-14 only quartz in quartz ribbons was measured. The foliation is indicated by the vertical line. The lineation is indicated by the arrow.

Quartz in Quartz Ribbons

SPECIMEN PS-86-4

93 DATA

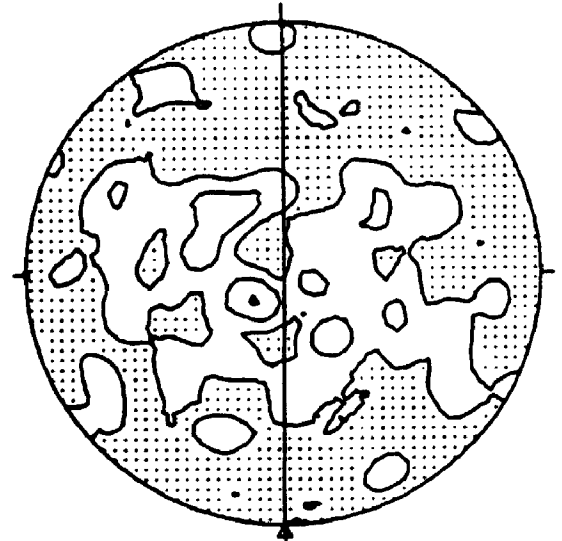


CONTOURED AT 1 2 3 POINTS PER 1.1 % AREA

Isolated Quartz grains

SPECIMEN PS-86-4

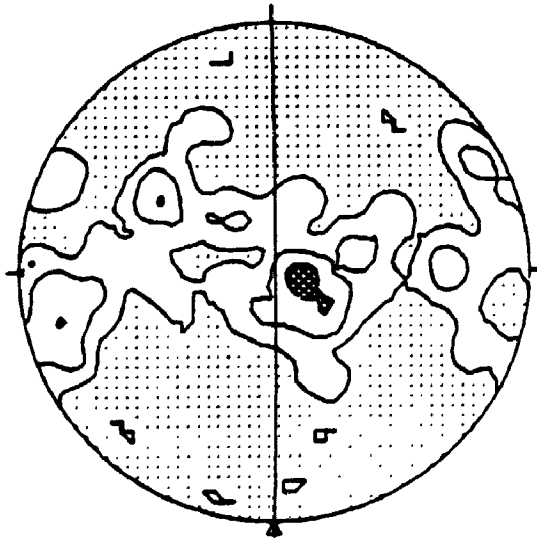
140 DATA



CONTOURED AT 1 3 5 POINTS PER 0.7 % AREA

SPECIMEN PS-85-12

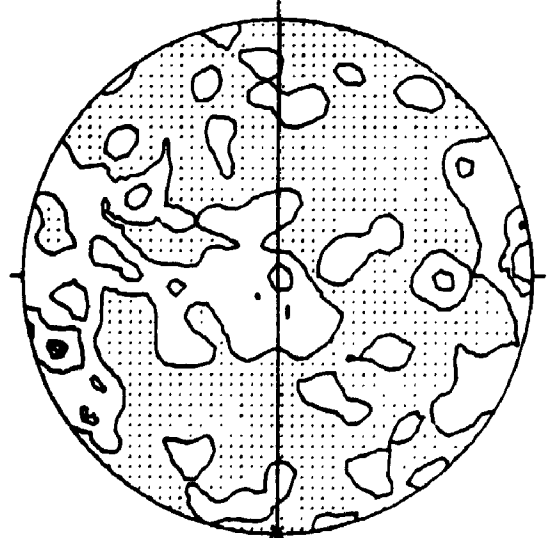
89 DATA



CONTOURED AT 1 3 5 POINTS PER 1.1 % AREA

SPECIMEN PS-85-12

218 DATA



CONTOURED AT 1 3 5 POINTS PER 0.4 % AREA

Fig. 6-1 continued

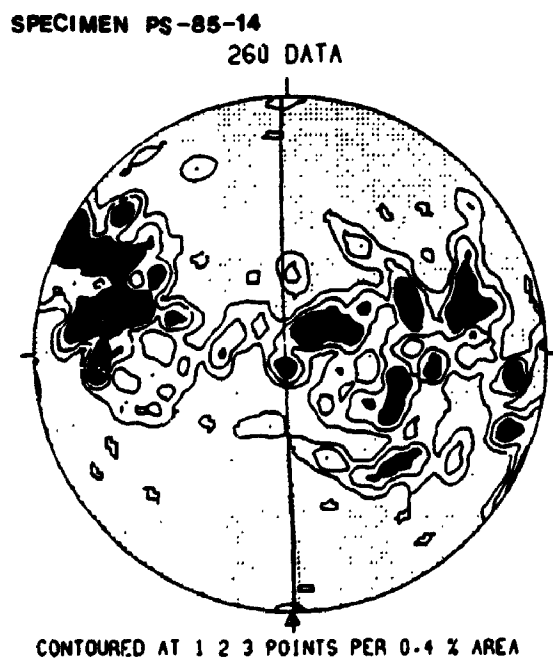
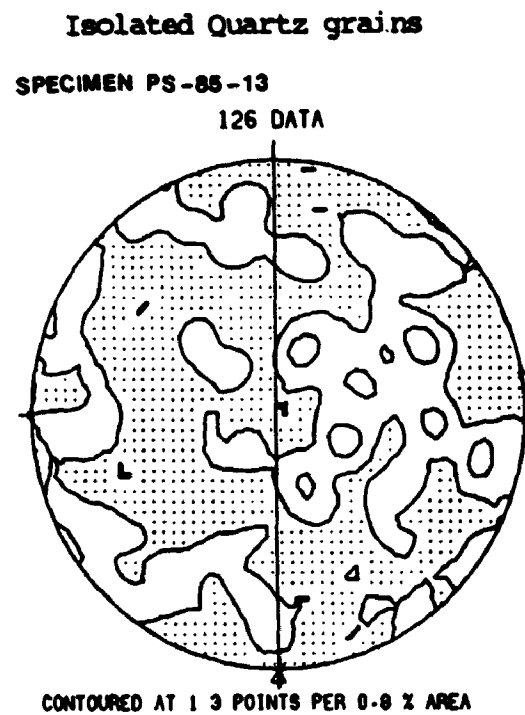
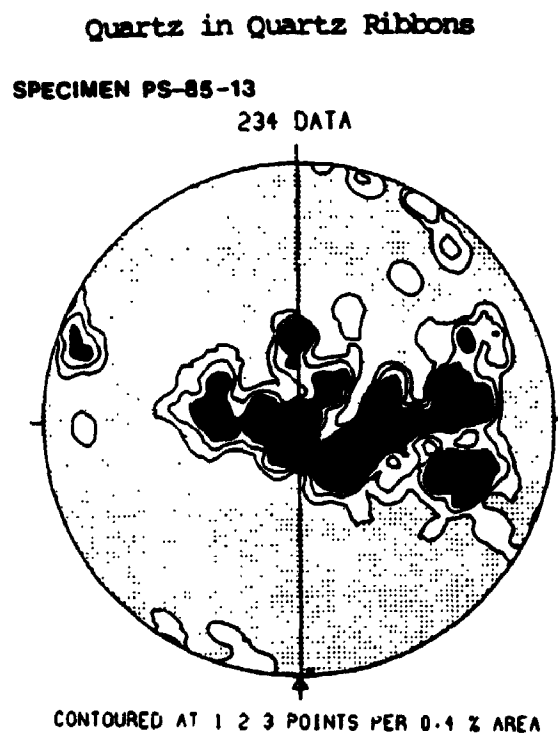
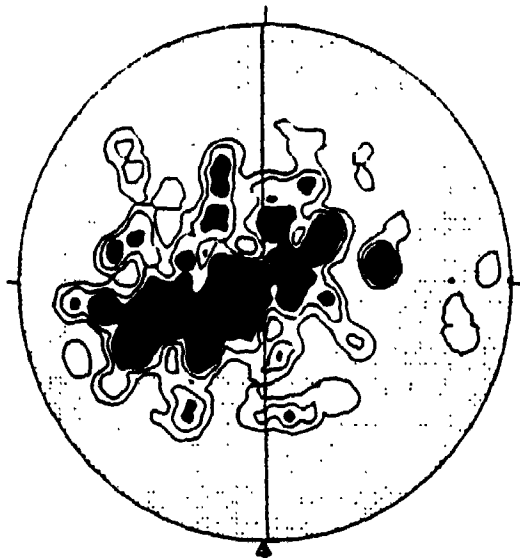


Figure 6-2. Quartz c-axis orientation patterns in anastomosing shear zones. For specimen PS-85-19 separate diagrams are presented for quartz in quartz ribbons and for isolated quartz grains. The foliation is indicated by the vertical line. The orientation of the lineation is indicated by the arrow.

Quartz in Quartz Ribbons

SPECIMEN PS-85-19

230 DATA

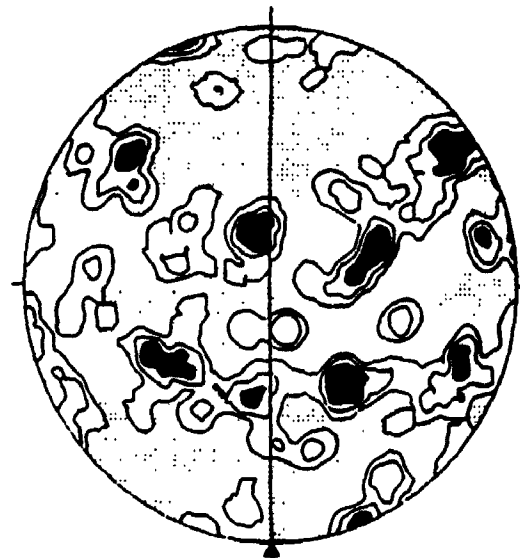


CONTOURED AT 1 2 3 POINTS PER 0.4 % AREA

Isolated Quartz grains

SPECIMEN PS-85-19

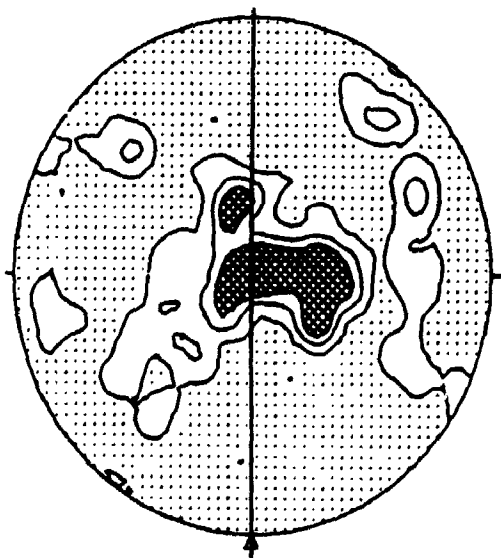
182 DATA



CONTOURED AT 1 2 3 POINTS PER 0.5 % AREA

SPECIMEN PS-85-16

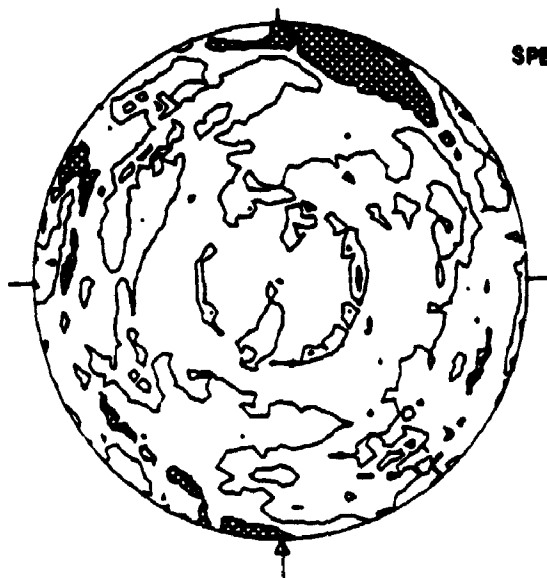
167 DATA



CONTOURED AT 1 3 5 POINTS PER 0.6 % AREA

Figure 6-3. The distribution of the poles to $\{10\bar{1}1\}$ of quartz in anastomosing shear zone specimen PS-85-16 and type II mylonite specimen PS-85-12. Data are plotted on the upper hemisphere of the equal area projection. Areas of maximum concentrations are indicated by cross-hatching. In both figures the foliation coincides with the plane of projection. The orientation of the lineation is indicated by the arrow.

SPECIMEN PS-85-16



CONTOUR VALUES 0.5 1.0 1.5

MINIMUM = 0.2

MAXIMUM = 2.0

UNIFORM = 4.1

SPECIMEN PS-85-12



CONTOUR VALUES 0.3 0.6 0.9 1.2

MINIMUM = 0.3

MAXIMUM = 1.4

UNIFORM = 109.6

consistent with the observed random orientation of c-axes (Fig. 6-3).

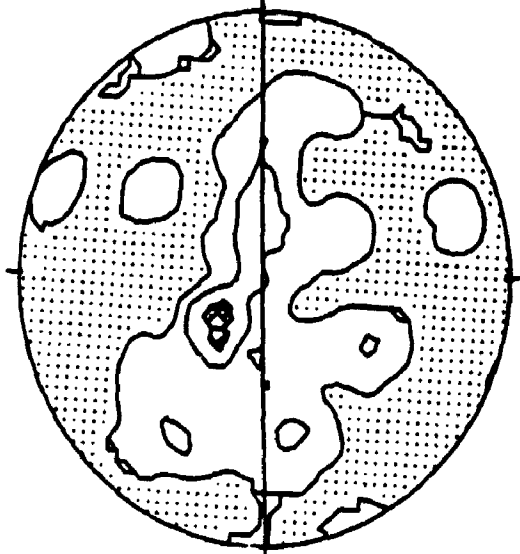
6.3.2 PLAGIOCLASE FELDSPAR FABRICS

Petrofabric analyses of plagioclase feldspar were conducted on six specimens representing weakly, moderately, and strongly modified anorthosite, type I and II mylonites and a planar shear zone. The orientations of the optic indicatrix axes of plagioclase were measured using a universal stage. From these data, orientation diagrams were prepared using an interactive version of a computer program written by Starkey (1970). The orientation diagrams were rotated to an orientation where the foliation is vertical and N-S and the lineation is horizontal. The orientation diagrams are reproduced as Figures 6-4, 6-5, 6-6, 6-7, 6-8 and 6-9. The mean areas occupied by different point concentrations, and their standard deviations, are presented in Appendix E. The area occupied by empty space in all the orientation patterns is within one standard deviation of 36.8 %, the value determined by Starkey (1977) to be characteristic of random orientation patterns. Nevertheless, some of the orientation diagrams of the optic indicatrix axes of plagioclase exhibit non-random patterns.

The X indicatrix axes exhibit a random orientation in the moderately modified anorthosite and the type I mylonite (Figs. 6-5 and 6-7). However, the X indicatrix axes tend to lie close to the foliation plane and normal to the lineation in the weakly and the strongly modified anorthosite (Figs. 6-4 and 6-6) and in the planar shear zone (Fig. 6-9), although in the latter the orientation pattern is more complex. In the type II mylonite, Fig. 6-8, the X axes tend to lie normal to the foliation. Similarly, the orientation of the Y indicatrix axes is randomly oriented in the strongly modified anorthosite and in the planar shear zone (Figs. 6-6 and 6-9). However, the Y indicatrix axes have a preferred orientation in the weakly modified anorthosite (Fig. 6-4). The Y axes lie in a girdle parallel to the foliation plane in the moderately modified anorthosite and the type I mylonite (Figs. 6-6 and 6-7), and in a girdle normal to the foliation in the type II mylonite (Fig. 6-8). The Z indicatrix axes exhibit a random orientation pattern in the weakly modified anorthosite, the strongly modified anorthosite, and in the planar shear zone (Figs. 6-4, 6-6 and 6-9). However, a preferred orientation of the Z indicatrix axes can be discerned in the remaining specimens. The Z indicatrix axes lie in a girdle normal to the foliation in the moderately modified anorthosite (Fig. 6-5), and in a girdle oblique to the foliation in the type I and the type

Figure 6-4. Orientation diagrams of the optical directions X, Y and Z of plagioclase grains from weakly modified anorthosite specimen PS-85-7. Orientation of the foliation is approximately N-S vertical. The lineation is nearly N-S horizontal. Equal area projection, upper hemisphere.

X
53 DATA

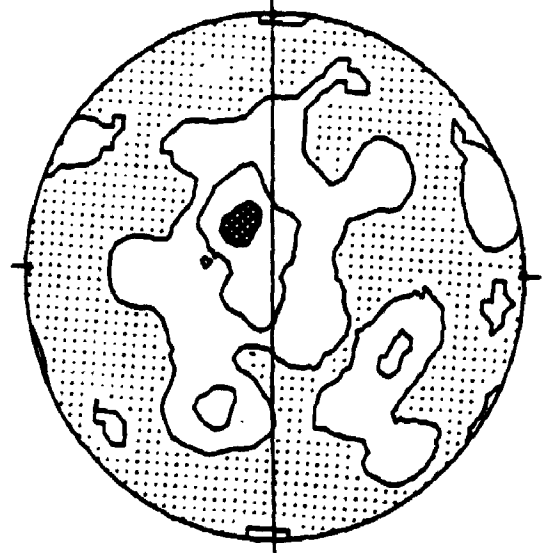


CONTOURED AT 1 3 5 POINTS PER 1.9 % AREA

SPECIMEN PS-85-7,
weakly modified anorthosite.

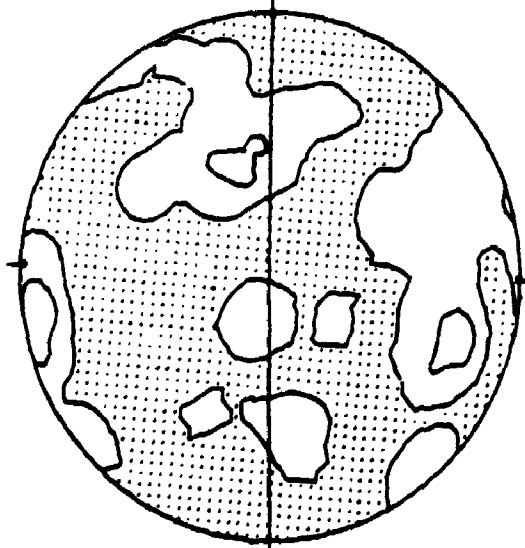
Plagioclase is An40-44.

Y
53 DATA



CONTOURED AT 1 3 5 POINTS PER 1.9 % AREA

Z
53 DATA

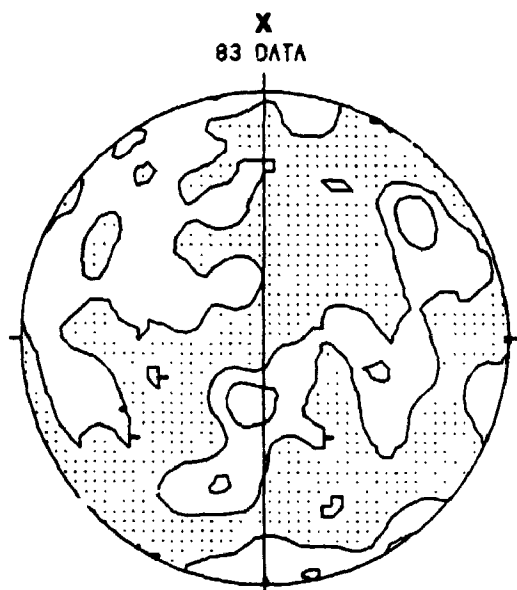


CONTOURED AT 1 3 POINTS PER 1.9 % AREA

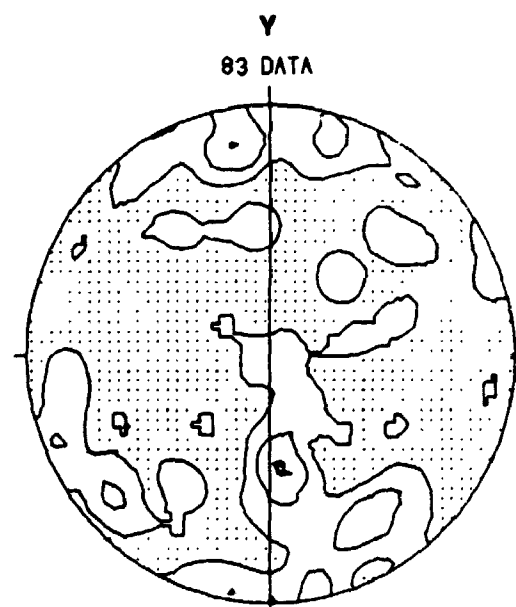
Figure 6-5. Orientation diagrams of the optical directions X, Y and Z of plagioclase grains from moderately modified anorthosite specimen PS-85-2. Orientation of the foliation is N-S vertical. The lineation is N-S horizontal. Equal area projection, upper hemisphere.

SPECIMEN PS-85-2,
moderately modified anorthosite.

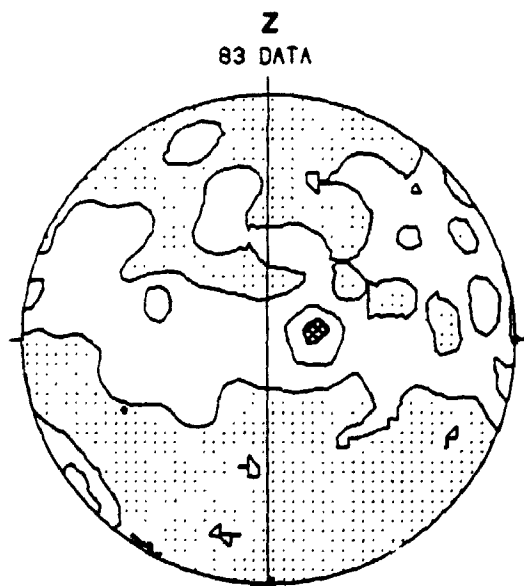
Plagioclase is An49-56.



CONTOURED AT 1 3 POINTS PER 1.2 % AREA



CONTOURED AT 1 3 5 POINTS PER 1.2 % AREA



CONTOURED AT 1 3 5 POINTS PER 1.2 % AREA

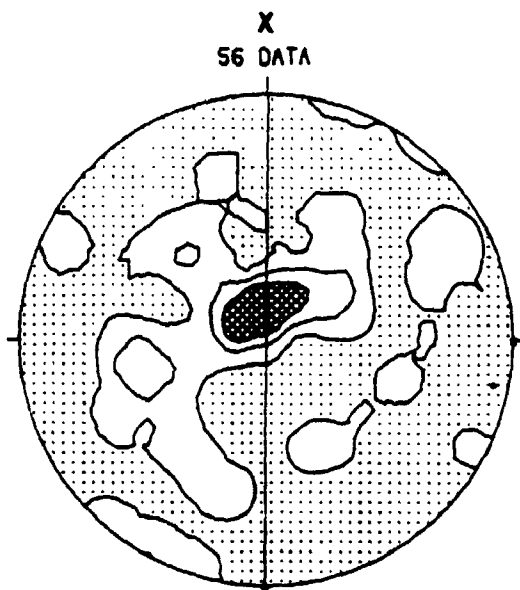
6

8.27

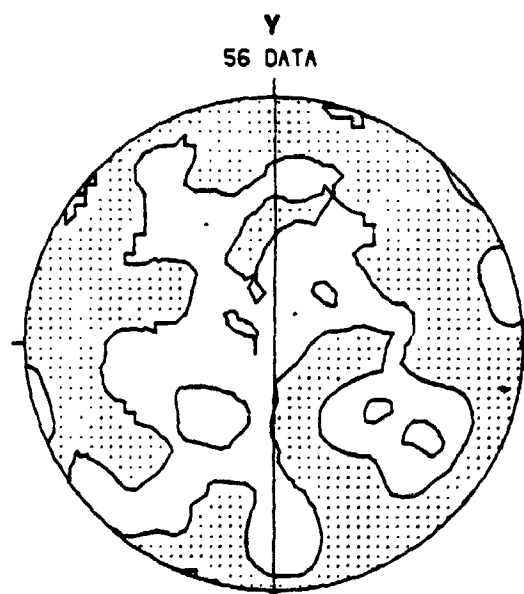
Figure 6-6. Orientation diagrams of the optical directions X, Y, and Z of plagioclase in strongly modified anorthosite specimen PS-86-14. Orientation of the foliation is N-S vertical. The lineation is horizontal. Equal area projection, upper hemisphere.

SPECIMEN PS-86-14,
strongly modified anorthosite.

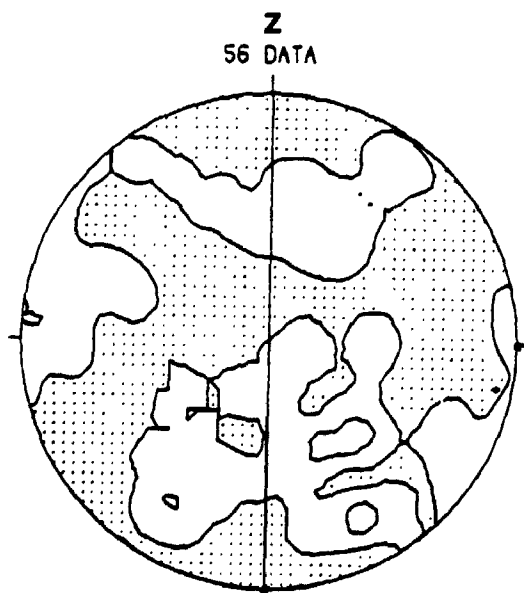
Plagioclase is An45-53.



CONTOURED AT 1.35 POINTS PER 1.7% AREA



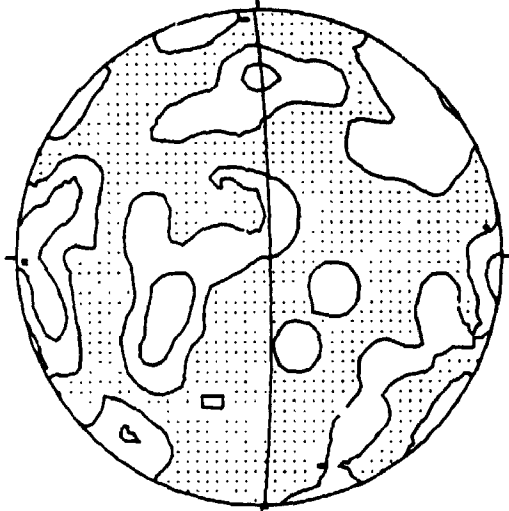
CONTOURED AT 1.3 POINTS PER 1.8% AREA



CONTOURED AT 1.3 POINTS PER 1.8% AREA

Figure 6-7. Orientation diagrams of the optical directions X, Y and Z of plagioclase in type I mylonite specimen PS-86-5. Orientation of the mylonitic foliation is approximately N-S vertical. The lineation is horizontal. Equal area projection, upper hemisphere.

X
83 DATA

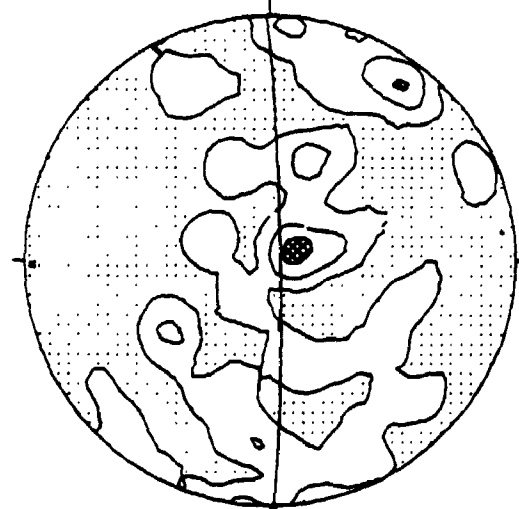


CONTOURED AT 1 3 POINTS PER 1.2 % AREA

SPECIMEN PS-86-5,

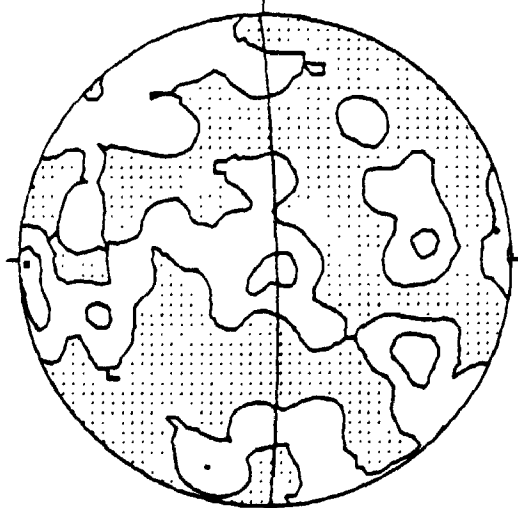
Plagioclase is An33-36.

Y
83 DATA



CONTOURED AT 1 3 5 POINTS PER 1.2 % AREA

Z
83 DATA



CONTOURED AT 1 3 POINTS PER 1.2 % AREA

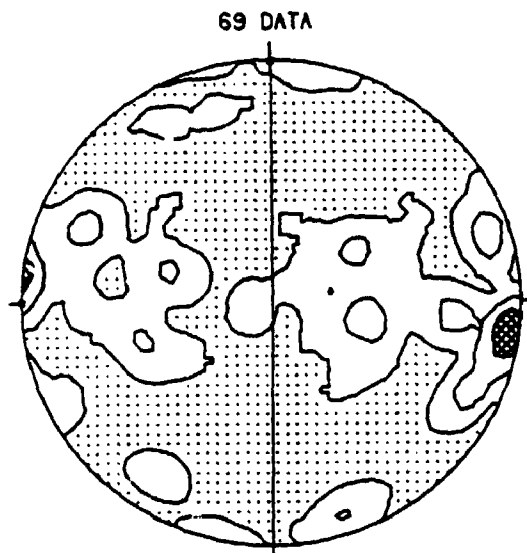
61

6

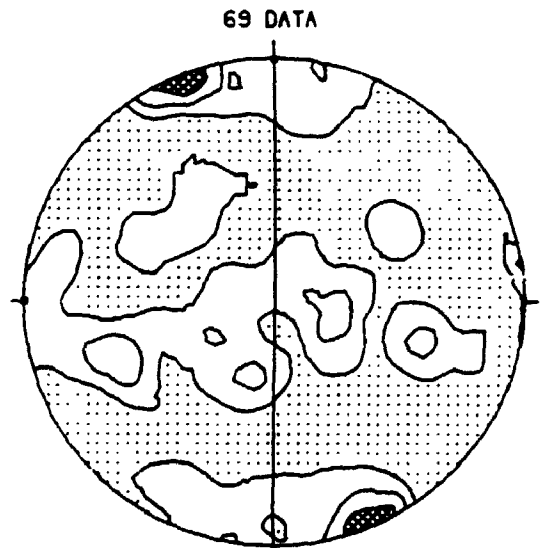
Figure 6-8. Orientation diagrams of the optical directions X, Y and Z of plagioclase in type II mylonite specimen PS-86-4. Orientation of the mylonitic foliation is N-S vertical. The lineation is horizontal. Equal area projection, upper hemisphere.

SPECIMEN PS-86-4,
type II mylonite.

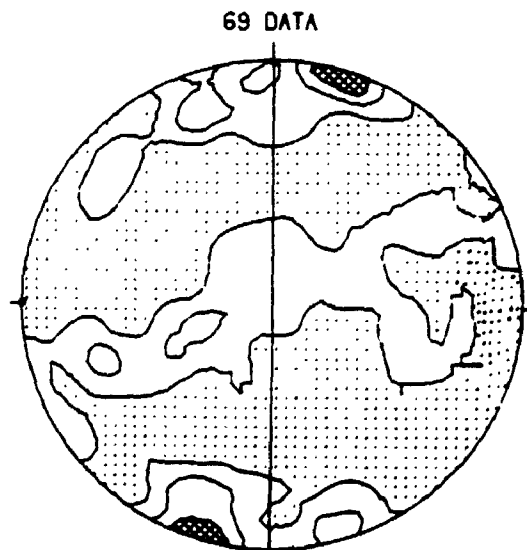
Plagioclase is An18-21.



CONTOURED AT 1 3 5 POINTS PER 1.4 % AREA



CONTOURED AT 1 3 5 POINTS PER 1.4 % AREA

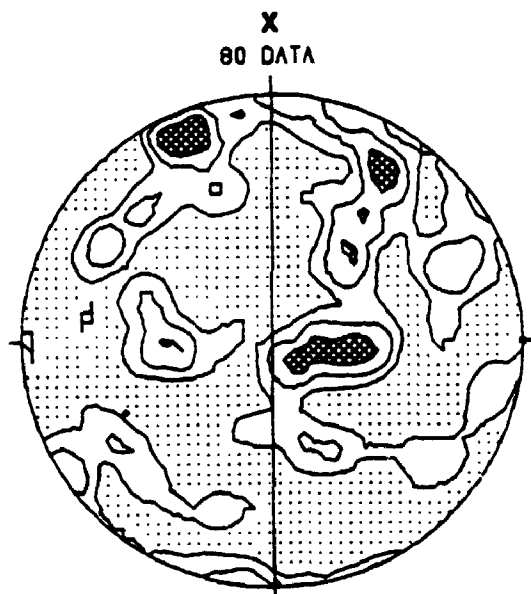


CONTOURED AT 1 3 5 POINTS PER 1.4 % AREA

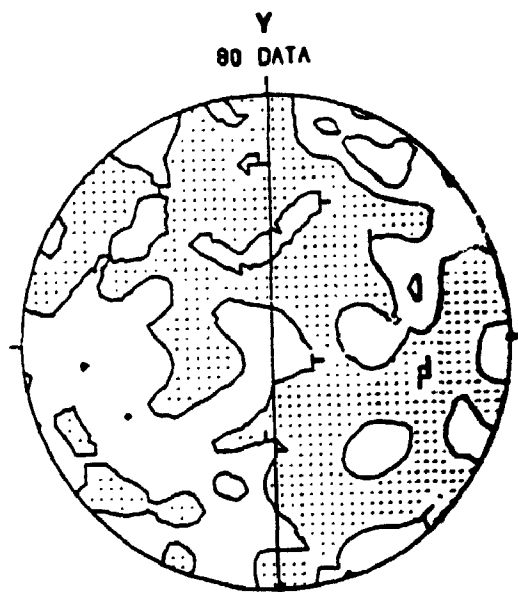
Figure 6-9. Orientation diagrams of the optical directions X, Y and Z of plagioclase in the strongly deformed center of a planar shear zone (specimen PS-85-2b). Orientation of the foliation is N-S vertical. The lineation is horizontal. Equal area projection, upper hemisphere.

SPECIMEN PS-85-2b,
strongly deformed center of a
planar shear zone.

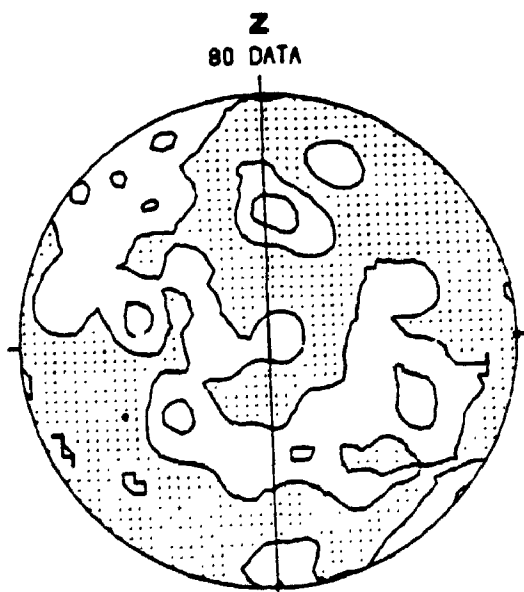
Plagioclase is An42-46.



CONTOURED AT 1 2 3 POINTS PER 1-2 % AREA



CONTOURED AT 1 3 POINTS PER 1-2 % AREA



CONTOURED AT 1 3 POINTS PER 1-2 % AREA

II mylonites (Figs. 6-7 and 6-8).

6.4 SUMMARY

The crystallographic orientation of quartz was investigated in six specimens of mylonites and anastomosing shear zones. The orientation of quartz c-axes in the quartz in quartz ribbons is preferred and displays two types of pattern. The first pattern consists of a single maximum and occurs in two of the anastomosing shear zones and one of the type II mylonite specimens. The second pattern of preferred orientation consists of a great circle girdle and occurs in the quartz ribbons in the remaining three specimens of type II mylonite. The orientation of the quartz c-axes in the isolated quartz grains is random.

The crystallographic orientation of plagioclase was investigated in six specimens representative of different degrees of modification of the Whitestone Anorthosite. The orientations of the optic indicatrix axes, X, Y and Z, of the plagioclase are random in some specimens, but non-random in others. The X and Y indicatrix axes tend to be oriented parallel to the foliation in the weakly and the strongly modified anorthosite. The X indicatrix axes lie in a girdle normal to the foliation in the type II mylonite. In the planar shear zone, the orientation

pattern is more complex. The Y indicatrix axes lie in a girdle parallel to the foliation in the moderately modified anorthosite and the type I mylonite. The Z indicatrix axes lie in a plane at a high angle to the foliation in the moderately modified anorthosite, the type I mylonite, the type II mylonite and in the planar shear zone.

CHAPTER 7

DISCUSSION: RESULTS AND GEOLOGICAL IMPLICATIONS

7.1 INTRACRYSTALLINE DEFORMATION

The observed crystallographic orientation patterns of plagioclase in all of the rocks investigated may be the result of syntectonic recrystallization. This has been observed microscopically during this study (Plate 4-1). Furthermore, White and Mawer (1986) reported syntectonic recrystallization of plagioclase observed using high resolution transmission electron microscopy in mylonites within the Parry Sound Shear Zone.

Tullis and Yund (1985) suggest that recrystallization of plagioclase plays an important role in the formation and the localization of ductile shear zones. Recrystallization is believed to have been important during deformation of the Whitestone Anorthosite where it is intersected by the Parry Sound Shear Zone.

The orientation patterns of c-axes in isolated quartz grains in the plagioclase-rich matrix of type II mylonites and the strongly deformed center of anastomosing shear zones are random. Similarly, the crystallographic orientation patterns of adjacent plagioclase grains, while non-random, are not sufficiently distinct. These observations suggest that grain boundary sliding, or some

other grain boundary process, was dominant in the plagioclase-rich matrix.

The preferred orientation patterns of quartz c-axes in the quartz ribbons of the mylonites and anastomosing shear zones from the Parry Sound Shear Zone suggest that dislocation creep was a prominent deformation process in quartz, where quartz was abundant.

One of the observed orientation patterns of quartz c-axes is characterized by a single maximum in the plane of foliation and normal to the lineation direction (see Fig. 6-2). Starkey (1979) suggested that similar fabrics in the Saxony Granulites were due to glide on prism $\langle a \rangle$ systems. Fabrics of this type have also been considered to result from deformation involving a rotational component (Schmid and Casey, 1982). Lister and Dornsiepen (1982) reported similar fabrics of c-axes to have developed in rocks of upper greenschist and amphibolite facies.

The second observed orientation pattern, typified by a distribution of quartz c-axes in a great circle girdle normal or at a high angle to foliation with multiple maxima (see Fig. 6-3), suggests that other slip systems may also have been active during the deformation of quartz. Fabric simulations by Taylor-Bishop-Hill analysis indicates similar orientation patterns, when basal $\langle a \rangle$ systems are allowed to operate (Lister and Williams, 1979). Lister and Dornsiepen (1982) suggested that such fabrics

formed under lower-middle amphibolite facies conditions.

Comparison of the girdle orientation patterns in specimens PS-85-12, PS-85-13 and PS-85-14 (Fig 6-3) with the skeletal c-axis patterns for coaxial deformation within different areas of the Flinn diagram (Lister and Williams, 1979; Schmid and Casey, 1986) indicate a deviation from the field of plain strain into the field of extension. This interpretation and the volume increases indicated by the results of chemical analysis reported in Chapter 5 suggest that there may have been significant dilatation during the development of type II mylonite and the anastomosing shear zones.

It has been demonstrated experimentally that at low temperature and/or fast strain rates quartz deforms by glide on basal $\langle a \rangle$ systems (Tullis et al., 1973). At high temperature and/or slow strain rates quartz deforms by glide on prism $\langle c \rangle$ systems (Tullis et al., 1973). It has been suggested that the basal/prism mechanism switch occurs at 600-700° C around 6 kbar mean stress (Lister and Dornsiepen, 1982). It is very likely that the different patterns observed in the mylonites of the Parry Sound Shear Zone indicate changes in metamorphic conditions, although factors other than temperature and strain rate may also have been important.

Microscopic evidence indicates that quartz may be the product of different hydrothermal events. This would be

consistent with the two types of mylonitic pegmatites of different ages recognized by van Breemen et al. (1986) in the Parry Sound region. The first type is syntectonic, whereas the second is late tectonic, and their ages are 1160 Ma and 1120 Ma respectively. If the introduction of quartz and pegmatites are considered to be due to the same fluid flux, there would thus have been two periods of silica-rich fluid introduction through the shear zone.

The two types of quartz ribbons identified on the basis of petrofabric analysis are also texturally distinct. Quartz ribbons exhibiting girdle orientation patterns have a grain size similar to that of other constituents, while quartz ribbons exhibiting single maximum c-axis orientation patterns have a grain size considerably greater than the average size of surrounding grains. Therefore, it is possible that the ribbons developed at the two occasions of silica influx.

In summary, the interpretation of the preferred orientation patterns of quartz c-axes suggests that a more complex strain path than simple shear occurred in mylonites of the Parry Sound Shear Zone. A departure from ideal simple shear is also noted in other major mylonite zones (e.g. Law, 1986). The observed different orientation patterns suggest that quartz was deformed under different conditions. The comparison of the orientation patterns with those reported from a variety of metamorphic terranes

suggests that lower to middle amphibolite facies conditions occurred during the deformation of quartz.

7.2 KINEMATIC HISTORY

The results of a recent geochronological study of the Whitestone Anorthosite and associated igneous rocks indicate that the Southwestern Grenville Province underwent crustal thickening from 1500 Ma until 1300 Ma (van Breemen et al., 1986). The ages of syntectonic pegmatites similar to those in type II mylonites in the Parry Sound Shear Zone (1159 Ma) and late tectonic pegmatites (1120 Ma) indicate that overthrusting of the Parry Sound Domain over the Britt Domain occurred over a period of at least 40 Ma (van Breemen et al., 1986).

The observed deformation of the Whitestone Anorthosite along the Parry Sound Shear Zone represents a progressive deformation with time. The moderately modified anorthosite was produced during an early phase of deformation. Penecontemporaneously, the scapolite-rich protomylonites (type I mylonites) were produced along the intersection between the Whitestone Anorthosite and the Parry Sound Shear Zone. The strongly modified anorthosite and quartz-bearing mylonites (type II mylonites) appear to be products of a later deformation. Chemical and mineralogical evidence suggest that weakly modified

anorthosite and anastomosing shear zones developed during this late stage or possibly later.

It is proposed that the age of scapolite-rich type I mylonites is that of initial overthrusting. This age must be older than 1159 Ma since this is the age of syntectonic pegmatites which occur in the later type II mylonites.

7.3 TECTONIC EVOLUTION

The Whitestone Anorthosite exhibits a mineral assemblage consisting of primary clinopyroxene and plagioclase (An60) (Mason, 1969; Thompson, 1983). This mineralogy represents a high temperature igneous assemblage. The weakly modified anorthosite exhibits a mineral assemblage consisting of hornblende, epidote, biotite, plagioclase (An40-56), scapolite (Me57-63) and, locally, chlorite. This mineralogy reflects moderate pressure, lower-middle amphibolite facies conditions (Miyashiro, 1961; Apter and Liou, 1983). The moderately modified anorthosite has a different mineral assemblage to that in weakly modified anorthosite with plagioclase (An48-58), scapolite (Me68-71), hornblende and almandine garnet as the dominant constituents. Recrystallized clinopyroxene with metamorphic corona is also present. This assemblage is characteristic of the moderate pressure conditions of middle to upper amphibolite facies

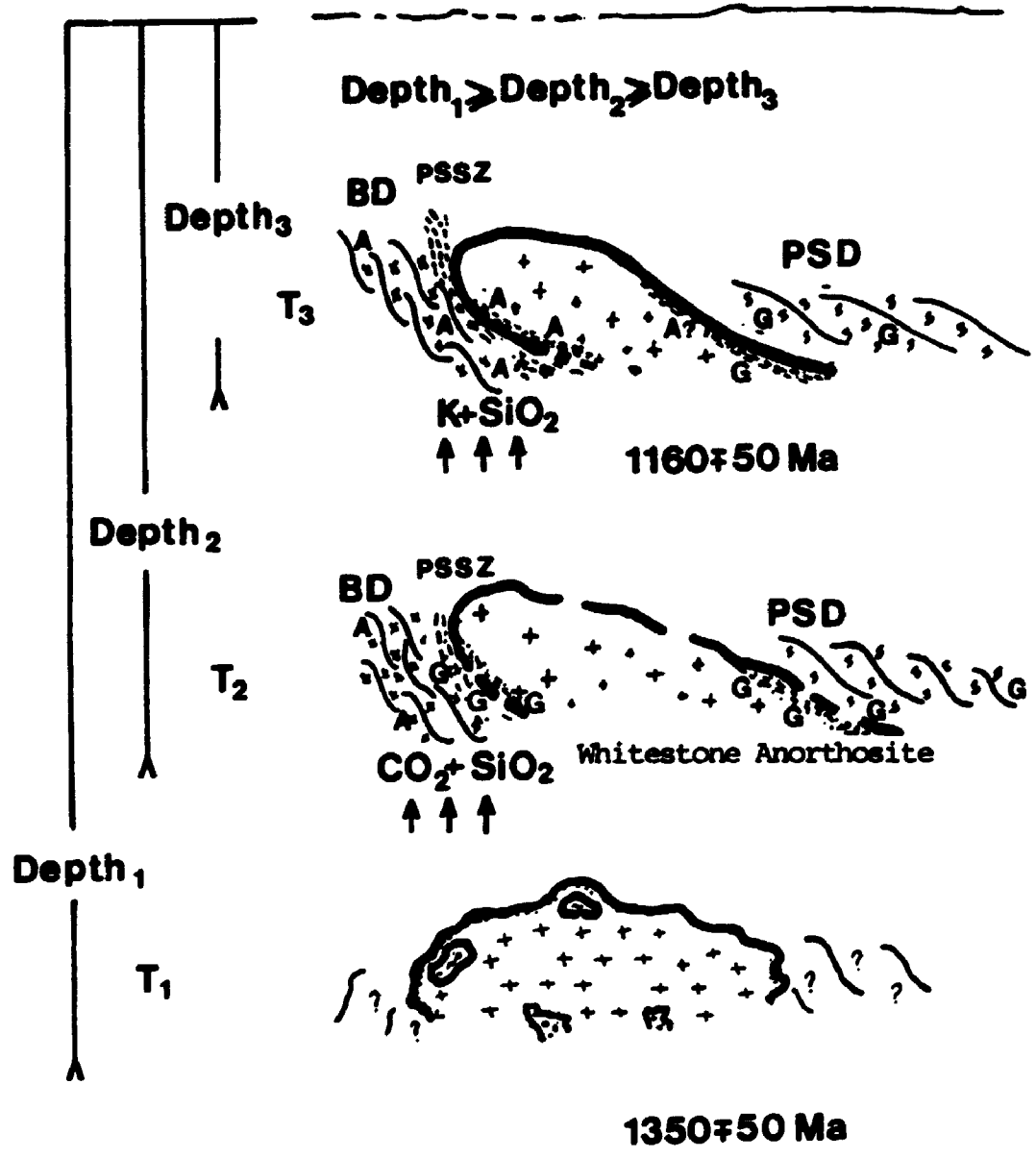
(Miyashiro, 1961; Fyfe et al., 1978).

Local shear zones and mylonites from Parry Sound also display distinct mineralogical and geochemical characteristics. Scapolite and calcite in planar shear zones and type I mylonites suggest a CO₂-dominated metasomatic event. Biotite, K-feldspar and ubiquitous quartz in anastomosing shear zones and type II mylonites are evidence for a potassium and silica dominated metasomatic event. This metasomatic event overprints the earlier CO₂ metasomatic event.

A possible kinematic model is, therefore, proposed for the deformation of the Whitestone at the contact with the Parry Sound Shear Zone, and the accompanying retrogression from granulite to lower amphibolite facies conditions. Three reference times t₁, t₂ and t₃ are arbitrarily chosen as being representative of the early, middle and late periods of the kinematic model for the Whitestone Anorthosite, which is represented schematically in Figure 7-1.

During the early period, events are sketchy and involve the crystallization of the Whitestone Anorthosite (or a larger igneous mass) at about 1350 Ma (van Breemen et al., 1986). van Breemen et al. suggest that the anorthosite formed during an extensive plutonism that affected the Central Gneiss Belt between 1500 and 1300 Ma.

Figure 7-1. Kinematic model for the deformation of the
Whitestone Anorthosite in the Parry Sound Shear Zone.



BD: Britt Domain
 PSD: Parry Sound Domain
 PSSZ: Parry Sound Shear Zone

A: Amphibolite facies
 G: Granulite facies

During the middle period, the deformation of the Whitestone Anorthosite occurred under medium pressure, granulite-upper amphibolite facies conditions ($T > 600^\circ \text{C}$). The upper amphibolite-granulite assemblage of the moderately modified anorthosite and the extensive metasomatic exchange at the margins of the Whitestone Anorthosite (Thompson, 1983) are indicative of these conditions. The presence of a pervasive foliation and refolded intrafolial folds in the moderately modified anorthosite suggests the occurrence of substantial thickening of the crust. Extensive CO_2 metasomatism in planar shear zones suggests progressive metamorphism within the underthrust plate. The absence of pegmatites in type I mylonites indicates either temperatures or water activity still unsuitable for partial melting (Fyfe et al., 1978). Type I mylonites developed where the shear zone intersected the Whitestone Anorthosite.

During the late period, lower grade metamorphic conditions prevailed, indicated by increasingly sodic plagioclase in the mineral assemblage of the strongly modified anorthosite proximal to the intersection of the Whitestone Anorthosite with the Parry Sound Shear Zone, and the sodic plagioclase and epidote bearing assemblage of the weakly modified anorthosite away from this intersection. Potassium and silica metasomatism in anastomosing shear zones and type II mylonites is the

consequence of fluid evolution. The appearance of feldspar megacrystals in the type II mylonite suggests partial melting in the underthrust block. A part of the silica and potassium rich fluids may have been transported by the silica melt (Fyfe et al., 1978). The zircon ages of pegmatites in type II mylonites suggest that deformation continued through 1159 Ma under lower amphibolite facies conditions (550-600°C). A change in the orientation of lineation with respect to the foliation reported by Schwerdtner (1987) suggests the possibility of a change in the regional stress regime. The composition of exsolved phases in feldspar single crystals has been interpreted by White and Mawer (1986) to indicate dislocation mobility continued until temperatures reached to 500°C (White and Mawer, 1986). The two generations of quartz identified above suggests that events during the late phase were complex and that there was a long and active tectonic history in the Parry Sound Region.

Windley (1986) has proposed a model for the tectonic evolution of the Grenville Province. He considers the Ottawa Orogeny (1150-1050 Ma) as a collision between the Central Gneiss Belt and the continental margin of the Central Metasedimentary Belt, and suggests a post-collision convergence and indentation to explain the formation of major northwest-directed thrust sheets in the Central Gneiss Belt. He suggests that the granulites of

the Parry Sound Domain with metamorphic zircon ages (1160-1170 Ma) close to the age of thrusting (1159 Ma) have formed at the deep levels of the thickened crust.

However, interpretations of the pegmatite ages from the Parry Sound Shear Zone presented here suggest a thrusting event prior to the Ottawa Orogeny (1150-1050 Ma). The pre-collision thrusting explains the occurrence of 1160 Ma and older ages of granulite facies rocks in the Parry Sound Domain. The pre-collision thrusting also accounts for the older metamorphic and emplacement ages observed in the central part of the Central Belt compared to the Central Metasedimentary Belt by Easton (1986).

FLUID EVOLUTION

The observed mineralogical and geochemical changes can be used to construct a fluid evolution model for the overthrust block in which the Whitestone Anorthosite occurs. This model comprises two stages. In the first stage, an inverted geothermal gradient develops in the overriding block, and a retrograde mineral assemblage forms. Also, the injection of an oxidizing fluid phase from the underthrust block produces significant changes in the oxidation state in the overthrust block, and the rocks of the overthrust plate become increasingly oxidized. In the second stage, progressively lower grade mineral

assemblages form in the overriding block. Originally oxidizing fluids derived from the underthrust plate become increasingly reducing. These contrasting states ultimately result in extensive veining and leaching along the path of rising fluid. Figure 7-1 shows different stages of fluid evolution in relation to the kinematic model.

The moderately modified anorthosite represents the overthrust plate at the first stage of the fluid evolution model. The mineral assemblage of the moderately modified anorthosite contains almandine garnet, calcium-rich plagioclase (An 59-48) and ferroan pargasitic amphibole, which suggest that the first stage of fluid evolution occurred at the high temperatures of the middle-upper amphibolite facies (in excess of 650°C) (Miyashiro, 1961; Fyfe et al., 1978). The minor occurrence of sphene and the relative abundance of ilmenite provide independent evidence for high temperatures (Moody et al, 1983).

The appearance of hematite-ilmenite exsolution lamellae in the moderately modified anorthosite indicates a change to an oxidizing state in the overthrust plate. The presence of these oxides suggests oxygen fugacities between the $\text{Fe}_2\text{O}_3 + \text{FeO}$ and $\text{Ni} + \text{NiO}$ buffers (Kretschmar, 1968). The oxidation index is in the vicinity of 50-52. The occurrence of up to 0.8 weight % sulphur in CO_2 -rich scapolites rather than in sulphides affords additional evidence for highly oxidizing conditions.

The gradation from the moderately modified anorthosite into type I mylonite along the intersection between the Whitestone Anorthosite and the Parry Sound Shear Zone is not associated with any mineralogical change other than the disappearance of hematite exsolution in ilmenite and the appearance of pyrite and pyrrhotite. The decreasing hematite exsolution is consistent with the observed gradual decrease of oxygen fugacity in the mylonites of the Parry Sound Shear Zone (see Table 5-3). The decrease may be attributed to an evolving fluid where the increasing fluid activity of the H_2O component was the result of diminishing CO_2 activity.

The weakly modified anorthosite represents the overriding plate at the second stage of the fluid evolution model. The epidote content of the weakly modified anorthosite suggests lower grade metamorphic conditions than those under which the moderately deformed anorthosite developed. The presence, locally, of chlorite and the high titanite to ilmenite ratio are additional evidence of these conditions.

The weakly modified anorthosite contains sulphides, but oxides are absent. This may indicate a reduction in the oxidation state of the overthrust plate (Froese, 1978).

Anastomosing shear zones, which are most readily observed in the weakly modified anorthosite, are enriched in sulphides. The appearance of sulphides may indicate

reduction in oxygen fugacity, and the observed low oxidation indices are consistent with this reduction (see Table 5-6). Reducing fluids enriched in hydrogen interact with rocks of different oxidation states, and remove Mg, Fe, Ca and Na and precipitate Si and K (Fyfe and Lonsdale, 1981). The deposition of pyrite and pyrrhotite may occur under these reducing conditions (Fyfe and Lonsdale, 1981).

The observed mineral assemblages and chemical compositions of the Whitestone Anorthosite could also be explained by the involvement of more than one type of fluid. However, this seems unlikely when the progressive geometry of the shear zone is considered. The progressive evolution of fluid under evolving conditions of the overthrust also provides a simpler explanation for the gradual modification of the rock chemistry across the Parry Sound Shear Zone.

The fluid evolution model presented here, based on the textural, mineralogical and chemical characteristics of the anorthosite, is similar to a more generalized model suggested by Fyfe (1986). The progressive changes of fluid composition in the overthrust setting of the Whitestone Anorthosite described above may explain in more detail the occurrences of complex mineral assemblages in similar tectonic settings.

CHAPTER 8

CONCLUSIONS

This study examines the processes accompanying the ductile deformation of the Whitestone Anorthosite in the Parry Sound Shear Zone. The method of investigation combines the study of mineralogy, chemistry and petrofabrics in the deformed anorthosite. The main conclusions are as follows.

i) The Whitestone Anorthosite displays progressive textural, mineralogical and chemical modifications where it is intersected by the Parry Sound Shear Zone. These modifications suggest an evolution of the deformation.

ii) The progressive mineralogical modifications of the Whitestone Anorthosite delimit the conditions of the deformation as moderate pressure type, upper to lower amphibolite facies.

iii) The chemical changes within the Whitestone Anorthosite are the result of rock-fluid interaction during deformation. Early CO_2 metasomatism and late K_2O and SiO_2 metasomatism indicate an evolution of the fluid environment of the overthrust block containing the Whitestone Anorthosite.

iv) Mass balance calculations indicate insignificant volume changes during transformations to CO_2 enriched type I mylonites and planar shear zones, but substantial

dilatations during transformations to SiO_2 and K_2O enriched type II mylonites and anastomosing shear zones.

v) Dislocation creep is an important deformation mechanism for quartz in ribbons under amphibolite and higher grade metamorphic conditions. A mechanism dominated by grain boundary sliding, or some other grain boundary process, is characteristic of isolated quartz and plagioclase in the matrix of type II mylonites and anastomosing shear zones. Syntectonic recrystallization is a dominant deformation mechanism for plagioclase in increasingly modified anorthosites and local shear zones.

vi) The magnitude of textural, mineralogical and chemical modifications in the deformed Whitestone Anorthosite indicates a long deformation history associated with the Parry Sound Shear Zone.

vii) The age of formation of the Parry Sound Shear Zone appears to be older than the currently proposed age of 1160 Ma.

viii) The older age of the Parry Sound Shear Zone, compared to the shear zones in the eastern Grenville Province, suggests an episode of thrusting prior to the main collision of the Ottawa Orogeny (1150-1050 Ma).

APPENDIX A

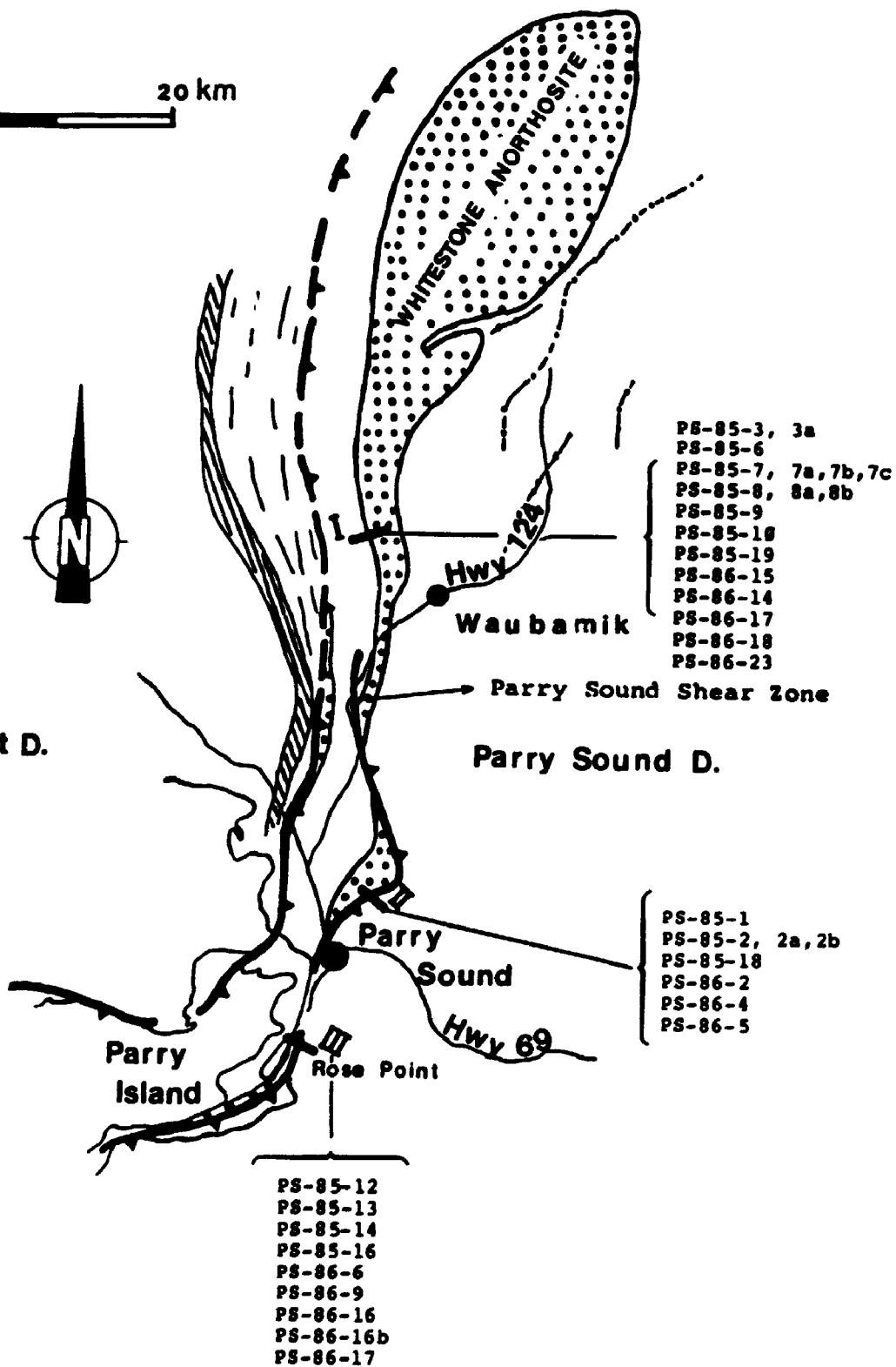
SAMPLE LOCATIONS

This map displays the locations of samples referenced in this thesis.

0 20 km



Britt D.

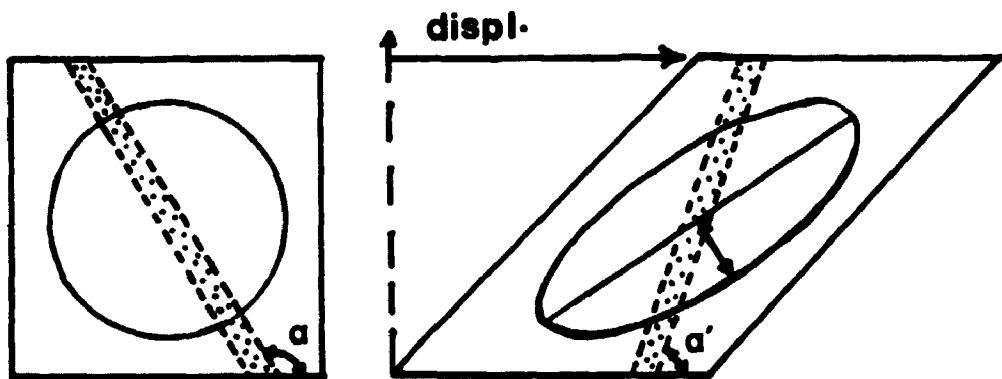


APPENDIX B

CALCULATIONS OF SHEAR STRAINS AND DISPLACEMENTS

The relationship between the orientations of linear features before and after deformation is:

$$Y = \cot \alpha' - \cot \alpha$$



where Y is the shear strain and α and α' are the initial and final angles between the linear feature and the shear plane. (see Figure above)

The approximate displacement = Y x width of the shear zone.

APPENDIX C

ELECTRON MICROPROBE ANALYSES

Mineral analyses were carried out using a Material Analyses Co. (MAC) microprobe and a KRISSEL CONTROL probe system V4CM6SPI in the Department of Geology at the University of Western Ontario. Data were reduced using the program MAGIC IV run on a PDP 11/65 computer. The microprobe operated under an excitation voltage of 15 KV, a sample current of 250 MA, a beam diameter of 1 to 3 microns and a counting time of 30 seconds or 20000 counts. The results are within 3% of the amount present, and the limit of detection is approximately 0.05%.

Natural minerals were used as standards for the analyses. For example, amphibole compositions were determined using albite as a standard for Na, orthopyroxene for Mg, Fe and Si, kaersutite for Al and Ti, diopside for Ca, and orthoclase for K. Analyses of plagioclase and scapolite involved the use of albite as standard for Na, An90 as a standard for Al, Si and Ca, and orthoclase for K. The sample numbers associated with analyses of various minerals are given above each table.

The plagioclase formulae were calculated on the basis of 32 oxygen atoms per structural unit. The amphibole formulae were calculated on the basis of 23 oxygen atoms per structural unit, and a cation total of 13 excluding Ca, Na, K (Leake, 1978). The garnet formulae were calculated on the basis of 24 oxygen atoms per structural unit. The scapolite formulae were determined on the basis of 12 (Si,Al) atoms per structural unit (Deer et al., 1966).

PLAGIOCLASE ANALYSES

SAMPLE #

PS-85-17

Weight % oxides

SiO ₂	54.51	54.83	55.04	54.24	55.11	54.03
Al ₂ O ₃	28.75	28.99	28.01	29.31	28.95	28.77
CaO	12.22	12.40	12.09	12.55	12.31	12.38
K ₂ O	0.04	0.04	0.03	0.01	0.01	0.00
Na ₂ O	4.70	4.73	4.85	4.55	4.89	4.50
Total	100.22	100.99	100.02	100.66	101.27	99.68

Numbers of cations on the basis of 32 oxygens

Si	9.83	9.81	9.93	9.74	9.83	9.79
Al	6.11	6.11	5.96	6.20	6.09	6.14
Ca	2.36	2.38	2.34	2.41	2.35	2.40
K	0.00	0.00	0.00	0.00	0.00	0.00
Na	1.64	1.64	1.70	1.58	1.69	1.58
Total	19.94	19.95	19.94	19.95	19.97	19.92

An content %	59	59	58	52	58	60
--------------	----	----	----	----	----	----

SAMPLE #

PS-85-8

Weight % oxides

SiO ₂	53.51	56.15	55.75	54.74	56.07	54.03
Al ₂ O ₃	29.96	28.31	28.15	28.14	28.68	30.13
CaO	11.69	9.64	9.59	9.52	9.78	11.86
K ₂ O	0.13	0.19	0.17	0.14	0.17	0.15
Na ₂ O	5.05	5.72	6.12	5.73	6.05	5.18
Total	100.34	100.01	99.78	98.27	100.75	101.35

Numbers of cations on the basis of 32 oxygens

Si	9.65	10.07	10.05	10.00	10.00	9.65
Al	6.37	5.99	5.98	6.06	6.03	6.34
Ca	2.26	1.85	1.85	1.86	1.87	2.27
K	0.03	0.04	0.04	0.03	0.04	0.03
Na	1.77	1.99	2.14	2.03	2.09	1.79
Total	20.07	19.95	20.05	19.99	20.04	20.09

An content %	56	48	46	47	47	55
--------------	----	----	----	----	----	----

SAMPLE #

PS-85-8b

Weight % oxides

SiO ₂	60.91	59.20	59.92	60.59	60.45	60.16
Al ₂ O ₃	24.77	25.08	24.77	25.02	24.85	24.43
CaO	7.61	7.44	7.39	7.41	7.54	7.42
K ₂ O	0.17	0.06	0.14	0.12	0.14	0.11
Na ₂ O	7.35	7.71	7.30	7.36	7.50	7.25
Total	100.81	99.49	99.52	100.50	100.48	99.37

Numbers of cations on the basis of 32 oxygens

Si	10.77	10.63	10.73	10.74	10.73	10.74
Al	5.16	5.31	5.23	5.23	5.20	5.22
Ca	1.44	1.43	1.42	1.40	1.43	1.40
K	0.04	0.01	0.03	0.03	0.03	0.03
Na	2.52	2.68	2.53	2.53	2.58	2.52
Total	19.93	20.07	19.94	19.92	19.97	19.92

An content %	36	35	36	35	35	35
--------------	----	----	----	----	----	----

SAMPLE #

PS-85-2

	Weight % oxides					
SiO ₂	57.55	55.88	55.34	56.43	55.36	54.88
Al ₂ O ₃	26.46	27.76	27.78	27.22	27.30	27.77
CaO	9.83	11.53	11.23	10.54	11.07	11.84
K ₂ O	0.24	0.11	0.20	0.18	0.20	0.19
Na ₂ O	5.79	4.81	5.21	5.20	5.37	4.54
Total	99.87	100.09	99.76	99.57	99.30	99.22

	Numbers of cations on the basis of 32 oxygens					
Si	10.33	10.05	10.00	10.18	10.05	9.97
Al	5.60	5.88	5.92	5.79	5.84	5.95
Ca	1.89	2.22	2.17	2.04	2.15	2.30
K	0.05	0.02	0.05	0.04	0.05	0.04
Na	2.01	1.68	1.82	1.82	1.89	1.60
Total	19.90	19.86	19.97	19.86	19.99	19.87
An content %	48	57	54	52	52	58

SAMPLE #

PS-85-2a

Weight % oxides

SiO ₂	53.66	54.10	56.61	56.07	55.62	57.06
Al ₂ O ₃	28.83	28.63	28.47	28.84	28.75	28.20
CaO	9.96	10.39	9.82	10.20	10.98	9.99
K ₂ O	0.21	0.24	0.25	0.27	0.19	0.38
Na ₂ O	6.27	5.77	6.18	6.02	5.61	6.12
Total	98.93	99.13	101.33	101.40	101.15	101.75

Numbers of cations on the basis of 32 oxygens

Si	9.80	9.85	10.05	9.96	9.92	10.10
Al	6.21	6.14	5.96	6.04	6.04	5.88
Ca	1.95	2.03	1.87	1.94	2.01	1.89
K	0.05	0.05	0.06	0.06	0.04	0.09
Na	2.21	2.04	2.13	2.07	1.94	2.10
Total	20.22	20.12	20.06	20.08	20.04	20.05

An content %

46

49

46

48

51

46

SAMPLE #

PS-85-2b

Weight % oxides

SiO ₂	58.75	56.49	57.63	56.46	57.74	58.75
Al ₂ O ₃	27.55	27.49	27.43	27.54	27.34	27.55
CaO	9.41	9.39	9.15	9.66	9.31	9.41
K ₂ O	0.21	0.24	0.22	0.22	0.22	0.21
Na ₂ O	5.61	6.26	6.23	6.42	6.55	5.61
Total	101.49	98.87	100.96	101.33	101.56	101.53

Numbers of cations on the basis of 32 oxygens

Si	10.34	10.16	10.24	10.31	10.25	10.34
Al	5.71	5.83	5.74	5.82	5.72	5.71
Ca	1.77	1.81	1.80	1.85	1.77	1.77
K	0.05	0.55	0.05	0.05	0.05	0.05
Na	1.91	2.18	2.14	2.23	2.25	1.91
Total	19.78	20.04	19.98	20.10	20.04	19.78

An content %	47	45	45	45	43	47
--------------	----	----	----	----	----	----

SAMPLE # PS-86-16

Weight % oxides

SiO ₂	56.63
Al ₂ O ₃	27.51
CaO	9.25
K ₂ O	0.22
Na ₂ O	6.76
Total	100.37

Numbers of cations on the basis of 32 (O)

Si	10.15
Al	5.81
Ca	1.77
K	0.05
Na	2.35
Total	20.14

An content % 42

SAMPLE #

PS-86-5

Weight % oxides

SiO ₂	58.26	58.62	58.37	58.14	59.25	58.01
Al ₂ O ₃	26.01	26.20	26.31	25.63	25.95	25.96
CaO	7.51	7.31	7.23	7.07	7.25	7.53
K ₂ O	0.26	0.27	0.27	0.30	0.25	0.30
Na ₂ O	7.41	7.31	7.46	7.66	7.70	7.16
Total	99.45	99.71	99.64	98.80	100.40	98.96

Numbers of cations on the basis of 32 oxygens

Si	10.48	10.50	10.47	10.52	10.54	10.48
Al	5.51	5.53	5.56	5.47	5.44	5.53
Ca	1.45	1.40	1.39	1.37	1.38	1.46
K	0.06	0.06	0.06	0.07	0.06	0.07
Na	2.58	2.54	2.59	2.69	2.66	1.60
Total	20.08	20.035	20.08	20.12	20.09	20.04

An content %	35	35	34	33	34	36
--------------	----	----	----	----	----	----

SAMPLE #

PS-86-4

Weight % oxides

SiO ₂	62.57	63.79	60.84	63.19	63.01	60.52
Al ₂ O ₃	22.42	22.36	23.57	22.31	21.89	23.41
CaO	4.35	4.00	5.88	4.62	3.89	5.81
K ₂ O	0.23	0.23	0.24	0.27	0.08	0.30
Na ₂ O	9.18	9.41	8.34	9.44	9.50	8.36
Total	98.75	99.79	98.87	99.83	98.37	99.40

Numbers of cations on the basis of 32 oxygens

Si	11.22	11.30	10.94	11.30	11.32	10.94
Al	4.74	4.67	4.99	4.67	4.63	4.99
Ca	0.84	0.76	1.13	0.88	0.75	1.21
K	0.05	0.05	0.05	0.06	0.04	0.07
Na	3.19	3.23	2.91	3.25	3.31	2.93
Total	20.03	20.01	20.04	20.09	20.03	20.06

An content %	20	19	28	21	18	27
--------------	----	----	----	----	----	----

AMHIBOLE ANALYSES

Weight % oxides

SiO ₂	43.97	42.91
TiO ₂	0.31	0.28
Al ₂ O ₃	12.09	12.28
Fe O	13.30	14.26
MgO	12.11	12.20
MnO	0.33	0.25
CaO	12.62	12.40
K ₂ O	0.87	0.81
Na ₂ O	1.21	1.29
Total	96.81	96.68

Numbers of cations on the basis of 23 oxygens

Si	6.50	6.35
Ti	0.03	0.03
^{iv} Al	1.49	1.64
^{vi} Al	0.61	0.49
Fe ²⁺	1.34	1.16
Fe ³⁺	0.30	0.60
Mg	2.66	2.69
Mn	0.04	0.03
Ca	1.99	1.96
K	0.16	0.15
NaM4	0.00	0.01
Na-A	0.34	0.35
Comp.	Pargst.	Mg Hast.

Weight % oxides

SiO ₂	38.79	39.45	39.26	38.46
TiO ₂	1.13	0.93	1.04	1.11
Al ₂ O ₃	13.98	14.17	14.06	14.77
Fe O	22.18	20.82	20.77	21.04
MgO	6.61	6.94	6.44	6.09
MnO	0.16	0.08	0.20	0.17
CaO	12.00	12.20	12.06	11.90
K ₂ O	2.61	1.68	1.57	1.70
Na ₂ O	1.14	1.00	1.08	1.08
Total	97.60	97.27	96.48	96.32

Numbers of cations on the basis of 23 oxygens

Si	5.96	6.05	6.09	5.98
Ti	0.13	0.10	0.12	0.13
^{iv} Al	2.04	1.94	1.90	2.01
^{vi} Al	0.49	0.61	0.66	0.70
Fe ²⁺	2.19	2.18	2.32	2.34
Fe ³⁺	0.65	0.48	0.36	0.40
Mg	1.51	1.58	1.49	1.41
Mn	0.02	0.01	0.02	0.02
Ca	1.97	2.00	2.00	1.98
K	0.31	0.32	0.31	0.33
NaM4	0.01	0.00	0.00	0.01
Na-A	0.32	0.29	0.32	0.32
Comp.	Hast.	Ferroan Pargst.	Ferroan Pargst.	Ferroan Pargst.

Weight % oxides

SiO ₂	38.48
TiO ₂	1.13
Al ₂ O ₃	14.43
Fe O	22.89
MgO	5.44
MnO	0.25
CaO	11.84
K ₂ O	1.67
Na ₂ O	1.36
Total	97.49

Numbers of cations on the basis of 23 oxygens

Si	5.97
Ti	0.13
^{iv} Al	2.02
^{vi} Al	0.61
Fe ²⁺	2.53
Fe ³⁺	0.43
Mg	1.26
Mn	0.03
Ca	1.97
K	0.33
NaM4	0.01
Na-A	0.39
Comp.	Ferroan Pargst.

SAMPLE #

PS-86-4

Weight % oxides

SiO ₂	38.63	38.22	38.10	37.88	37.90
TiO ₂	1.25	1.32	1.36	1.36	1.03
Al ₂ O ₃	12.34	14.74	12.49	12.77	14.30
Fe O	26.25	22.80	25.53	25.69	22.50
MgO	4.43	6.06	4.30	4.38	5.43
MnO	0.14	0.23	0.14	0.22	0.28
CaO	11.17	12.16	12.22	11.35	11.82
K ₂ O	1.56	2.07	1.74	1.55	1.69
Na ₂ O	1.70	1.18	1.56	1.83	1.25
Total	97.47	98.88	96.44	97.03	96.20

Numbers of cations on the basis of 23 oxygens

Si	6.09	5.86	6.08	6.00	5.96
Ti	0.15	0.15	0.16	0.16	0.12
^{iv} Al	1.90	2.13	1.92	1.99	2.04
^{vi} Al	0.38	0.52	0.42	0.40	0.61
Fe ²⁺	2.94	2.35	2.99	2.94	2.49
Fe ³⁺	0.52	0.56	0.42	0.47	0.47
Mg	1.04	1.38	1.02	1.03	1.27
Mn	0.02	0.03	0.02	0.03	0.04
Ca	1.88	1.99	1.92	1.92	1.99
K	0.31	0.40	0.35	0.31	0.34
NaM4	0.06	0.00	0.04	0.04	0.00
Na-A	0.45	0.34	0.44	0.52	0.38
Comp.	Hast.	Hast.	Ferroan Pargst.	Hast.	Ferroan Pargst.

Weight % oxides

SiO ₂	38.25	38.07	39.47
TiO ₂	1.22	1.23	1.19
Al ₂ O ₃	14.03	14.23	14.05
Fe O	22.07	21.99	21.39
MgO	5.96	5.87	6.87
MnO	0.09	0.00	0.04
CaO	11.95	11.92	11.97
K ₂ O	1.78	1.83	1.62
Na ₂ O	1.27	1.22	1.22
Total	96.62	96.36	97.82

Numbers of cations on the basis of 23 oxygens

Si	5.98	5.96	6.03
Ti	0.14	0.14	0.14
^{iv} Al	2.01	2.03	1.96
^{vi} Al	0.56	0.60	0.57
Fe ²⁺	2.46	2.47	2.25
Fe ³⁺	0.42	0.40	0.47
Mg	1.39	1.37	1.56
Mn	0.01	0.00	0.00
Ca	2.00	2.00	1.96
K	0.35	0.36	0.31
NaM4	0.00	0.00	0.02
Na-A	0.38	0.37	0.34
Comp.	Ferroan Pargst.	Ferroan Pargst.	Ferroan Pargst.

GARNET ANALYSES

SAMPLE #

PS-85-2

Weight % oxides

SiO ₂	37.04	37.64	37.46	36.87	37.19
Al ₂ O ₃	20.70	20.36	20.33	20.52	20.27
Fe ₂ O ₃	27.12	26.67	27.53	27.29	27.12
MnO	1.47	2.57	0.47	0.85	0.72
MgO	2.14	2.41	2.22	1.98	1.94
CaO	10.63	9.71	11.10	11.37	11.11
Total	99.10	99.36	99.11	98.88	98.35

Numbers of cations on the basis of 24 oxygens

Si	5.96	6.03	6.01	5.95	6.02
Al	3.92	3.85	3.85	3.90	3.87
Fe	3.65	3.57	3.70	3.68	3.67
Mn	0.20	0.35	0.06	0.12	0.10
Mg	0.51	0.58	0.53	0.48	0.47
Ca	1.83	1.67	1.91	1.98	1.93
Alm.	64.22	63.94	65.20	63.88	64.44
Gross.	32.25	29.82	33.68	34.10	33.82
Pyrrp. content %	8.29	9.34	8.57	7.63	7.59
Spess.	3.53	6.24	1.13	2.02	1.73

SAMPLE #	PS-86-5				
	Weight % oxides				
SiO ₂	37.10	36.97	38.32	36.99	37.36
Al ₂ O ₃	20.96	20.88	20.87	20.79	20.49
Fe ₂ O ₃	26.31	26.69	26.74	26.55	27.53
MnO	1.20	1.49	1.33	1.55	1.30
MgO	2.44	2.82	2.94	2.03	1.95
CaO	10.82	10.04	10.28	11.85	11.32
Total	98.83	98.89	100.48	99.76	99.95

Numbers of cations on the basis of 24 oxygens

Si	5.96	5.94	5.96	5.92	5.97
Al	3.97	3.95	3.86	3.92	3.86
Fe	3.53	3.59	3.61	3.55	3.68
Mn	0.16	0.20	0.15	0.21	0.18
Mg	0.58	0.68	0.51	0.48	0.46
Ca	1.86	1.73	2.02	2.03	1.94
Alm.	65.57	65.00	62.51	61.31	63.51
Gross.	33.49	31.33	34.89	35.06	33.46
Pyrp. content %	9.51	10.91	8.03	7.71	7.42
Spess.	2.94	3.68	2.60	3.63	3.04

SAMPLE #	PS-86-4				
	Weight % oxides				
SiO ₂	37.70	36.71	37.14	36.63	37.26
Al ₂ O ₃	20.46	21.14	20.43	20.39	20.30
Fe ₂ O ₃	29.00	28.38	28.64	29.02	28.88
MnO	1.71	1.88	1.70	2.41	2.36
MgO	1.47	1.39	1.41	1.29	1.29
CaO	9.45	9.88	9.50	8.99	9.12
Total	99.79	99.38	98.82	98.73	99.21

Numbers of cations on the basis of 24 oxygens

Si	6.05	5.92	6.02	5.97	6.03
Al	3.87	4.02	3.90	3.92	3.87
Fe	3.89	3.83	3.88	3.96	3.91
Mn	0.23	0.26	0.23	0.33	0.32
Mg	0.35	0.33	0.34	0.31	0.31
Ca	1.62	1.71	1.65	1.57	1.58
Alm.	67.70	66.09	67.34	67.52	67.23
Gross.	28.26	29.48	28.62	26.80	27.20
Pyrp. content %	5.76	5.46	5.58	5.08	5.08
Spess.	4.04	4.43	4.05	5.68	5.56

SCAPOLITE ANALYSES

SAMPLE #

PS-85-8

Weight % oxides

SiO ₂	46.73	47.37	47.46	46.82	48.14
Al ₂ O ₃	27.24	27.10	26.60	26.61	26.61
CaO	16.74	16.43	15.97	15.66	15.68
K ₂ O	0.40	0.34	0.33	0.38	0.37
Na ₂ O	3.57	4.11	3.77	4.41	4.65
SO ₃	0.03	0.55	0.46	1.17	0.50
Cl	0.46	0.47	0.53	0.38	0.57
Total	94.70	95.89	94.60	94.96	95.94

Numbers of ions on the basis of 12 (Si, Al)

Si	7.10	7.14	7.19	7.16	7.27
Al	4.89	4.85	4.79	4.83	4.72
Ca	2.75	2.68	2.62	2.59	2.54
K	0.07	0.06	0.06	0.07	0.07
Na	1.06	1.21	1.12	1.32	1.36
S	0.00	0.06	0.05	0.13	0.05
Cl	0.11	0.12	0.13	0.09	0.14
Me content %	71	68	69	65	64

SAMPLE #

PS-85-8b

	Weight % oxides				
SiO ₂	49.52	49.25	48.36	48.38	50.43
Al ₂ O ₃	26.27	26.26	26.16	26.63	26.62
CaO	13.88	14.67	15.43	15.44	14.28
K ₂ O	0.39	0.42	0.34	0.34	0.41
Na ₂ O	4.64	5.31	5.05	4.96	5.52
SO ₃	0.78	0.73	1.46	1.49	0.68
Cl	0.63	0.73	0.56	0.54	0.66
Total	95.47	96.35	96.79	95.24	97.95

Numbers of ions on the basis of 12 (Si, Al)

Si	7.39	7.36	7.32	7.27	7.37
Al	4.60	4.63	4.67	4.72	4.62
Ca	2.23	2.37	2.52	2.50	2.26
K	0.07	0.08	0.06	0.06	0.07
Na	1.35	1.55	1.49	1.45	1.58
S	0.08	0.08	0.16	0.16	0.07
Cl	0.16	0.18	0.14	0.13	0.16
Me content %	61	59	62	62	58

SAMPLE #

PS-85-2

Weight % oxides

SiO ₂	45.21	45.06	45.49	46.49
Al ₂ O ₃	27.73	27.43	27.54	27.51
CaO	18.14	17.33	17.67	17.82
K ₂ O	0.14	0.12	0.13	0.16
Na ₂ O	3.38	3.45	3.46	3.58
SO ₃	0.91	1.04	0.99	0.55
Cl	0.03	0.03	0.01	0.05
Total	95.52	94.43	95.28	96.11

Numbers of ions on the basis of 12 (Si, Al)

Si	6.97	7.03	6.97	7.10
Al	5.02	4.96	5.02	4.89
Ca	3.00	2.89	2.93	2.93
K	0.02	0.02	0.02	0.02
Na	1.01	1.04	1.03	1.06
S	0.10	0.12	0.11	0.06
Cl	0.00	0.00	0.00	0.01

Me content %	74	73	73	73
--------------	----	----	----	----

SAMPLE

PS-85-2a

Weight % oxides

SiO ₂	46.61	47.46	46.13	47.12
Al ₂ O ₃	27.88	27.65	27.95	27.50
CaO	17.35	17.35	17.41	17.32
K ₂ O	0.25	0.33	0.27	0.34
Na ₂ O	3.55	3.96	3.33	3.54
SO ₃	0.49	0.21	0.29	0.34
Cl	0.27	0.35	0.30	0.37
Total	96.12	96.49	95.38	96.15

Numbers of ions on the basis of 12 (Si, Al)

Si	7.03	7.10	6.99	7.10
Al	4.96	4.87	5.00	4.89
Ca	2.80	2.78	2.83	2.79
K	0.04	0.06	0.02	0.06
Na	1.03	1.15	0.98	1.03
S	0.05	0.02	0.03	0.03
Cl	0.06	0.08	0.07	0.09
Me %	72	69	73	72

SAMPLE #

PS-85-2b

Weight % oxides

SiO ₂	46.56	47.24	47.30	46.99	47.03
Al ₂ O ₃	27.29	27.41	27.23	27.20	27.26
CaO	16.41	16.88	17.24	16.57	16.84
K ₂ O	0.39	0.38	0.36	0.34	0.35
Na ₂ O	3.75	3.53	3.91	3.99	3.98
SO ₃	0.40	0.66	0.38	0.45	0.35
Cl	0.36	0.38	0.46	0.46	0.41
Total	94.81	96.09	96.42	95.53	95.80

Numbers of ions on the basis of 12 (Si, Al)

Si	7.10	7.14	7.14	7.14	7.14
Al	4.89	4.85	4.85	4.85	4.85
Ca	2.70	2.75	2.81	2.70	2.75
K	0.07	0.07	0.07	0.06	0.06
Na	1.11	1.04	1.15	1.17	1.17
S	0.04	0.07	0.04	0.05	0.04
Cl	0.09	0.09	0.11	0.11	0.10

Me content %	69	71	70	68	69
--------------	----	----	----	----	----

SAMPLE #

PS-86-16

Weight % oxides

SiO ₂	46.32	47.26	45.25
Al ₂ O ₃	28.61	27.29	27.48
CaO	17.83	17.78	17.95
K ₂ O	0.25	0.23	0.20
Na ₂ O	3.62	3.84	3.26
SO ₃	0.04	0.14	0.06
Cl	0.15	0.16	0.14
Total	96.67	96.55	94.21

Numbers of ions on the basis of 12 (Si, Al)

Si	6.94	7.14	7.03
Al	5.05	4.85	4.96
Ca	2.86	2.90	3.00
K	0.04	0.04	0.03
Na	1.05	1.13	0.98
S	0.00	0.01	0.00
Cl	0.03	0.03	0.03

Me content %	72	71	74
--------------	----	----	----

SAMPLE #

PS-86-5

Weight % oxides

SiO ₂	47.51	47.34	46.86	48.46
Al ₂ O ₃	27.42	27.64	27.54	26.77
CaO	16.88	17.10	16.43	16.24
K ₂ O	0.41	0.39	0.39	0.42
Na ₂ O	3.71	3.71	3.71	4.26
SO ₃	0.39	0.21	0.23	0.17
Cl	0.40	0.39	0.44	0.51
Total	96.72	96.78	95.60	96.83

Numbers of ions on the basis of 12 (Si, Al)

Si	7.18	7.09	7.05	7.27
Al	4.81	4.90	4.94	4.72
Ca	2.73	2.77	2.68	2.63
K	0.07	0.07	0.07	0.08
Na	1.08	1.08	1.09	1.24
S	0.04	0.02	0.02	0.01
Cl	0.10	0.09	0.11	0.13
Me content %	70	70	70	66

APPENDIX D

GEOCHEMICAL ANALYSES

Fifteen specimens from the modified anorthosite and mylonites were analyzed. Analyses are listed in the following tables along with specific gravity measurements. Analyses were performed on a Phillips 1450 X-ray fluorescence spectrometer in the analytical facilities of the Geology Department at the University of Western Ontario. All major elements were analyzed from fusion discs and using international standards. The discs were prepared from a mixture of 2 grams of spectroflux (lithium tetraborate, lithium carbonate, and lanthanum oxide), 0.37 grams of sample and 0.02 grams of NaNO_3 . The blend was placed in a platinum crucible and fused at 1000°C for two minutes. The molten mixture was poured into a circular mold where it acquired a disc-shape. These discs were analyzed with a Rh tube target under 60 KV and 40 mA, using the U.S.G.S. standards PCC-1, DTS-1 and BCR-1. Major element abundances were determined against the monitor FS-94. The total iron was listed as Fe_2O_3 . Loss on ignition was determined by heating 1 gr of sample at 1100°C for two hours.

Analytical error for major elements except Na_2O , K_2O and P_2O_5 is less than 3%. Analytical error for Na_2O , K_2O and P_2O_5 is 5-7%. Uncertainty for trace elements is within 12%, except for Nb, Pb and La, which is 20%.

The specific gravities of samples were determined by weighing the samples in air and in water. The dry weight divided by the difference between the two measurements times the specific gravity of water is equal to the specific gravity of the the sample.

The ratios of ferric to ferrous iron were determined by a titration method. A mixture of 0.25 grams of sample, and 0.10 grams of ammonium metavanadate was dissolved in 5 ml of 40% HF. After 24 hours, 15 ml of 10% H_2SO_4 and 3 to 5 drops of diphenyl sulphate indicator were added. Standardized ferrous ammonium sulphate was titrated against the excess pentavalent vanadium in the mixture. The amount of ferrous iron oxidized by the ammonium metavanadate is proportional to the amount of metavanadate consumed during the reaction. The reproducibility of all analyses was checked by repeating the analyses at least once. When the difference was greater than 10%, the result was ignored.

Trace elements were determined from pressed pellets using a W tube target at 60 KV and 40 mA with reference to international standards. Results were reduced with the computer program TRACE developed at the University of Western Ontario.

Rare earth abundances were determined by instrumental neutron activation analyses in the analytical facilities of the Geology Department at U.W.O. Detection limits for elements are : La - 0.5 ppm; Ce - 1.0 ppm; Nd - 3 ppm; Sm - 0.01 ppm; Eu - 0.05 ppm; Tb - 0.1 ppm; Yb - 0.05 ppm; and Lu 0.01 ppm. Uncertainty in ppm per element is La, Tb and Yb \pm 5%; Ce, Nd \pm 3%; Sm \pm 1%; Eu, Lu \pm 5%.

SAMPLE #	PS-85-3	PS-86-14	PS-86-16 b
SiO ₂	53.00	53.82	63.87
TiO ₂	0.20	0.30	1.27
Al ₂ O ₃	27.23	22.30	12.88
Fe ₂ O ₃	1.67	4.61	10.66
MnO	0.02	0.07	0.19
MgO	0.93	2.39	1.63
CaO	10.47	11.08	4.55
K ₂ O	0.59	0.56	1.83
P ₂ O ₅	0.01	0.13	0.29
Na ₂ O	3.91	3.83	3.10
LOI	0.92	0.50	0.63
Total	98.93	99.59	100.90
S.G.	n.d.	n.d.	n.d.

SAMPLE #	PS-85-3a
SiO ₂	68.55
TiO ₂	0.72
Al ₂ O ₃	15.96
Fe ₂ O ₃	2.79
MnO	0.03
MgO	1.93
CaO	5.86
K ₂ O	1.09
P ₂ O ₅	0.08
Na ₂ O	2.09
LOI	1.10
Total	100.20
S.G.	n.d.

SAMPLE #	PS-85-17	PS-85-7	PS-85-2	PS-86-5	PS-86-4
Nb	0	0	3	5	18
Zr	0	0	0	67	511
Y	10	11	24	23	63
Sr	725	611	620	625	523
Rb	0	23	3	6	58
Ba	180	168	150	223	856
Ga	19	23	23	26	17
La	0	0	0	0	37
Pb	0	5	11	12	13
Zn	28	43	78	79	115
Cu	4	5	39	16	13
Ni	10	20	9	7	6
Co	34	36	61	41	43
Cr	21	30	1	18	0
V	42	101	124	115	108
S	0	351	2759	1054	212

SAMPLE #	PS-85-7a	PS-85-7b	PS-85-7c
Nb	3	3	4
Zr	341	119	221
Y	0	0	9
Sr	675	493	564
Rb	85	47	63
Ba	681	1695	1401
Ga	20	14	21
La	135	36	122
Pb	7	14	7
Zn	54	23	37
Cu	23	2	4
Ni	23	3	9
Co	51	55	37
Cr	14	2	3
V	78	3	36
S	601	0	0

SAMPLE #	PS-85-17	PS-85-7	PS-85-7a	PS-86-7b	PS-85-7c	PS-86-4
La	3.0	2.8	40.5	106.7	123.2	47.2
Ce	3.0	2.7	52.4	138.4	74.7	26.1
Nd	6.5	6.9	23.9	64.3	60.4	64.5
Sm	0.7	0.9	2.3	6.6	6.9	13.6
Eu	0.6	0.3	0.5	1.0	0.4	1.3
Tb	0.0	0.1	0.0	0.7	0.1	0.6
Yb	0.3	0.2	0.2	0.6	0.2	3.1
Lu	0.0	0.0	0.0	0.0	0.0	0.5
Ta	0.1	0.3	1.2	0.6	0.3	0.4
Hf	0.1	0.2	5.9	6.7	4.4	4.0
Sc	7.1	6.5	0.9	3.3	1.3	5.8
Cs	0.0	0.4	0.4	0.8	0.3	0.3
Th	0.1	0.1	13.1	28.4	24.4	1.9

APPENDIX E

ORIENTATION DATA

The mean areas occupied by different point concentrations of quartz c-axes and the optic directions X, Y and Z of plagioclase were obtained by a computer program written by Starkey (1970). They are derived by sampling the data in intervals of $n/10$, where n is the total sample size.

Quartz in Quartz Ribbons

Isolated Quartz grains

SAMPLE #	Conc.	Quartz in Quartz Ribbons		Isolated Quartz grains	
		Means	Sigma	Means	Sigma
PS-85-19	0	54.15	2.38	38.01	4.13
	1	21.10	3.51	34.14	4.68
	2	10.85	2.08	19.72	4.41
	3	6.23	2.22	6.19	1.88
	4	3.61	1.49	1.37	1.20
	5	1.95	1.06	1.05	0.67
	6	1.37	0.69	0.43	0.18
	7	0.59	0.47		
	8	0.51	0.29		
	9	0.25	0.07		
	10	0.00	0.00		

SAMPLE #	Conc.	Quartz in Quartz Ribbons	
		Means	Sigma
PS-85-16	0	49.55	8.04
	1	27.95	8.71
	2	10.48	4.49
	3	4.33	2.19
	4	3.52	1.11
	5	2.14	0.57
	6	1.12	0.64
	7	0.91	0.75
	8	0.65	0.43
	9	0.69	0.25
	10	0.18	0.04
	11	0.05	0.05

Quartz in Quartz Ribbons

Isolated Quartz grains

	Conc.	Means	Sigma		Means	Sigma
	0	53.83	4.32		36.76	4.37
	1	21.00	4.22		37.96	4.36
	2	10.95	2.39		16.33	3.43
SAMPLE #	3	6.72	2.13		6.41	1.82
PS-85-13	4	3.57	0.77		2.03	1.84
	5	1.97	0.73		1.10	0.58
	6	1.21	0.64		0.24	0.16
	7	0.71	0.32		0.05	0.00
	8	0.22	0.17			
	9	0.28	0.24			
	10	0.36	0.00			

	Conc.	Means	Sigma
	0	48.69	7.17
	1	23.93	6.11
SAMPLE #	2	14.51	4.11
PS-85-14	3	7.16	1.37
	4	3.70	1.30
	5	1.18	0.86
	6	1.21	0.79
	7	0.45	0.24
	8	0.23	0.04

Quartz in Quartz Ribbons Isolated Quartz grains

	Conc.	Means	Sigma	Means	Sigma
	0	49.91	11.06	41.09	5.68
SAMPLE #	1	25.10	11.73	31.45	6.87
PS-86-4	2	11.06	5.61	17.22	5.34
	3	6.62	2.31	7.29	2.84
	4	4.29	1.40	2.11	1.31
	5	1.76	1.46	1.45	0.98
	6	2.41	1.03	1.33	0.07
	7	0.71	0.82	0.00	0.00
	8	0.15	0.00		

	Conc.	Means	Sigma	Means	Sigma
	0	44.41	5.68	40.50	7.02
SAMPLE #	1	29.62	8.36	33.35	7.04
PS-85-12	2	13.40	5.85	16.31	4.83
	3	7.46	2.19	6.84	1.63
	4	3.91	1.96	1.85	1.35
	5	1.35	1.42	1.18	0.79
	6	0.41	1.42	1.12	0.67
	7			0.92	0.00
	8			0.10	0.00

REFERENCES

- Apted, M.J., and J.G. Liou, 1983. Phase relations among greenschist, epidote-amphibolite and amphibolite in a basaltic system. *Am. Jour. of Science* **283-A**, 328-354.
- Beach, A., 1980. Retrogressive metamorphic processes in shear zones with specific reference to the Lewisian Complex. *Jour. of Struct. Geol.* **2**, 257-263.
- Borges, F.S. and S.H. White, 1980. Microstructural and chemical studies of sheared anorthosites, Roneval, South Harris. *Jour. of Struct. Geol.* **2**, 273-280.
- Davidson, A., 1984. Identification of ductile shear zones in the Southwestern Grenville Province of the Canadian Shield. In Precambrian Tectonics Illustrated, edited by A. Kroner and R. Greiling, E. Schweizerbart'sche Verlagsbuchhandlung, Stuttgart, 263-279.
- Davidson A., and Morgan, W.C., 1981. Preliminary notes on the geology east of Georgian Bay, Grenville Structural Province, Ontario. In Current Research, Part A, Geol. Surv. Canada, paper **81-A**, 291-298.
- Davidson, A., N.G. Culshaw, and L. Nadeau, 1982(a). A tectono-metamorphic framework for part of the Grenville Province, Parry Sound Region, Ontario. In Current Research, Part A, Geol. Surv. Canada, paper

82-1A, 175-190.

- Davidson, A., N.G. Culshaw, and L. Nadeau, 1982(b). Tectonic features in the Central Gneiss Belt, Parry Sound Region, Ontario. Guide for the 1982 field excursion 1-3 October, 190p.
- Deer, W. A., Howie, R.A., and Zussman, J., 1966. An Introduction to the Rock Forming Minerals. Longman Group, Great Britain, 528pp.
- Easton, R.M., 1986. Geochronology of the Grenville Province. In The Grenville Province, edited by J.M. Moore, A. Davidson and A.J. Baer, Geol. Assoc. of Canada, special paper 32, 127-174.
- Ernst, W.G., 1976. Petrologic Phase Equilibria. W.H. Freeman and Company, San Francisco, 333p.
- Fyfe, W.S., 1986. Fluids in Deep Continental Crust. In Reflection Seismology: The Continental Crust 14, AGU, 33-39pp.
- Fyfe, W.S. and P. Lonsdale, 1981. Ocean floor hydrothermal activity. In The Oceanic Lithosphere, The Sea, edited by C. Emiliani, John Wiley, New York, 589-638 pp.
- Fyfe, W.S., N.J. Price and A.B. Thompson, 1978. Fluids in the Earth's Crust. Elsevier, Amsterdam, 383 pp.
- Froese, E., 1978. Oxidation and reduction reactions. In Applications of Thermodynamics to Petrology and Ore Deposits: a short course, edited by Greenwood, H.J.

2, 84-97.

- Gresens, R.L., 1967. Composition-volume relationships of metasomatism. *Chemical Geology* 2, 47-65.
- Goldsmith, J.R., 1982. Review of the behavior of plagioclase under metamorphic conditions. *Am. Mineral.* 67, 643-651.
- Haughton, D.R., 1970. Plagioclase-scapolite equilibrium. *The Can. Mineralogist* 10, 855-870.
- Hietanen, A., 1967. Scapolite in the Belt series in the St. Joe-clearwater region, Idaho. U.S. Geol. Survey Sp. Paper 86, 56pp.
- Hewitt, D.F., 1967. Geology and mineral deposits of the Parry Sound-Huntsville area. Ontario Department of Mines, Geological Report 52, 65pp and Map 2118.
- Jensen L.N. and J. Starkey, 1985. Plagioclase microfabrics in a ductile shear zone from the Jotun Nappe, Norway. *Jour. Struct. Geol.* 7, 527-539.
- Kerrich, R., W.S. Fyfe, B.E. Gorman, and I. Allison, 1977. Local modification of rock chemistry by deformation. *Contrib. Mineral. Petrol.* 65, 183-190.
- Kretchmar, U.H., 1968. A study of the opaque minerals of the Whitestone Anorthosite, Dunchurch, Ontario. Unpublished M.Sc. Thesis, McMaster, Hamilton, Ontario.

- Lacy, W.C., 1960. Geology of the Dunchurch area, Ontario, Canada. *Bull. Geol. Soc. Am.* 71, 1713-1718.
- Laird, J., and A.L. Albee, 1981. Pressure temperature and time indicators in mafic schist: Their application to reconstructing the polymetamorphic history of Vermont. *Am. Jour. Sci.* 281, 127-175.
- Law, R.D., 1986. Relationships between strain and quartz crystallographic fabrics in the Roche Maurice quartzites of Plougastel. *Jour. Struct. Geol.* 8, 413-513.
- La Tour, T.E., 1974. An examination of metamorphism and scapolite in the Skalkaho Region, Southern Sapphire Range, Montana. Unpublished M.Sc. Thesis, University of Montana, Montana.
- Leake, B.E., 1978. Nomenclature of amphiboles. *Min. Mag.* 42, 533-563.
- Lister, G.S. and P.F. Williams, 1979. Fabric development in shear zones: theoretical control and observed phenomena. *Jour. Structural Geol.* 4, 283-297.
- Lister, G.S. and U.F. Dornsiepen, 1982. Fabric transitions in the Saxony granulite terrain. *Jour. Structural Geol.* 4, 81-92.
- Martignole, J., 1986. Some questions about crustal thickening in the central part of the Grenville Province. In The Grenville Province, edited by J.M.

- Moore, A. Davidson and A.J. Baer, Geol. Assoc. of Canada, special paper 32, 327-340.
- Mason, I.M., 1969. Petrology of the Whitestone Anorthosite. Unpublished Ph.D. Thesis, McMaster University, Hamilton, Ontario.
- Miyashiro, A., 1961. Evolution of metamorphic belts. Jour. Petrology, 2, 277-3-11.
- Moody, J.B., D. Meyer, J.E Jenkins, 1983. Experimental characterization of the greenschist/amphibolite boundary in mafic systems. Am. Jour. Sci. 283, 48-92.
- Mummery, B.C., 1972. Coronite amphibolites from the Whitestone area, Parry Sound, Ontario. Unpublished Ph.D. Thesis, McMaster University, Hamilton, Ontario.
- Nadeau, L., 1984. Deformation of leucogabbroic rocks at Parry Sound, Ontario. Unpublished M.Sc. thesis, Carleton University, Ottawa, Ontario.
- Quirke, T.T., 1930. Key Harbour Sheet. Geological Survey of Canada, Map 239A.
- Platt, J.P. and J.H. Behrmann, 1986. Structures and fabrics in a crustal shear zone, Betic Cordilleras, S.E. Spain. Jour. of Struct. Geol. 8, 15-34.
- Ramsay, J.G., 1980. Shear zone geometry: A review. Jour. Struct. Geol. 2, 83-99.
- Ramsay, J.G. and I. Allison, 1979. Structural Analysis of Shear Zones in an alpinised Hercynian Granite.

- Schweiz. Mineral. Petrogr. Mitt. 59, 251-279.
- Robbins D.W. and R.G.J. Strens, 1972. Charge-transfer inferromagnesian silicates: The polarized electronic spectra of trioctahedral micas. Mineral. Mag. 38, 551-563.
- Schmid, S.M. and Casey, M. 1986. Complete texture analysis of commonly observed quartz c-axes patterns. Am. Geophys. Un., geophys. Monogr. 36, 263-286.
- Schwerdtner, W.M, 1987. Interplay between folding and ductile shearing in the Proterozoic crust of the Muskoka - Parry Sound Region, central Ontario. Can. Jour. Earth Sci. 24, 1507-1526.
- Segall, P. and Simpson C., 1986. Nucleation of ductile shear zones on dilatant fractures. Geology 14, 56-59.
- Shieh, Y.N. and Schwarcz H.P., 1974. Oxygen isotope studies of granite and migmatite, Grenville province of Ontario, Canada. Geochim. Cosmochim. Acta 38, 21-45.
- Sibson, R.H., 1977. Fault rocks and fault mechanisms. Geol. Soc. of London Journal 133, 191-213.
- Sinha, K.A., D.A. Hewitt, and D.J. Rimstidt, 1986. Fluid interaction and element mobility in the development of ultramylonites. Geology 14, 883-886.
- Starkey, J., 1964. An X-ray method for determining the orientation of selected crystal planes in

- polycrystalline aggregates. *Am. Jour. Sci.*, **262**, 735-752.
- Starkey, J., 1970. A computer program to prepare orientation diagrams. In Experimental and Natural Rock Deformation, edited by P. Paulitsch, Berlin, Springer Verlag, Berlin, 51-74 pp.
- Starkey, J., 1977. The contouring of orientation data represented in spherical projection. *Can. Jour. Earth Sci.* **14**, 268-277.
- Starkey, J., 1979. Petrofabric analysis of saxony granulites by optical and X-ray diffraction methods. *Tectonophysics* **58**, 201-219.
- Stockwell, C.H., 1970. Geology of the Canadian Shield, introduction. In Geology and Economic Minerals of Canada, edited by R.J.W. Douglas, Geol. Survey of Canada Economic Geology Report, **1**, 43-54.
- Thompson, D.L., 1983. The nature of anorthosite-country rock interaction during granulite facies metamorphism: An example from the Whitestone Anorthosite. Unpublished M.Sc. Thesis, McMaster University, Ontario.
- Tullis, J.A., Christie, J.M. and Griggs, D.T., 1973. Microstructures and preferred orientations of experimentally deformed urtz. *Bull. Geol. Soc. Am.*, **84**, 297-314.

- Tullis, J.A., and R.A. Yund, 1985. Dynamic recrystallization of feldspar: A mechanism for ductile shear zone formation. *Geology*, 13, 238-241.
- van Breemen, O., A. Davidson, W.D. Loveridge and R.W. Sullivan, 1986. U-Rb zircon geochronology of Grenville tectonites, granulites and igneous precursors, Parry Sound, Ontario: some preliminary results. In The Grenville Province, edited by J.M. Moore, A. Davidson and A.J. Baer, Geol. Assoc. of Canada, special paper 32, 191-207.
- van Breemen, O. and A. Davidson, 1988. Recent U-Pb dating, Southwestern Grenville Province. Grenville workshop, programs and abstracts, 17.
- Vauchez, A., 1987. The development of discrete shear-zones in a granite: stress, strain and changes in deformation mechanisms. *Tectonophysics* 133, 137-156.
- Vocke, R.D. Jr., G.H. Hanson and M. Grunfelder, 1987. Rare earth element mobility in the Rofna Gneiss, Switzerland. *Contrib. Mineral. Petrol.* 95, 145-154.
- White, J.W. and C.K. Mawer, 1986. Extreme ductility of feldspars from a mylonite, Parry Sound, Canada. *Jour. Struct. Geol.* 8, 133-143.
- Wilson, C.J.L., 1975. Preferred orientation in quartz ribbon mylonites. *Geol. Soc. of America Bull.* 86, 968-974.

- Windley, B.F., 1986. Comparative tectonics of the Western Grenville and the Western Himalaya. In the Grenville Province, edited by J.M. Moore, A. Davidson and A.J. Baer, Geol. Assoc. Canada Special Paper 31, 341-348.
- Wynne-Edwards, H.R., 1972. The Grenville Province. In Variations in Tectonic Styles in Canada, Edited by R.A. Price and R. J.W. Douglas, Geol. Assoc. of Can., Spec. Pap. 11, 263-334.

VITA

NAME: Hayrettin Koral

YEAR OF BIRTH: 1954

**POST-SECONDARY
EDUCATION AND
DEGREES:** Istanbul University
Istanbul, Turkey
1973-1977 B.Sc.

Rensselaer Polytechnic
Institute
Troy, New York
1981-1983 M.Sc.

The University of Western
Ontario
London, Ontario
1983-1988 Ph.D.

**RELATED WORK
EXPERIENCE:** Demonstrator
The University of Western
Ontario
1983-1986

Teaching Assistant
Rensselaer Polytechnic
Institute
1982

Research Assistant
Istanbul University
1977-1979

Teaching Assistant
Istanbul University
1977-1980

PUBLICATIONS:

(1) Koral, H. & J. Starkey (1987). Quartz deformation in mylonites of the Parry Sound Shear Zone. Abstr., Canadian Tectonics Meeting, Thunder Bay, Ontario.

(2) Koral, H. & J. Starkey (1987). Ductile deformation of the Whitestone Anorthosite: Progressive changes within the Parry Sound Shear Zone. Abstr, 7th International Tectonics Conferance, Kingston, Ontario.

- Windley, B.F., 1986. Comparative tectonics of the Western Grenville and the Western Himalaya. In the Grenville Province, edited by J.M. Moore, A. Davidson and A.J. Baer, Geol. Assoc. Canada Special Paper 31, 341-348.
- Wynne-Edwards, H.R., 1972. The Grenville Province. In Variations in Tectonic Styles in Canada, Edited by R.A. Price and R. J.W. Douglas, Geol. Assoc. of Can., Spec. Pap. 11, 263-334.